INTERMEDIATE STRAIN RATE BEHAVIOR OF TWO STRUCTURAL ENERGETIC MATERIALS

A Thesis
Presented to
The Academic Faculty

by

Nitin R Patel

In Partial Fulfillment
of the Requirements for the Degree
Masters of Science in Mechanical Engineering

Georgia Institute of Technology

October 2004

INTERMEDIATE STRAIN RATE BEHAVIOR OF TWO STRUCTURAL ENERGETIC MATERIALS

Approved by:

Dr. Min Zhou, Advisor
School of Mechanical Engineering
Georgia Institute of Technology

Dr. David McDowell
School of Mechanical Engineering
Georgia Institute of Technology

Dr. Naresh Thadhani
School of Materials Science & Engineering
Georgia Institute of Technology

Date Approved: October 20, 2004

DEDICATION

To my parents, who have given me the strength to accomplish anything I desire

To my brother, who has served as an ideal role-model for me, making me strive to become more than just the "Other Guy"

To my girlfriend, Courtney, whose love and encouragement make each day a pleasure to live

ACKNOWLEDGMENTS

I would like to express my sincere gratitude to my advisor, Dr. Min Zhou, who has provided me with invaluable support and guidance throughout my stay at Georgia Tech. I would also like to thank my committee members, Dr. David McDowell and Dr. Naresh Thadhani, for all of their assistance with the project.

This study was conducted as part of the AFOSR MURI at Georgia Tech. I would like to give a special thanks to everyone working as part of the MURI for their insight and assistance.

I would like to specially thank Louis Ferranti, Matt McGill, Dan Eakins, and the rest of Dr. Thadhani's research group for their help with the material synthesis portion of this study. I would like to also thank David Sarver, Robert Cooper, John Graham, and the rest of the Mechanical Engineering Machine Shop for their help with specimen preparation and experimental testing. I also want to thank Ghazal Saheli, Ryan Austin, and Dr. Garmestani for their help with the modeling work done in this study.

I would like to express my gratitude towards Greg Ingram, for teaching me all there is to know about the lab equipment, Vikas Tomar, Wuwei Liang, Sam Martin, and Ambarish Kulkarni for their guidance and friendship throughout my stay at Georgia Tech. A special thanks goes out to all of my friends here at Georgia Tech, back in Arizona, and all over the country for all the good times we have had.

TABLE OF CONTENTS

LIST OF TABLES

LIST OF FIGURES

SUMMARY

A new class of materials, known as multi-functional energetic structural materials (MESMs), has been developed. These materials possess both strength and energetic functionalities, serving as candidates for many exciting applications. One of such applications is ballistic missiles, where these materials serve as part of structural casing as well as explosive payload.

In this study, the dynamic compressive behavior of two types of MESMs in the intermediate strain rate regime is investigated. The first type is a thermite mixture of Al and Fe_2O_3 particles suspended in an epoxy matrix. The second type is a shock compacted mixture of Ni and Al powders. Compression experiments on a split-Hopkinson pressure bar (SHPB) apparatus are carried out at strain rates on the order of 10^3 s^{-1}. In addition, a novel method for investigating the dynamic hardness of the Al + Fe_2O_3 + Epoxy materials is developed. In this method, high-speed digital photography is used to obtain time-resolved measurements of the indentation diameter throughout the indentation process.

Experiments show that the shock compacted Ni-Al material exhibits a rather ductile behavior and the deformation of the Al + Fe_2O_3 + Epoxy mixtures is dominated by the polymer phase and significantly modulated by the powder phases. The pure epoxy is ductile with elastic-plastic hardening, softening, and perfectly plastic stages of deformation. The Al and Fe_2O_3 particles in Al + Fe_2O_3 + Epoxy mixtures act as

reinforcements for the polymer matrix, impeding the deformation of the polymer chains, alleviating the strain softening of the glassy polymer matrix at lower levels of powder contents (21.6 - 29.2% by volume), and imparting the attributes of strain hardening to the mixtures at higher levels of powder contents (21.6 - 49.1% by volume). Both the dynamic and quasi-static hardness values of the Al + Fe_2O_3 + Epoxy mixtures increase with powder content, consistent with the trend seen in the stress-strain curves.

To quantify the constitutive behavior of the 100% epoxy and the Al + Fe_2O_3 + Epoxy materials, the experimentally obtained stress-strain curves are fitted to the Hasan-Boyce model. This model uses a distribution of activation energies to characterize the energy barrier for the initiation of localized shear transformations of long chain polymeric molecules. The results show that an increase in powder content increases the activation energy, decreases the number of transformation sites, causes redistribution of applied strain energy, and enhances the storage of inelastic work. These effects lead to enhanced strength and strain hardening rate at higher levels of powder content.

CHAPTER I
INTRODUCTION AND BACKGROUND

1.1 Introduction

In engineering design, there are many different classes of materials, two of which are structural and energetic materials. Structural materials are capable of sustaining loads and are found in common engineering applications such as buildings, bridges, and automobiles. Energetic materials posses the capability of releasing large amounts of energy through exothermic reactions and are typically used as explosives. The combination of the strength and energetic properties creates a new class of materials known as multi-functional energetic structural materials (MESMs).

A typical energetic material that would serve as part of MESMs can be made up of two or more components that react with each other when a certain reaction initiation energy level is achieved. The reaction is initiated by the rupture of the bonds of constituents within the energetic material (Owens 1996). The rupture of bonds must be initiated by the introduction of a large amount of stress or heat to the energetic material.

The design of an energetic material is very flexible and can allow for use in many different applications. It is this flexibility that poses the largest challenge when tailoring an energetic material for a particular engineering application due to the constant compromise in the reaction and the strength characteristics. The “stronger” a MESM is, the more difficult it may be to initiate reaction and it may also decrease the energetic characteristics of the material.

1.1.1 Applications of Energetic Materials

Due to the energetic capabilities of the material, it follows that energetic materials have many uses in military applications. Popular applications of MESMs include explosives, explosive aids, and explosive structures. Conventional explosives are comprised of energetic materials that possess extremely high energetic characteristics, commonly known as high-energetic materials. An explosive aid can be a medium to high energetic material that acts as a casing for bombs or mines. Explosive structures possess the ability to withstand structural stresses and loads, yet when the initiation of the chemical reaction takes place, energy will be released. Although all of these applications are of interest, the applications of energetic structures have recently become particularly interesting.

The unique characteristics of MESMs make them attractive choices for applications such as missiles, where the strength allows for it to serve as a portion of the casing. An increase of the onboard payload of the missile is accomplished by the introduction of energy stored within the MESMs that is not present in other typical structural materials, such as steel (Chen et al. 2002).

The two main types of missiles that can benefit from MESMs are target-penetrating missiles (TPMs) and explode-on-contact missiles (ECMs). A TPM must be capable of penetrating meters of earth and many layers of concrete prior to detonation. The design of TPMs must be robust and capable of handling very high stress levels prior to detonation. ECMs typically do not encounter such high levels of stress. The primary sources of loading for ECMs is generally limited to the flight on the aircraft, ignition, and flight towards the target.

The general design of a missile that incorporates an energetic material substitutes part of the traditional steel casing with MESMs in the area surrounding the explosive payload (Figure 1). The structural properties of the MESMs allow a TPM to withstand the loading during the penetration of its target, while the energetic properties of the material enhance the detonation capabilities of both TPMs and ECMs.

The chemical makeup of MESMs introduces problems not seen in metals such as steel. The stability, initiation parameters, and long-term storage effects of the material can effect its energetic functionality. It is important that the energetic material does not encounter premature initiation, the results of which would be catastrophic.

Energetic materials can be tailored to initiate when specific levels of stresses are attained, such as those generated by the penetration of the target or a shockwave generated by the detonation of the onboard explosives, resulting in a rapid increase in temperature. In order to prevent a premature reaction, the energetic system must have the reaction initiated by a higher level of stress than that it would see during handling, flight, or firing of the missile.

1.2 Objectives and Approach

An important parameter to understand when dealing with an energetic material is the initiation of the chemical reaction, which occurs at a high state of stress or an elevated temperature. However, in the application of ballistic missiles, it is very important to not only know the initiation conditions, but it is also important to understand the constitutive response of the material under dynamic loading. Due to the nature of ballistic impacts and penetration of missile into its target, the majority of the loading that a missile endures

is in the dynamic regime, on the order of 10^3 s^{-1}. Testing in the dynamic regime allows for relatively inexpensive tests to be carried out onto a wide range of materials and material compositions. This allows for the selection of materials with the optimum strength and energetic characteristics to be tested within the high strain-rate regime, which requires much more expensive tests. In order to get a complete understanding of the dynamic constitutive response, novel experimental techniques are used. A method for the creation of controlled porosity allows for the investigation into the constitutive behavior of specimens with significant void content, while dynamic indentation experiments provide insight into the resistance of penetration and the wear properties of the specimens tested. The experimental data will also be fit to a constitutive model to better explain the deformation mechanisms present under dynamic loading. This allows for the observation of changes in the mechanisms over the range of material compositions used in this study.

1.3 Reactive Metal Powder Systems

There are a variety of different chemical reactions that are capable of generating the heat required to classify them as energetic materials. Two material systems are investigated in this study, the first being an aluminum and iron oxide mixture. This reactive metal powder system undergoes the following chemical reaction when the initiation stress state is reached,

$$Fe_2O_3 + 2Al \xrightarrow{stress} 2Fe + Al_2O_3 \left(\Delta H_R = -282 \frac{kJ}{mol} \right). \quad (1.1)$$

The second material system that is investigated is a nickel and aluminum mixture. The chemical reaction for initiation of this system is,

$$3Ni + Al \xrightarrow{stress} Ni_3Al + oxidation \left(\Delta H_R = -159 \frac{kJ}{mol} \right). \quad (1.2)$$

1.4 Methods of Synthesis for Energetic Materials

There are several techniques that can be used to create energetic structural materials. From an energetic standpoint, the interaction between the reactive constituents dictates the reactive capabilities of the material; the more interaction, the more reaction. Increasing the strength of the structure of the material requires a compromise in the energetic functionality. The following synthesis methods represent only a small number of the current techniques used to create MESMs.

1.4.1 Sol-Gel Synthesis

The sol-gel method is a novel technique that allows for the creation of a porous, metal-oxide matrix through the evaporation of a solution containing a metal salt, alcohol, and a gelation agent (Figure 2a). The resulting material matrix has both a high surface area and high levels of porosity. Metal fuel particles can be introduced into the pores of the oxide matrix prior to gelation to create an energetic sol-gel material (Figure 2b).

The creation of materials using the sol-gel process has many advantages. The synthesis of the material is simple due to the fact that it can be done with the use of general laboratory equipment. Another benefit of this process is that the particles within the metal-oxide matrix are on the order of nanometers, allowing for a more homogeneous material to be created, as well as increasing the reactivity. The smaller particles decrease the overall porosity within the material, thus increasing its strength. The energetics of sol-gel material is enhanced by the high surface area of the metal-oxide matrix, allowing

for greater potential for reaction with the metal fuel particles located within the pores (Figure 3).

Flexibility in the synthesis of sol-gel materials allows the material to be tailored to a variety of applications by increasing the strength, manipulating the porosity, and varying the elements that make up the sol-gel. Due to the variety of applied loads that an energetic material sees when used in an application such as a missile, it must be able to not only withstand significant compressive loading, but it will also be required to withstand both shear and torsional loading. To strengthen the sol-gel material to withstand these different loads, carbon fibers (or other high strength fibers), metallic glass cores, steel rods, or nanotubes can be added at the micro or nano level. Alignment of reinforcement particles can significantly increase the strength of the sol-gel material in a specific direction. The density of the sol-gel can be manipulated by controlling the evaporation rates and styles of the liquid phase of the gel. Slow evaporation of the solvent results in a xerogel, which is ~50% porous; supercritical extraction of the solvent produces a highly porous, low-density aerogel (Tillotson et al. 1998). In order to vary the make-up of the sol-gel material, a technique of controlled distribution of various transition metal oxides into a silica matrix has been developed (Curran 1999). Ti, V, Cr, and recently, Fe, Co, and Ni are some of the materials that have successfully been introduced into the silica matrix.

Despite the various advantages of the sol-gel method, there have been difficulties in creating viable specimens. The sol-gel material has a tendency to crack during the final stages of evaporation especially during the creation of large specimens. In addition,

the size and shape of sol-gel materials is limited due to the gelation stage of the synthesis process.

1.4.2 Shock Compaction

Another synthesis technique used to create energetic materials is shock compaction. This method allows the compression of powders together, without the need for a binder system. The close compaction of the powders results in enhanced interaction between reactive constituents, and the simplicity of the system allows for a uniform distribution of particles.

The compression of the metallic powders is carried out by detonating explosives that are packed around a cylinder which contains the reactive powders, generating a shockwave that propagates through the material, resulting in the creation of a solid material. A mandrel, which is a stable, metallic rod, can be placed in the center of the powders to be compacted to absorb the wave and prevent poor compaction in the center due to misalignment. Lee and Thadhani (1998) were able to create titanium carbide (TiC) through the shock compaction method. The solid resulting from the shock compaction method was observed to have no visible cracks and optical micrographs revealed a densely packed microstructure of agglomerates of carbon surrounded by Ti particles.

Although the shock compaction method has the capability of producing very dense, homogenous solids, there are limitations to this method. Difficulty will arise while trying to compact large portions of powders at once. Cracks often occur within the

shock compacted material as well. Due to the complexity of wave propagation, intricate shapes cannot be easily created using this method; only cylindrical units can be produced.

1.4.3 Epoxy Binder Matrix

Another approach to creating an energetic material is to suspend the energetic powders within a polymer matrix. Commercially available epoxy resin and hardeners can be used to create the polymer phase of the material. There has been a great deal of work in the general area of epoxy-based polymers due to their versatile use. The use of epoxy in structural materials requires investigation into the synthesis of epoxy-based polymers, characterization of their constitutive behavior, and methods of reinforcing the epoxy matrix.

Significant mechanical testing of basic, commercially available epoxy systems has been explored. An epoxy system comprised of EPON 828 resin and T-403 hardener was tested at various strain rates in compression by Chen and Zhou (1998). It was discovered that the peak compressive stress increased as the strain rate increased. The highest peak stress achieved was approximately 180 MPa. Large differences between the strain rate effect within the quasi-static and dynamic tests were observed. Quasi-static tests showed a large increase in strength with increasing strain rate, indicating strain-rate hardening dominating the deformation due to the low heat generation during plastic deformation. Conversely, the increase in strain rate in the dynamic testing regime yielded very little difference in the strength, most likely attributed to the balance between strain-rate hardening and thermal softening within the material due to an increase in the heat generated during plastic deformation at high rates.

The same EPON 828/T-403 epoxy system was later tested in tension under dynamic and quasi-static loading by Chen et al. (2002). Tension tests revealed a maximum peak stress of approximately 80 MPa. Unlike the compression testing, the dynamic tests did not yield a large variance due to the strain rate. However, it was discovered that the fracture method of quasi-static tests varied from the dynamic tests. Under quasi-static loading, fracture was observed to take place in a ductile manner, with necking of the gauge section taking place. Conversely, dynamic testing revealed that fracture occurred in a brittle manner. The brittle fracture sites tended to be at the ends of the gauge section, where the cross-section of the specimens transitioned from the flat gauge section to a fillet radius. Fracture occurring in this region is most likely attributed to stress concentrations created during the machining process. It is also likely that the premature fracture masked the effect of strain rate on the maximum peak stress in this study.

Recent work is being done to introduce nanotubes into polymeric materials to increase their strength (Garmestani et al. 2003). The addition of nanotubes can play a great role in enhancing the strength characteristics; in fact, it has been found that the modulus of a cast composite film comprised of polystyrene with a 5% volume fraction of carbon nanotubes has an increase of 100% in its modulus compared to the material without nanotubes. Nanotubes, when properly distributed and oriented within a material, can carry large amounts of load that the matrix material would normally be forced to carry on its own.

The introduction of nanotubes into a polymer matrix will result in random dispersion and orientation. Magnetic field-induced alignment orients the nanotubes in the

same direction within the matrix. Al-Haik et al. (2004) conducted a study in which nanotubes were introduced into an Aeroepoxy matrix and aligned using magnetic fields of 0, 15 and 25 T. Nanoindentation techniques were used to characterize the mechanical properties of the different configurations. It was observed that the fields at 0, 5 and 25 T produced average hardness values of 1.70, 2.42 and 3.24 GPa, respectively. The average calculated values of the elastic modulus were 22.95, 27.20, and 31.23 GPa, respectively. It can clearly be seen that the mechanical characteristics of a material can greatly be increased with the inclusion and proper orientation of nanotubes as reinforcement to the polymer matrix.

1.5 Experimental Methods

There are many methods for testing the mechanical behavior of materials. Testing of materials in the intermediate-strain rate regime (10^2-10^4 s^{-1}) is of particular interest for applications such as ballistic penetrators, armor, and machine tooling. A wide variety of experimental methods are conducted in the intermediate-strain rate regime, and in this study, we focus on the use of the split-Hopkinson pressure bar (SHPB) apparatus and dynamic indentation.

1.5.1 Dynamic Compression Testing

Bertram Hopkinson (1914) developed a method to study the propagation of dynamic pressure waves initiated by an explosion or ballistic impact. Hopkinson proposed that a bullet impacting the end of a long, elastic, metal rod would produce a pressure wave that would propagate down the length of the rod. The duration of the

pressure wave begins when the bullet first impacts the end of the rod and terminates when the bullet is fully arrested.

Hopkinson devised a method to study the pressure waves with the use of a ballistic pendulum, which consisted of a long, metal rod (incident bar), a short metal rod of the same diameter (momentum bar), and a catch box (momentum trap). The incident bar and momentum trap were both suspended horizontally by four strings, allowing them to move horizontally while remaining in the same plane. The momentum bar was affixed to the free end of the incident bar with a magnetic solenoid.

A pressure wave was initiated in the incident bar by either the detonation of an explosive or the impact of a bullet on the free end of the bar. The pressure wave propagates down the incident bar, through the incident bar/momentum bar interface, and into the momentum bar. When the compressive wave reaches the free end of the momentum bar, it reflects back as a tensile wave of the same profile and amplitude. When the tensile wave returns to the incident bar/momentum bar interface, it breaks the bond created by the magnetic field, sending the momentum bar into the momentum trap. The horizontal displacements of both the incident bar and momentum trap are used to calculate the momentum trapped in the momentum bar.

R.M. Davies (1948) later studied Hopkinson's apparatus and noted some of the disadvantages and limitations of his method. The first was that the adhesion between the incident and momentum bars created large errors in tests that were run at low impact pressures. The second disadvantage that he noted was that Hopkinson's results were unable to produce any relation between pressure and time for the wave propagating within the bar.

Davies modified Hopkinson's apparatus with the incorporation of condensers to measure the propagation of pressure waves within the incident bar. Two condensers were used in this apparatus, one that is oriented around the circumference of the incident bar, and one located at the end of the incident bar. For slow movements or impacts on the bar, the two conductors move together, showing no change in relative displacement. However, for high-amplitude impulses, the condenser located on the bar will register a change in capacitance first, while the condenser at the end of the bar has yet to detect the wave. The ability to measure the pressure wave with the use of the condensers allowed Davies to overcome the limitations of Hopkinson's method. Davies noted three important assumptions required for pressure waves traveling within metal rods:

1. Propagating waves traveling through the bar must be elastic
2. Waves must not distort as the travel through the bar
3. The pressure pulse must evenly be distributed within the entire cross-section of the bar

Further improvements to the Hopkinson apparatus were made by Klosky (1949), who incorporated two pressure bars with a specimen sandwiched in between them to measure the dynamic compressive behavior. This system is commonly referred to as the Klosky bar apparatus and is also referred to as the split-Hopkinson pressure bar (SHPB) apparatus. The use of and incident bar and a transmission bar allows for the study of the dynamic response of materials at higher rates of loading. Further revisions of the SHPB apparatus were made by Lindholm (1964), who used strain gauges to capture the wave propagation with better resolution. A comprehensive review of current SHPB techniques in compression, tension, and torsion has been documented by Follansbee (1985).

1.5.2 Hardness Testing and Dynamic Indentation

Hardness testing has been widely used to gauge a materials resistance to indentation and to give insight into wear resistance and durability. A typical quasi-static hardness test involves applying a force to a penetrator located on the material surface and measuring the effects of its penetration into the material. One of the more widely used hardness testing methods is the Brinell hardness test (ASTM E-10), which is conducted by penetrating a steel ball indenter into the surface of the specimen (Figure 4).

The material behavior during a quasi-static hardness test results in three stages of deformation, elastic deformation, plastic deformation, and elastic recovery. In the initial stages of load application during a Brinell hardness test the material deforms elastically. When the stress exceeds the elastic limit, plastic flow occurs within the material along with continued elastic deformation (Figure 4). Removal of the applied load will allow for a portion of the deformed material to recover elastically.

The applied load (F), diameter of indenter (D), and diameter of the indentation measured after the removal of the load (d) are used to calculate the Brinell hardness using the following equation:

$$HBW = 0.102 \times \frac{2F}{\pi D\left(D - \sqrt{D^2 - d^2}\right)}. \qquad (1.3)$$

Another common experiment carried out to measure the hardness of materials is microindentation hardness testing. The Vickers microindentation test (ASTM E-384) utilizes a square based, pyramidal-shaped, diamond indenter with face angles of 136º (Figure 5). A Vickers microindentation experiment requires the penetration of the indenter into the surface of the test material at a set load and dwell time. At the

conclusion of the indentation, the indenter is moved, and the size of the indent is measured optically under a microscope. The mean length of the diagonals of the indent (d) is used along with the force (P) to calculate the Vickers hardness,

$$HV = 1854.4 \times \frac{P}{d^2}. \qquad (1.4)$$

Despite hardness testing being a useful gauge of a materials response to quasi-static penetration, it does not provide insight into the deformation characteristics of a material under dynamic loading conditions. Tabor (1948) conducted an investigation into the dynamic hardness of metals. In his study, a drop weight diamond indenter was dropped from a known height onto the surface of the test metal and the rebound height of the indenter was measured. Using the initial height of the indenter, rebound height, and the volume of the indentation, the energy required to plastically deform the material under dynamic conditions can be calculated. A limitation to Tabor's method is the inability to measure the applied load throughout the duration of the experiment. Tabor relied on previously known material properties that may also be rate dependent, such as the Young's modulus, yield strength, and work hardening coefficient.

Subhash et al. (1999) developed a method for dynamic Vickers indentation of metals that utilized a modified Hopkinson bar apparatus and a load cell to capture the time-resolved loading history throughout the indentation process. To calculate the dynamic Vickers hardness, the maximum force from the load cell and final indention dimensions were used. Results from this experiment showed that the dynamic hardness of metals was higher than the static hardness values measured. The trend in the observed dynamic hardness behavior was found to be consistent with the previously reported rate-sensitivity of metals tested.

1.6 The Hasan-Boyce Model

To quantify the constitutive behavior of the polymer-based materials, the deformation mechanisms must be studied. Deformation of glassy polymers is dominated by local rearrangements of molecules. If the local energy barrier, known as the activation energy, is exceeded by the strain energy due to the applied stress, localized regions of polymeric chain movement will occur. The creation of a significant number of these regions, known as transformation sites, allows for the flow of polymeric chains, and ultimately, inelastic deformation of the material.

Hasan and Boyce (1995) developed a model to characterize the nonlinear viscoelastic and the post-yield behavior of single-phase polymers. This model, known as the Hasan-Boyce model, uses a distribution of activation energies to characterize the energy barrier of localized shear transformations.

Error! Reference source not found. represents the rate-dependent behavior of the polymer used in this study. Initially, the deformation of the polymer is linear elastic in nature, which can be seen by the region marked as A. With increasing deformation, regions with low activation energy transform at considerable rates, giving rise to nonlinear stress-strain behavior (region B). Once a site begins to transform, the material surrounding it, which possesses higher activation energy, begins to elastically store the corresponding transformation energy, preventing multiple shear transformations within the same volume by increasing the effective activation energy.

Further increase in the stress leads to the transformation of regions with progressively higher activation energy, resulting in increasing nonlinearity in the stress-

strain curve, as seen in region C. As the number of transformed sites increases, the amount of surrounding material capable of storing the corresponding transformation energy decreases. When the surrounding material is no longer capable of storage, the creation of defects within the material that have low activation energy leads to strain softening of the material, as seen in region D. The material evolves into a steady-state flow from the strain softening state due to regions of liquid-like mobility within the material. There is a slight work hardening effect in the material at significant inelastic strain levels, known as orientation hardening, which is caused by the reorientation of the polymeric chains during flow (region E).

The following equations were developed by Lu et al. (2001) to describe the viscoelastic and viscoplastic behavior of single-phase polymers using the Hasan-Boyce model. The inelastic strain rate is given by,

$$\dot{\gamma}^p = \left(\dot{\gamma}_1^p + \dot{\gamma}_2^p\right) \times \left[\exp\left\{ \frac{\tau \cdot \Delta v_\tau^*(T)}{kT} \right\} - \exp\left\{ \frac{-\tau \cdot \Delta v_\tau^*(T) + S}{kT} \right\} \right], \quad (1.5)$$

where $\dot{\gamma}_1^p$ and $\dot{\gamma}_2^p$ are two functions that contribute to the inelastic strain rate, τ is the equivalent shear stress, $\Delta v_\tau^*(T)$ is the shear activation volume, k is the Boltzmann constant, T is the absolute temperature, and S is the local transformation strain energy. The shear activation volume is given by,

$$\Delta v_\tau^*(T) = \Delta v_{\tau 0}^* + \lambda\left(T - T_0\right), \quad (1.6)$$

where $\Delta v_{\tau 0}^* = \Delta v_\tau^*(T_0)$ is taken at room temperature and λ is a material parameter. $\dot{\gamma}_1^p$ and $\dot{\gamma}_2^p$ are given as,

$$\dot{\gamma}_1^p = \dot{\gamma}_0 \cdot e^{-a\eta} \frac{\sqrt{2} + (2-\eta)e^{3\pi(1-\eta)/4}}{\left[1+(1-\eta)^2\right]\left(\sqrt{2}+2e^{3\pi/4}\right)}, \tag{1.7}$$

$$\dot{\gamma}_2^p = \dot{\gamma}_0 \cdot e^{-a'\eta} \frac{\sqrt{2}e^{\pi(1/4-\eta)} + (2+\eta)e^{\pi(1-\eta/4)}}{\left[1+(1+\eta)^2\right]\left(\sqrt{2}e^{\pi/4}+2e^{\pi}\right)}, \tag{1.8}$$

where $\dot{\gamma}_0$ is the pre-exponential factor, $\eta = 1/(kT)$, a is an internal variable that characterizes the mean of the distribution of order, and $a' = a + (\pi\alpha^{-1})/2$, which is another internal variable that characterizes the standard deviation of the distribution of disorder.

The internal variables a, α^{-1}, and S are used to capture the evolution of microstructural disorder. The rates of change of these three internal variables are given by

$$\dot{a} = (a - a_{eq}) f(\gamma^p)\omega, \tag{1.9}$$

$$\dot{\alpha}^{-1} = -\left[\alpha^{-1} - \alpha_{eq}^{-1}\right]\omega, \tag{1.10}$$

$$\dot{S} = \beta(\tau\dot{\gamma}^p) - S\omega, \tag{1.11}$$

where a_{eq} and α_{eq}^{-1} are steady-state values and $f(\gamma^p) = \exp\left(-\xi\exp(-\xi\gamma^p)\right)$ is used to reflect the fact that creation of sites with low activation energy occurs at the onset of inelastic strain. β represents the rate of storage of inelastic work, which falls off with increasing elastic strain, is given by $\beta = \beta_1\left[1+\beta_2\exp(-\beta_3\gamma^p)\right]$, where β_1, β_2, and β_3 are material parameters. The effective frequency, ω, is given by

$$\omega = \frac{\omega_0}{\dot{\gamma}_0}\dot{\gamma}^p, \tag{1.12}$$

where ω_0 is the fundamental attempt frequency.

The overall strain rate, $\dot{\gamma}^{total}$, consists of an elastic and an inelastic part, i.e.,

$$\dot{\gamma}^{total} = \frac{\dot{\tau}}{\mu} + \dot{\gamma}^{p}, \tag{1.13}$$

where μ is the shear modulus of the material.

The Hasan-Boyce model can be extended to include the temperature change due to adiabatic heat generation. Under the assumption that all the plastic work is converted to heat during an adiabatic process, the rate of temperature change is given by

$$\dot{T} = \frac{\dot{W}^{p}}{\rho c}, \tag{1.14}$$

where ρ is the mass density, c is the specific heat, and $\dot{W}^{p}$ is the rate of plastic work per unit volume. Since

$$\dot{W}^{p} = \tau \dot{\gamma}^{p}, \tag{1.15}$$

the rate of temperature change is

$$\dot{T} = \frac{\tau \dot{\gamma}^{p}}{\rho c}. \tag{1.16}$$

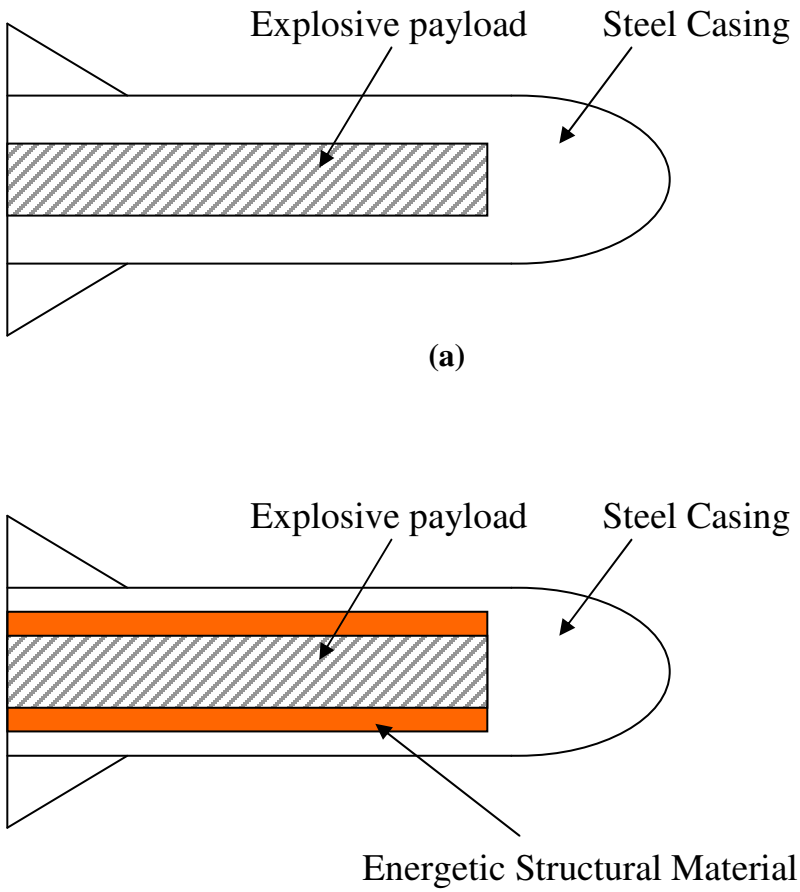

Figure 1: (a) Traditional missile and (b) a missile employing use of Energetic Structural Materials

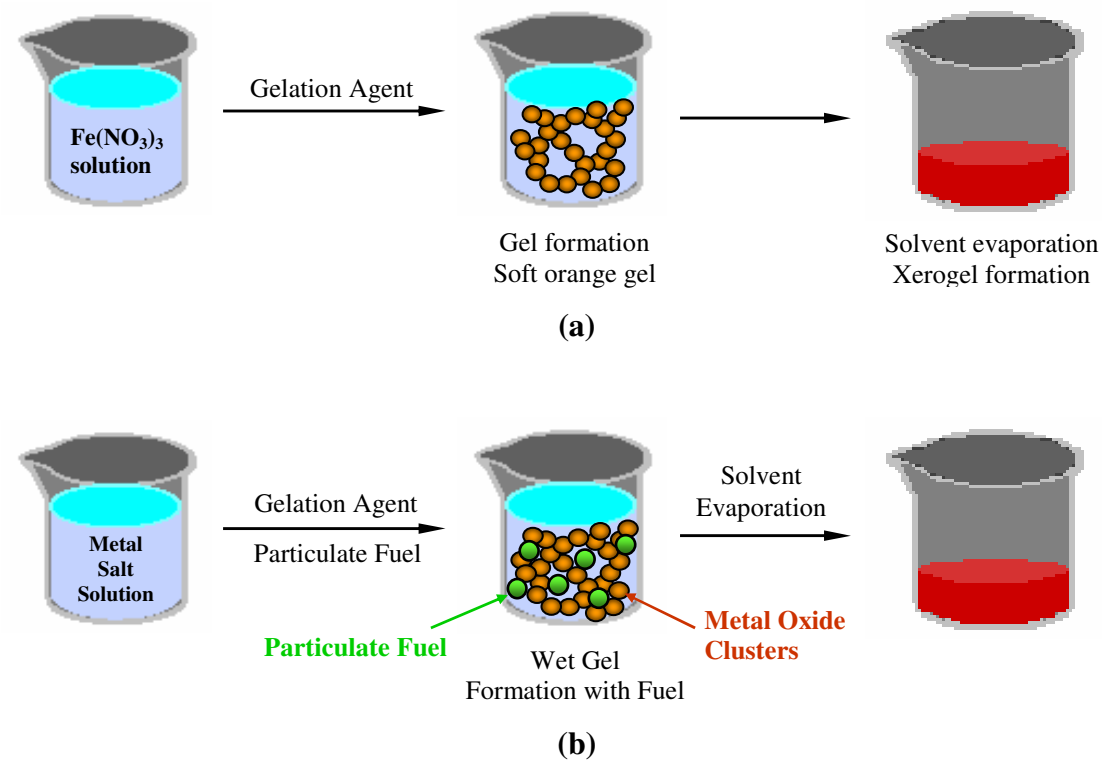

Figure 2: (a) Synthesis of sol-gel material and (b) addition of metal fuel particles to create an energetic sol-gel material

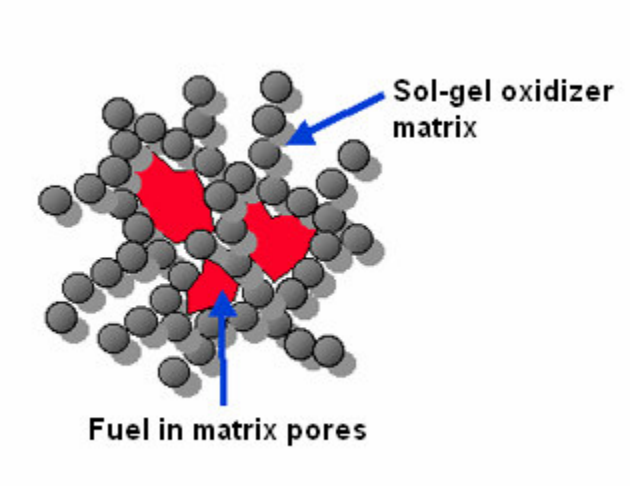

Figure 3: Enhanced interaction between matrix and fuel particles

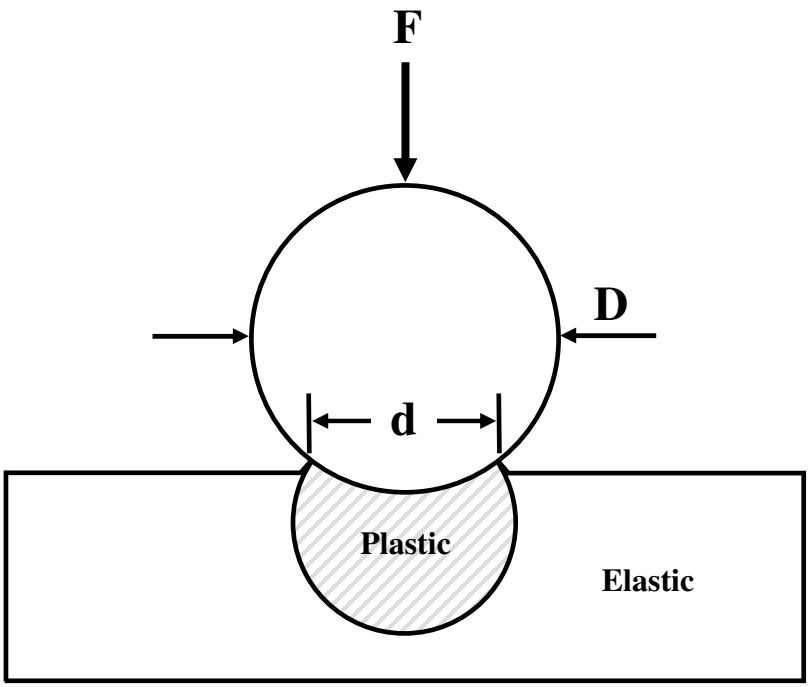

F – Test Force (N)
D – Diameter of indenter (mm)
d – Diameter of indentation (mm)

Figure 4: Schematic of Brinell hardness test

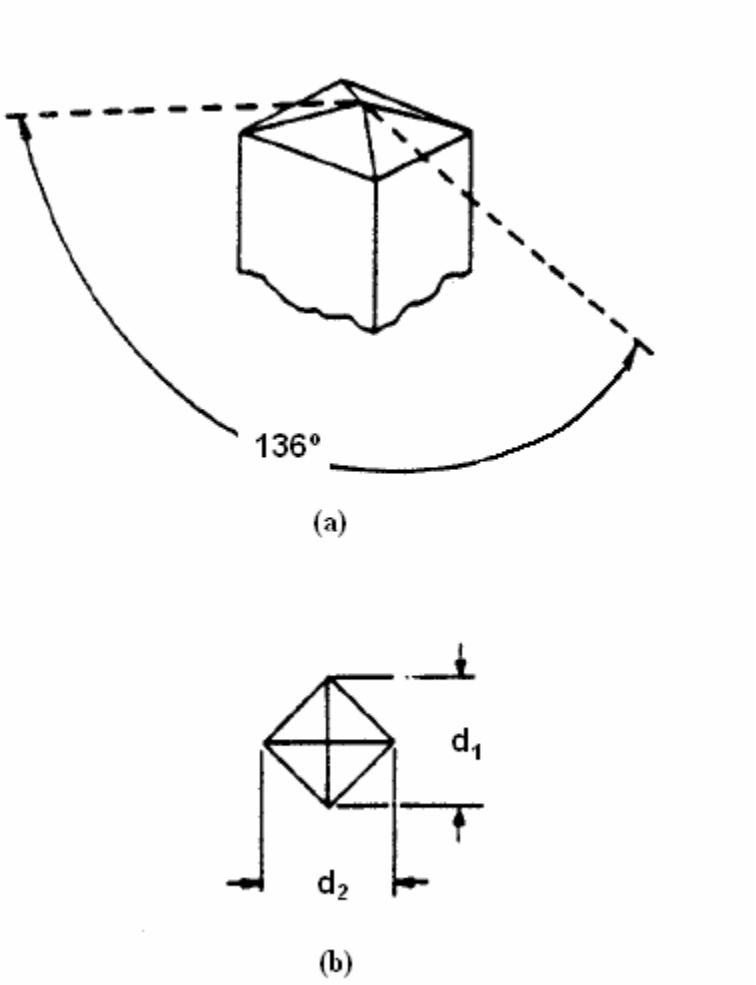

(ASTM E-384)

Figure 5: (a) Vickers indenter and (b) indentation geometry

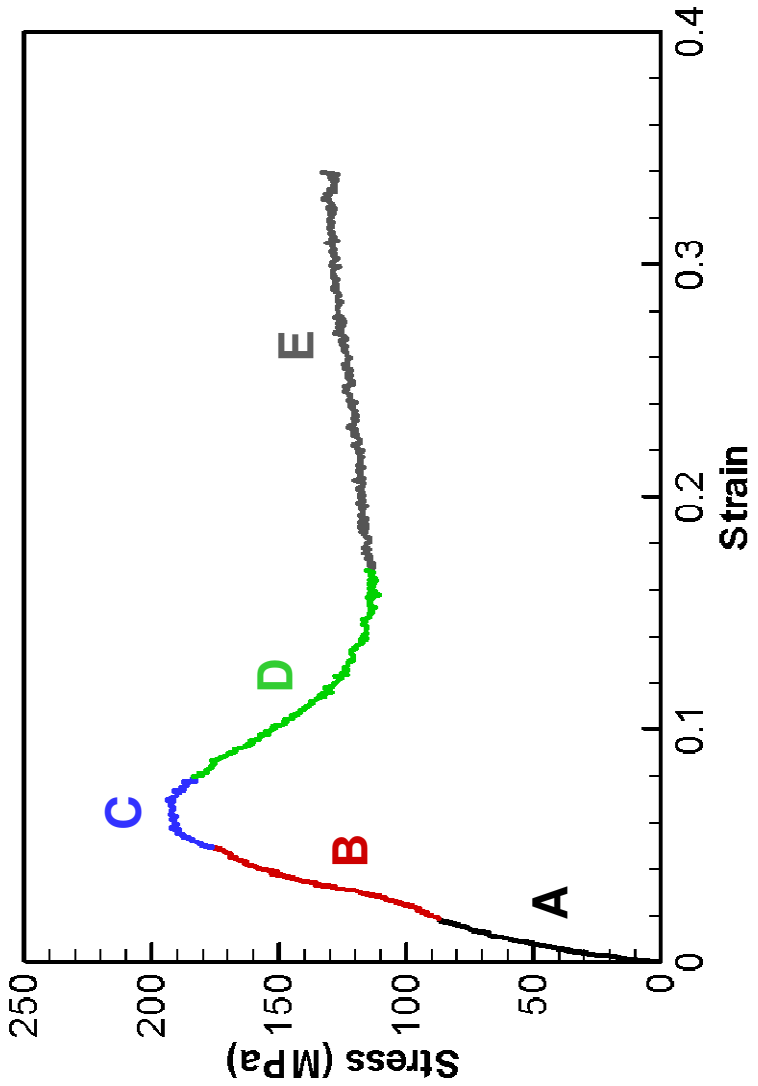

Figure 6: Viscoelastic behavior of EPON 826/Diethanolamine

CHAPTER II
EXPERIMENTAL APPARATUS AND PROCEDURES

2.1 Theory and Operation of the Split-Hopkinson Pressure Bar Apparatus

Ballistic missiles are required to perform under a wide range of conditions and withstand high impact forces. Because of this, one of the properties that is of the most interest is the dynamic compressive strength. The split-Hopkinson pressure bar (SHPB) apparatus can be used to investigate the strength of the MESMs in this study due to loading in the intermediate-strain rate regime (strain rates on the order of 10^2-10^4 s^{-1}).

2.1.1 The Split-Hopkinson Pressure Bar Apparatus

The SHPB apparatus is used to investigate the dynamic compressive behavior of the materials in this investigation. The amplitude and duration of the loading pulse can be varied in SHPB experiments by changing the velocity and length of the striker bar. The resulting time-resolved mechanical response of the specimen is captured by high-speed digital oscilloscopes.

A traditional SHPB apparatus that is used for dynamic compression experiments consists of a striker, incident, and transmission bar (Figure 7). A gas gun, whose pressure controls the velocity of the striker bar, is used to propel the striker bar towards the incident bar. Teflon o-rings on the striker bar minimize the friction of the bar as it travels down the barrel of the gas gun. The impact of the striker bar on the incident bar creates an elastic stress wave that propagates down the incident bar towards the specimen, which

is sandwiched between the incident bar and transmission bar. Upon reaching the incident bar/specimen interface, the wave partly reflects back into the incident bar as a tensile wave; the rest of the wave is transmitted into the specimen, and subsequently into the transmission bar.

A high-speed digital oscilloscope records the output from strain gauges mounted on the surface of the incident and transmission bars. The outputs from the strain gauges include the three stress waves of interest: the incident wave, reflected wave, and the transmitted wave. Figure 8 is a plot of the oscilloscope readout capturing the waves of interest, where compression is taken to be positive voltage. The incident wave is used to quantify the pulse duration, while the reflected wave is used to calculate the strain rate. The strain rate can be integrated to find the strain history of the specimen, while the transmitted wave is used to calculate the stress history in the specimen. The combination of the stress and strain history from the transmitted and reflected waves the stress-strain relationship can be determined. A more detailed discussion of the calculations used for analysis will follow.

The SHPB apparatus that is used in this study (Figure 9) utilizes bars that are constructed of VASCOMAX C-350 maraging steel that are heat treated to a hardness of 59 on the Rockwell C scale and have a common diameter of 19.05 mm. The approximate tensile yield strength of the bar material is 2.29 GPa. The length of the striker bar is 585 mm, the incident bar is 1575 mm, and the transmission bar is 1270 mm. A shock-absorbing stopper mechanism is placed at the free end of the transmission bar to prevent excessive horizontal movement of the bars.

The strain gauges used, supplied from Micro Measurements Group, Inc., are of model number WK-06-250BF-10C, with a gauge factor of 2.05 and a nominal resistance of 1000 Ω. At each location on the pressure bars, two strain gauges are mounted diametrically opposite each other to negate the effects of any bending that may occur in the bars. Each set of strain gauges is connected to its own Wheatstone bridge, which is individually powered by a Hewlett Packard E3617A DC power supply set to an excitation voltage of 30 V. The outputs from the Wheatstone bridges are recorded by a Nicolet Pro 42 high-speed digital oscilloscope, which is set to record data at a resolution of 500 nanoseconds.

The time duration of the loading pulse is typically twice the time it takes for a stress wave to travel the length of the striker bar,

$$t = \frac{2 \cdot L_0}{C_0}, \tag{2.1}$$

where t is the pulse duration, L_0 is the length of the striker bar, and C_0 is the longitudinal velocity in the pressure bars,

$$C_0 = \sqrt{\frac{E}{\rho}}, \tag{2.2}$$

where E and ρ are the Young's Modulus and density of the pressure bar material.

The magnitude of the stress wave is determined by the velocity of the striker bar,

$$\sigma = \frac{E \cdot v_0}{2 \cdot C_0}, \tag{2.3}$$

where v_0 is the velocity of the striker bar.

The strain rate that the specimen experiences can be calculated,

$$\frac{\partial \varepsilon}{\partial t} = \dot{\varepsilon} = \frac{v_1 - v_2}{L}, \tag{2.4}$$

where L is the length of the specimen and v_1 and v_2 are the velocities of the incident bar/specimen interface and the specimen/transmission bar interface, given by

$$v_1 = C_0 \left(\varepsilon_I - \varepsilon_R \right) \text{ and} \tag{2.5}$$

$$v_2 = C_0 \cdot \varepsilon_T, \tag{2.6}$$

where ε_I, ε_R, and ε_T are the strains measured in the strain gauges due to the incident, reflected, and transmitted waves respectively.

The strain measured in the incident and transmission bar strain gauges is a function of the output voltage V_O of the Wheatstone bridge, strain gauge factor and the excitation voltage,

$$\varepsilon = \frac{2 \cdot V_O}{f \cdot V_E}. \tag{2.7}$$

Combining the equations above give us the strain rate as a function of the strain gauge readings,

$$\frac{d\varepsilon}{dt} = \dot{\varepsilon} = \frac{C_0}{L} \left[\varepsilon_I(t) - \varepsilon_R(t) - \varepsilon_T(t) \right]. \tag{2.8}$$

The average stress in the specimen is given by:

$$\sigma(t) = \frac{P_1(t) + P_2(t)}{2 \cdot A_s}, \tag{2.9}$$

where P_1 and P_2 are the forces on the incident bar/specimen and specimen/transmission bar interfaces respectively and A_s is the cross-sectional area of the specimen. The forces at the incident bar/specimen and specimen/transmission bar interfaces are given by

$$P_1 = E \cdot A_b \left[\varepsilon_I(t) + \varepsilon_R(t) \right], \tag{2.10}$$

$$P_2 = E \cdot A_b \cdot \varepsilon_T(t), \tag{2.11}$$

where A_b is the cross-sectional area of the pressure bar.

Substituting the forces back into the average stress equation the stress based on the waves measured by the strain gauges is,

$$\sigma(t) = \frac{E}{2}\frac{A_b}{A_s}\left[\varepsilon_I(t) + \varepsilon_R(t) + \varepsilon_T(t)\right]. \tag{2.12}$$

During uniform deformation of the specimen, the stress at the incident bar/specimen and specimen/transmission bar interfaces will be equal, thus,

$$\varepsilon_I(t) + \varepsilon_R(t) = \varepsilon_T(t). \tag{2.13}$$

The strain rate and stress equations can be simplified to:

$$\frac{d\varepsilon}{dt} = \dot{\varepsilon} = \frac{-2 \cdot C_0}{L}\varepsilon_R(t), \tag{2.14}$$

$$\sigma(t) = E \cdot \frac{A_b}{A_s} \cdot \varepsilon_T(t). \tag{2.15}$$

2.1.2 High-Speed Digital Imaging

An IMACON 200 high-speed digital camera, supplied by DRS Data & Imaging Systems Inc., is used to capture images of the compression tests when imaging is required (Figure 10). The IMACON 200 is capable of recording 16 frames with a resolution of 1200x980 pixels per frame at a frame rate of up to 200 million frames/second. The IMACON 200 is triggered by the oscilloscope upon the incident wave reaching the strain gauges on the incident bar. The delay on the camera is 160 μs, the approximate time for the pressure wave to travel from the incident bar strain gauges to the incident bar/specimen interface.

A Photogenic PowerLight 2500DR flash is used to provide back lighting for the images. The PowerLight 2500DR is triggered by the IMACON 200, and a preflash of 100 μs is used to allow for the flash to ramp up to the usable light output prior to images being taken. A 105 mm f/2.8D AF Nikor lens is used to focus the IMACON 200 onto the specimen with backlighting provided by the PowerLight 2500DR.

2.1.3 Separation of Waves for Extended Analysis

The traditional time period in which the mechanical response of a material is investigated when using the SHPB apparatus is restricted to the time duration of the loading pulse. Analysis beyond this duration may become complicated due to the interference caused by waves reflecting off the free end of the bars and subsequently passing through the strain gauges (Figure 11).

Lundberg and Henchoz (1977) developed a set of equations that allowed for extended analysis based on a SHPB apparatus with two sets of strain gauges on each bar. The ability to measure the wave propagation at two points on each bar, known as the two-point method, allows the extended histories of strain, normal force, and particle velocity to be examined. However, traditional SHPB apparatus, such as the one used in this study, tend to have only one set of strain gauges on the incident bar and one set of gauges on the transmission bar, requiring significant modifications be made to allow for two-point measurements.

Park and Zhou (1999) developed a method for extending the time period for which data can be extracted using only one set of strain gauges and the known end conditions of the pressure bars. This method allows for analysis of data recorded by a

SHPB apparatus that uses only one set of properly placed gauges per pressure bar, such as the one used in this study. The assumed known conditions for a suitable SHPB apparatus (Figure 9) are:

1. The impact end of the incident bar is traction free except when it is in contact with the striker bar
2. The right end of the transmission bar is traction free until it makes contact with the stopper mechanism

The motion of a wave through a slender cylindrical rod can be described by the one-dimensional wave equation,

$$\frac{\partial^2 u}{\partial x^2} = \frac{1}{C_0^2}\frac{\partial^2 u}{\partial t^2}. \tag{2.16}$$

The general solution to this equation is

$$u(x,t) = u_1\left(t - \frac{x}{C_0}\right) + u_2\left(t + \frac{x}{C_0}\right), \tag{2.17}$$

where the two terms represent the motion of the wave forms in the positive and negative x-direction. The longitudinal strain equation is expressed as

$$\varepsilon(x,t) = \varepsilon_1\left(t - \frac{x}{C_0}\right) + \varepsilon_2\left(t + \frac{x}{C_0}\right), \tag{2.18}$$

where $\varepsilon(x,t) = \partial u(x,t)/\partial x$. The particle velocity may be written as

$$v(x,t) = C_0\left[-\varepsilon_1\left(t - \frac{x}{C_0}\right) + \varepsilon_2\left(t + \frac{x}{C_0}\right)\right], \tag{2.19}$$

where $v(x,t) = \partial u(x,t)/\partial t$.

Figure 12 illustrates the Lagrangian diagram of wave propagation in cylindrical bars (Park and Zhou 1999). A set of strain gauges is mounted at a distance a from the impact end of the incident bar. Substitution of $x = a$ into Equation (2.18) gives

$$\varepsilon_A(t) = \varepsilon_1(t - t_a) + \varepsilon_2(t + t_a), \tag{2.20}$$

where $\varepsilon_A(t) = \varepsilon(a,t)$ and $t_a = a / C_0$.

Equations for the separation of the waves within the incident bar will be investigated first. The duration of impact between the striker and incident bars is $2L_0 / C_0$, where L_0 is the length of the striker bar. In order for the first reflected wave and the incident wave to be recorded without interference, it is required that $L_0 < (L - a)$.

For the time period $t < T - t_a$, the reflected wave has yet to reach the strain gauge at $x = a$, thus,

$$\varepsilon_2(t + t_a) = 0. \tag{2.21}$$

Combining Equations (2.20) and (2.21), the longitudinal strain can be represented by

$$\varepsilon_A(t) = \varepsilon_1(t - t_a). \tag{2.22}$$

For $T - t_a < t < T + t_a$, the incident wave fully passes through the strain gauge, thus,

$$\varepsilon_1(t - t_a) = 0. \tag{2.23}$$

Combining Equations (2.20) and (2.23), the longitudinal strain becomes

$$\varepsilon_A(t) = \varepsilon_2(t + t_a). \tag{2.24}$$

For $t > T + t_a$, both ε_1 and ε_2 may be non-zero. The known end condition of a traction free boundary at $x = 0$ can be used, thus,

$$\varepsilon_1(t) + \varepsilon_2(t) = 0. \tag{2.25}$$

Combining Equations (2.20) and (2.25), the longitudinal strain becomes

$$\varepsilon_A(t) = -\varepsilon_2(t - t_a) + \varepsilon_2(t + t_a). \tag{2.26}$$

Combining Equations (2.21) - (2.26) and changing variables such that $(t - t_a) \to \xi$ and $(t + t_a) \to \eta$, the strain functions ε_1 and ε_2 can be represented by the measured strain history ε_A as:

$$\varepsilon_1(\xi) = \begin{cases} \varepsilon_A(\xi + t_a), & \xi < T - t_a \\ 0, & T - 2t_a < \xi < T \\ -\varepsilon_2(\xi) & \xi > T \end{cases}, \tag{2.27}$$

and

$$\varepsilon_2(\eta) = \begin{cases} 0, & \eta < T \\ \varepsilon_A(\eta - t_a), & T < \eta < T + 2t_a \\ \varepsilon_2(\eta - 2t_a) + \varepsilon_A(\eta - t_a) & \eta > T + 2t_a \end{cases}. \tag{2.28}$$

Equations for the separation of waves within the transmission bar will now be investigated. The values of *L* and *a* for the transmission bar may be different than those that were used on the incident bar. While investigating the transmission bar, $t = 0$ occurs when the transmitted wave enters the specimen/transmission bar interface.

For $t < T - t_a$, the conditions are the same as in the incident bar, and equations (2.21) and (2.22) are valid.

For $t > T - t_a$, $\varepsilon_1(t - t_a)$ and $\varepsilon_2(t + t_a)$ may be non-zero. The traction free boundary at $x = L$ can be used, thus,

$$\varepsilon_1\left(t - \frac{L}{C_0}\right) + \varepsilon_2\left(t + \frac{L}{C_0}\right) = 0. \tag{2.29}$$

Combining Equations (2.20) and (2.29),

$$\varepsilon_1(t-t_a)=\varepsilon\left(t-T+t_a\right)+\varepsilon_A(t). \tag{2.30}$$

Combining Equations (2.21), (2.22), (2.29), and (2.30), and changing variables such that $(t-t_a)\rightarrow\xi$ and $(t+t_a)\rightarrow\eta$, the strain functions ε_1 and ε_2 can be represented by the measured strain history ε_A as:

$$\varepsilon_1(\xi)=\begin{cases}\varepsilon_A(\xi+t_a), & \xi<T-2t_a\\ \varepsilon_1(\xi+2t_a-T)+\varepsilon_A(\xi+t_a), & \xi>T-2t_a\end{cases}, \tag{2.31}$$

and

$$\varepsilon_2(\eta)=\begin{cases}0, & \eta<T\\ -\varepsilon_1(\eta-T), & \eta>T\end{cases}. \tag{2.32}$$

The extended analysis of the stress-strain relationship using the one-point method allows for investigation into the unloading characteristics of the specimens tested using the apparatus in this study.

2.1.4 Soft Recovery Method with the Split-Hopkinson Pressure Bar

Dynamic compression tests conducted on the SHPB apparatus generates loading of the specimen with defined loading pulse, but due to reflection of the waves off the free ends of the pressure bars, reloading of the specimen will occur. Nemat-Nasser et al. (1991) presented a technique of stress reversal that allowed for the soft recovery of compressive specimens. Changes to the standard SHPB apparatus are:

1. Incident bar with a threaded hole on impact end
2. Threaded flange
3. Short striker bar
4. Incident tube
5. Reaction mass

Figure 13 illustrates the setup of components for the stress reversal technique. The flange is located on the impact end of the incident bar, followed by the incident tube and the reaction mass. The incident tube has the same cross-sectional area and length as the striker bar and is made of the same material as all the pressure bars. The cross-sectional area of the flange is twice that of the striker and incident bars, and it is the same diameter as the outer diameter of the incident tube. The incident tube makes contact with the flange on one side and the reaction mass on the other. The reaction mass is a large steel disc with a hole in the center to allow for the incident bar to pass through.

The impact of the striker bar into the flange creates a common compressive stress wave in both the incident tube and bar. The compressive wave travels down the incident tube and upon reaching the incident tube/reaction mass interface, it reflects within the tube as a compressive wave. The identical lengths of the striker bar and incident tube allow for the proper timing of the reflected compressive wave in the incident tube reaching the flange just as the striker bar has completed imparting the incident wave. The compressive wave in the incident tube serves two functions upon reaching the flange:

1. Creation of a tensile wave in the incident bar closely following the loading compressive wave (Figure 14)
2. Impact between the flange and striker bar

The compressive incident wave imparts loading upon the specimen for the full time duration, but the trailing tensile wave reverses the force on the incident bar/specimen interface, effectively limiting the loading to one defined loading pulse. The contact between the flange and striker bar sends the striker bar away from the incident bar, preventing subsequent accidental loading.

In this study, the use of an 1880 mm long incident bar with a threaded hole on the impact end is used for the attachment of the flange. A shortened striker bar of length 184 mm and 19.05 mm diameter is used. The incident tube has an outer diameter of 27.0 mm and a length of 184 mm as well. The time duration of loading for the soft recovery experiments is 80 μs.

2.1.5 Vickers Microindentation Hardness

Vickers microindentation hardness tests are carried out on Al + Fe_2O_3 + Epoxy specimens using a Leco MHT Series 200 apparatus. The 50x objective lens is used to bring the specimen into focus and examine the indentation. A dwell time of 15s is used with a force of 0.050 kgf to produce the indentation. Measurements of the diagonal distances of the indent (Figure 15) are made on the digital images of the indent on the computer, and hardness values are automatically calculated by the program.

2.1.6 Dynamic Indentation Using the SHPB Apparatus

Dynamic Brinell hardness tests are carried out on the SHPB apparatus using a 3.175 mm steel ball indenter (Figure 16). An aluminum fixture is used to hold the steel ball indenter against the end of the incident bar such that only the indenter makes contact with the bar, preventing the loading wave to transfer into the fixture and not the specimen. The transmitted wave from the SHPB is used to calculate the application of load over the time duration of the experiment. The soft recovery method is used to ensure that only one loading pulse is applied to the specimen. The methods described in the ASTM E-10 Standard for Brinell hardness testing are followed as closely as possible.

Post-indentation diameter measurements of a polymeric material may be inaccurate due to the recovery of the indented region caused by to the rate-dependent behavior of the polymer. Because of this, the IMACON 200 high-speed digital camera is used to measure the indentation diameter throughout the experiment (Figure 17). Diameter measurements are recorded every 25 μs during each indentation with the camera, however, it can not be guaranteed that the maximum indentation diameter is captured in one of the frames. To resolve this issue, the known diameter measurements and their corresponding force values are used to calculate the hardness of the materials in this study.

2.1.7 Experimental Procedure

A thin layer of silicone lubricant is spread onto the loading ends of both the incident and transmission bars prior to the insertion of the specimen. The lubricant reduces friction on the specimen/bar interface, limiting any shear or barreling effects. The impact end of the incident bar is moved to within 20 mm from the right edge of the gas gun barrel to ensure flush contact between the striker and incident bars upon contact.

The strain gauges are connected to the powered Wheatstone bridges and then to the digital oscilloscope. The oscilloscope is set up to be triggered from the strain gauges on the incident bar with at 20% pretrigger to ensure all data is collected. The sweep length of the oscilloscope is set to 4000 data points at a resolution of 500 nanoseconds, resulting in total time duration of 2 milliseconds.

The gas gun is pressurized with compressed air to the desired pressure. Upon firing the gun, the striker bar is sent down the barrel of the gun, impacts the incident bar,

and the compressive stress wave is created. The wave propagates through the incident bar, and upon reaching the strain gauges, the oscilloscope is triggered, recording the data for the time duration. Data from the oscilloscope is analyzed to calculate the time-resolved loading history of the specimen.

2.2 Material Synthesis and Preparation

2.2.1 Al + Fe_2O_3 + Epoxy

The primary material of focus in this study is the thermite mixture of Al + Fe_2O_3 suspended in an epoxy binder matrix. The epoxy used to form the matrix is comprised of bisphenol A (Shell Chemicals, Epon™ 826) as the resin and Diethanolamine (DEA) as the hardener. Aluminum powder with an approximate particle size of 1.0 μm (Figure 18) and Fe_2O_3 powder with an approximate particle size of 0.1 μm (Figure 19) are used with the epoxy to create a viable energetic material. This method provides a safe, easy, and convenient way of manufacturing the energetic material in our own facilities at The Georgia Institute of Technology.

The constituents of the Al + Fe_2O_3 + Epoxy materials are measured according to a previously determined ratio by weight. For the mass of the epoxy, Epon 826 comprises 92.31% and DEA comprises 7.69%. For the mass of the solids, Al powder comprises of 25.26% and Fe_2O_3 comprises of 74.74%. The volume and volume fraction values for the constituents used in the various Al + Fe_2O_3 + Epoxy mixtures used in this study are listed in Table 1. A detailed description of the synthesis procedure of Al + Fe_2O_3 + Epoxy material can be found in Appendix A.

The proper amounts of EPON 826 resin, aluminum powder, Fe_2O_3 powder, and DEA hardener are mixed, degassed, and poured into aluminum molds that are lined with mold release. The molds are placed in an oven to cure at approximately 100ºC for 24 hours to cure. This synthesis method allows for the creation of Al + Fe_2O_3 + Epoxy materials with varying levels of binder to allow for investigation into the change in the constitutive behavior across this range (Figure 20).

2.2.2 Synthesis Issues of Al + Fe_2O_3 + Epoxy

Typical applications for the commercially available epoxy EPON 826 include fiber reinforced composites, electrical casings, construction, electrical, and aerospace adhesives. The addition of a large volume fraction of particles on the micron scale is not a conventional application, and because of this, several synthesis issues arise:

1. Porosity in cured material
2. Increased viscosity at low epoxy levels
3. Incomplete curing of cast materials

The first synthesis issue was the high levels of porosity found in preliminary specimens. The porosity, although sometimes not visible on the surface, was apparent due to the varying density values of specimens cut from the same rod; occasionally, specimens contained visible pores (Figure 21). The cause of this problem is the method of degassing the epoxy prior to curing. Originally, the epoxy mixture was poured into the aluminum molds, which were then degassed under vacuum in a desiccator. The small cross-sectional area of the molds (~285 mm^2) can restrict the movement of the air bubbles towards the top of the mold. An attempt to reproduce consistent porosity levels

within specimens was unsuccessful, however, degassing the epoxy mixture in a larger container (with a cross-sectional area of ~7850 mm^2), and then pouring the mixture into the aluminum molds solves this issue and allows for the creation of uniformly dense specimens.

The second synthesis issue encountered was extremely high viscosity in mixtures whose binder content was decreased below 40%. Incomplete wetting and mixing of powders introduced large agglomerates of Al and Fe_2O_3 within the solids. For mixtures with high powder content (>29.2% solids), the addition of powders in portions, as opposed to at one time, improved the mixing for the initial portions, but difficulty in mixing the later portions was still present. Heating of the epoxy/powder mixture alleviates this by decreasing the viscosity of the mixture, resulting in improved mixing of the final portion of the powders.

To further aid in decreasing the viscosity during synthesis, a solvent was added to the mixture. Toluene is chosen due to its low boiling point and non-reactive nature with the constituents used, allowing for it to decrease the viscosity during mixing and degassing, while evaporating during the curing cycle. The Toluene is added as 5% of the weight of the solid powders.

The curing procedure was modified due to the addition of the powders to the epoxy matrix. The recommended curing time of 12 hours (at ~100ºC) is doubled to guarantee that the epoxy is given enough time to settle around the solids and the Toluene may evaporate out. To allow for the Toluene to fully evaporate out of the material, the molds are opened up after the 24 hour curing cycle and placed back into the oven for another 24 hours at ~100ºC. The material is placed under a fume hood for an additional

5-6 days to allow for full polymerization of the epoxy to take place prior to machining the material.

2.2.3 Al + Fe_2O_3 + Epoxy Specimen Design

The cast Al + Fe_2O_3 + Epoxy materials are machined using standard lathe and cutting saw machines. The diameter of the cast rods is reduced using a lathe in The Georgia Institute of Technology Mechanical Engineering Machine Shop. A cutting speed of 540 rpm is used along with a final feed rate of 0.036 in/rotation to achieve a smooth surface finish. Cylindrical specimens are cut from these rods using a Buehler ISOMET 4000 Linear Precision Saw with a diamond-tipped cutting blade. The ends of the cylindrical specimens are polished such that they are perpendicular to the sides and parallel to each other. The specimens used in this study have a diameter of 6.35 mm and a length of 6.35 mm (Figure 22).

The effect of porosity is of interest to study the mechanical response of the material with respect to the void content. A controlled porosity method is used to allow for a controlled level of porosity to be created within fully dense materials. The use of a 0.64 mm diameter drill bit to drill holes within specimens allows for the creation of porosity at defined volume fractions (Figure 23). Two configurations are used to create void contents of ~3% and ~6% (Figure 24). Configuration #1 is an array of three holes drilled down the spine of the cylinder. Configuration #2 consists of two similar arrays, the second orientated 90º to the first. The controlled porosity method allows for the introduction of voids into specimens, however, it does not simulate the size and distribution of natural porosity.

2.2.4 Ni-Al

The Ni-Al material that is used in this study was created using the shock compaction method. The compaction layout is arranged such that the powders to be compacted are placed in the inner seamless steel cylinder (50.8 mm inner diameter, 57.0 mm outer diameter, 152.4 mm in length), which is surrounded by an outer steel cylinder (68.6 mm inner diameter, 76.2 mm outer diameter, 165.1 mm in length). A small gap (~11.6 mm) is maintained between the two concentrically placed steel cylinders. ANFO or ANFOIL explosives are packed around the second cylinder, but within a third, large cylinder that is made of PVC (Figure 25).

The product of this shock compaction is a cylinder 80 mm in diameter and 152 mm in length (Figure 26). The outer steel ring is removed on a lathe, and the resulting cylinder is cut into discs of various thicknesses using a diamond-tipped cutting saw. The faces of the discs are lapped to remove machining marks and to create parallel faces. An electrical discharge machining (EDM) apparatus is used to cut cylindrical specimens of different diameters out of the discs.

In this study, Ni-Al cylindrical specimens with a diameter of 5.36 mm and a thickness of 2.75 mm are subjected to various loading rates ranging from 1400-1800 s^{-1} using the SHPB apparatus. The soft recovery method is employed to subject the specimens to a single loading pulse and prevent fracture of the material.

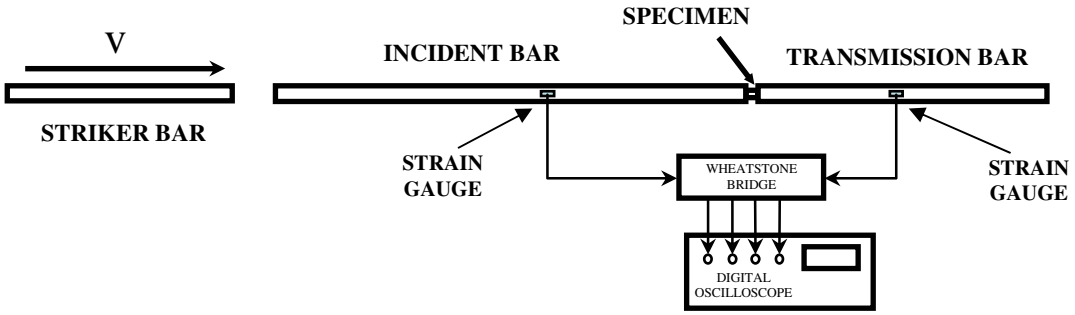

Figure 7: Schematic of split-Hopkinson pressure bar apparatus

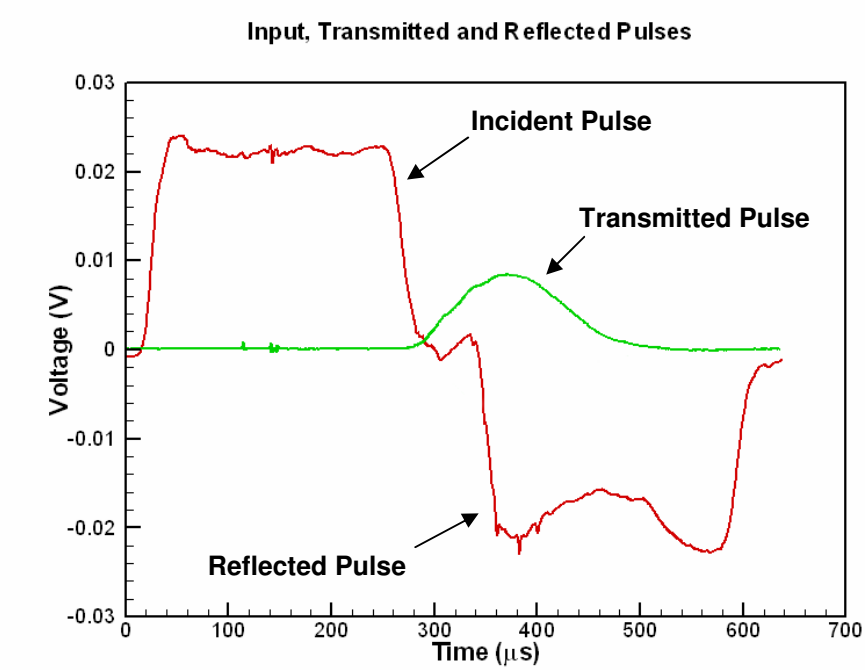

Figure 8: SHPB compression experiment digital oscilloscope readout

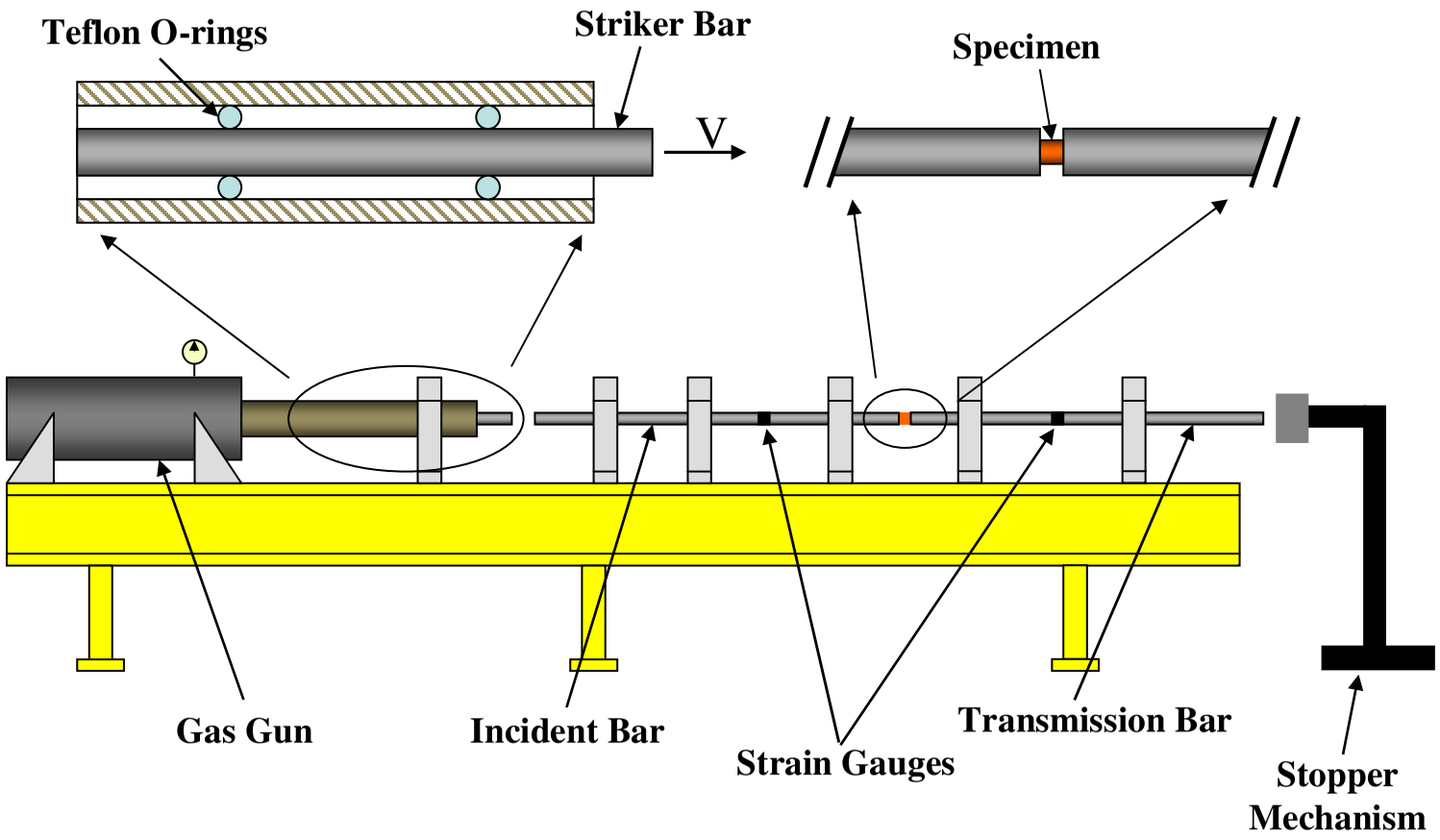

Figure 9: An illustration of the split-Hopkinson pressure bar apparatus at The Georgia Institute of Technology

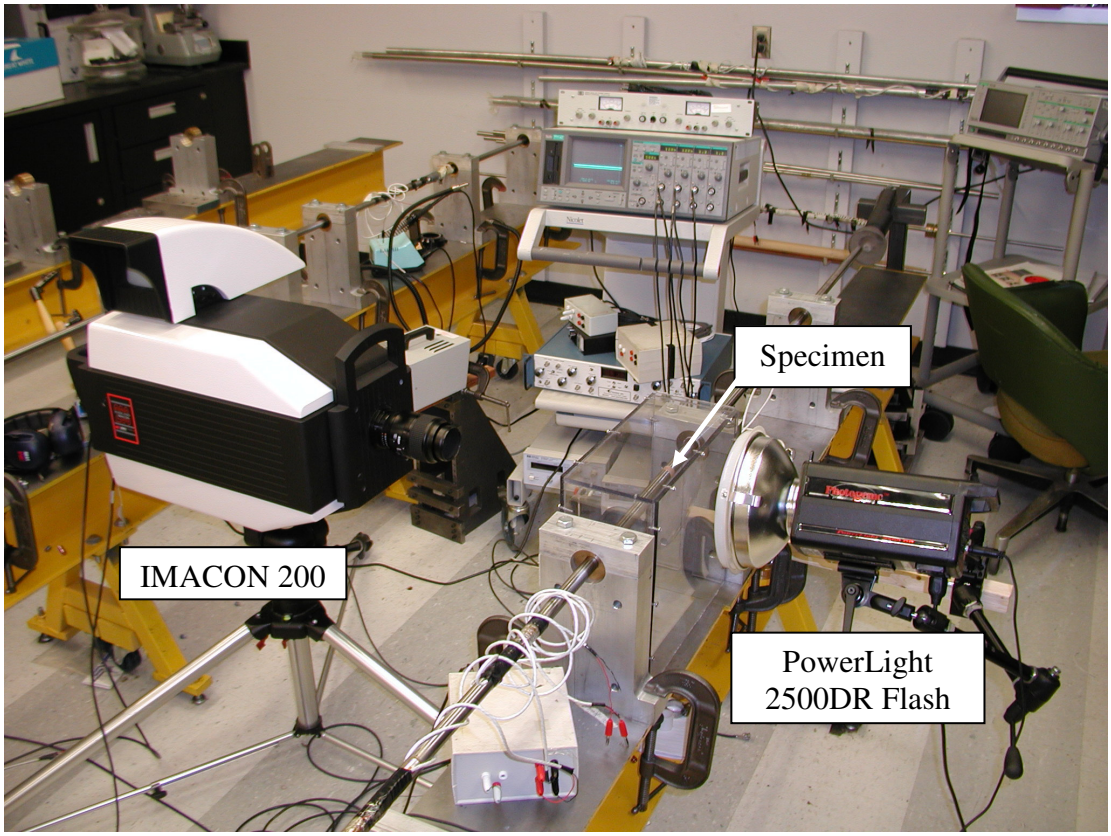

Figure 10: The split-Hopkinson pressure bar apparatus at The Georgia Institute of Technology

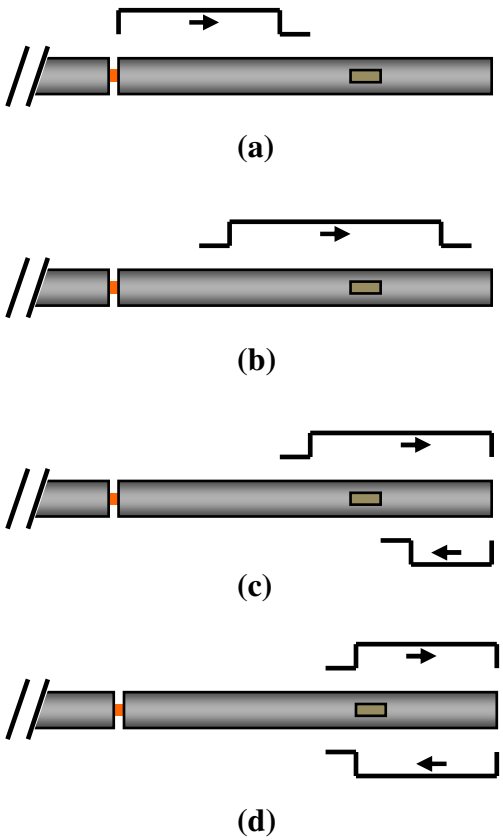

Figure 11: Schematic representation of pressure wave (a) entering transmission bar, (b) passing through strain gauge, (c) reflecting off free end of bar, and (d) interference between transmission wave and reflected wave

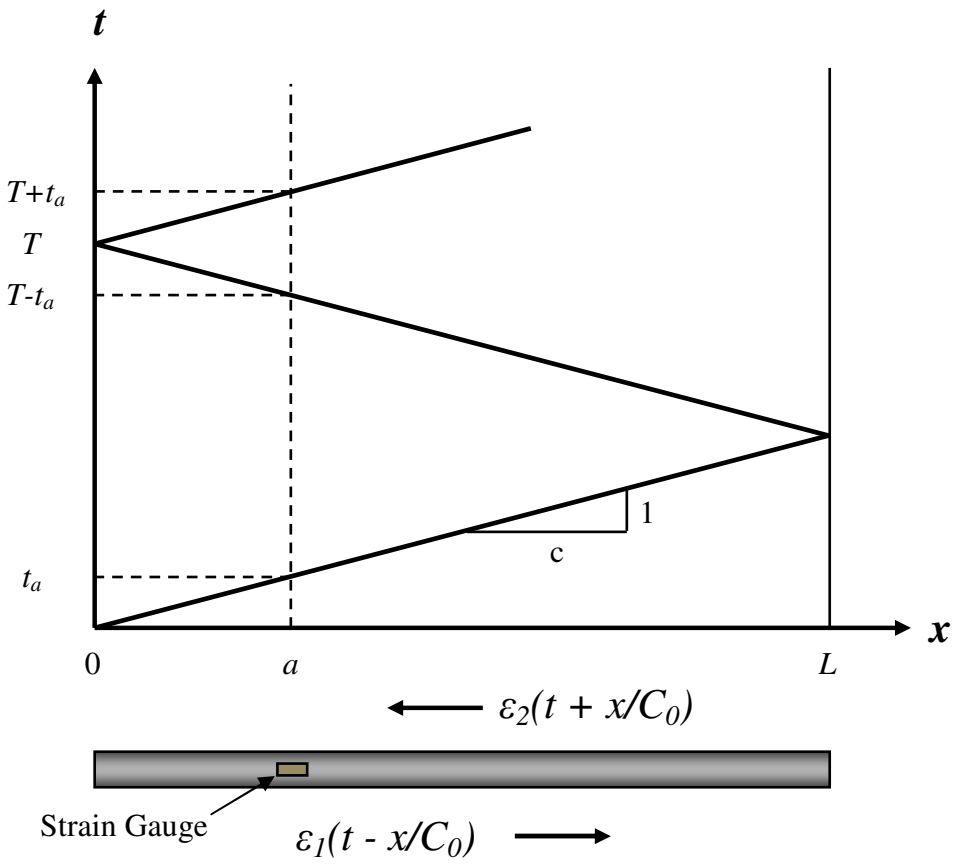

Figure 12: Lagrangian diagram of longitudinal waves in cylindrical bars (Park and Zhou 1999)

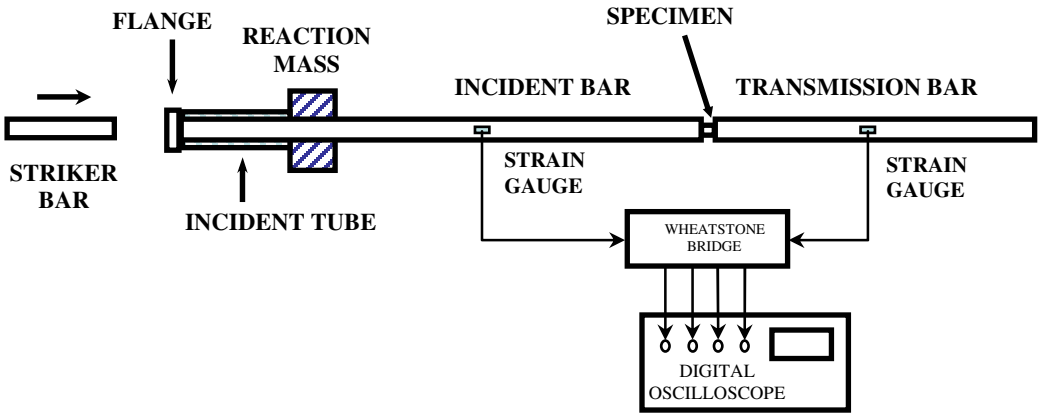

Figure 13: Schematic of SHPB apparatus modified for the Soft-Recovery Method

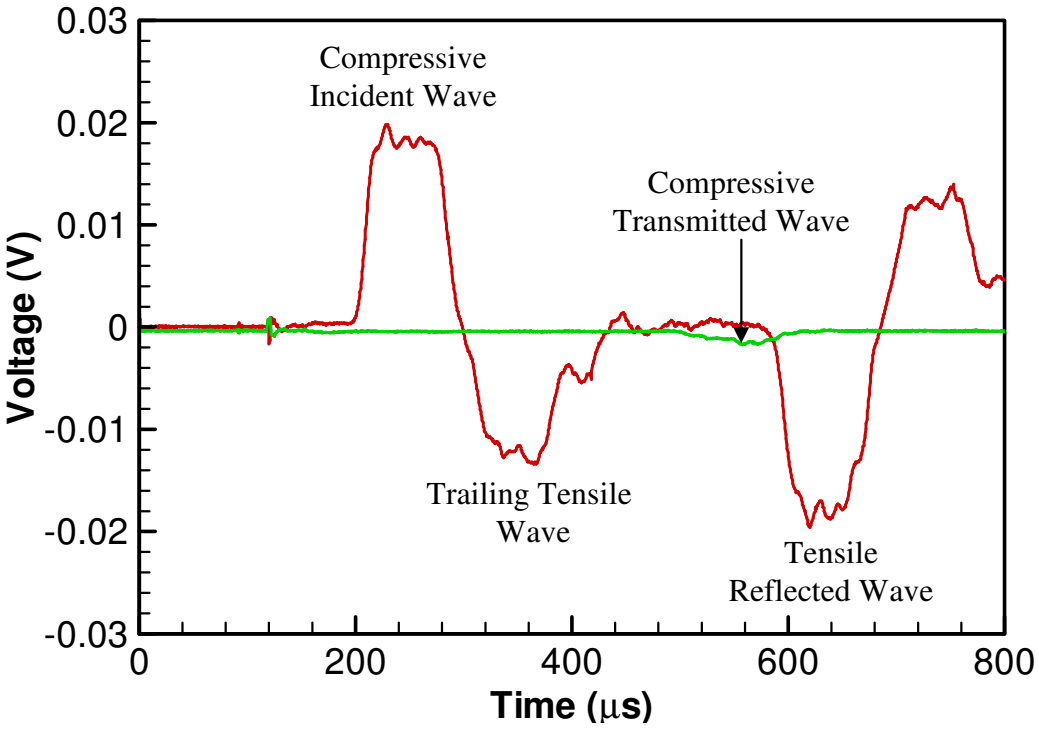

Figure 14: Oscilloscope readout from the SHPB apparatus using the Soft-Recovery Method

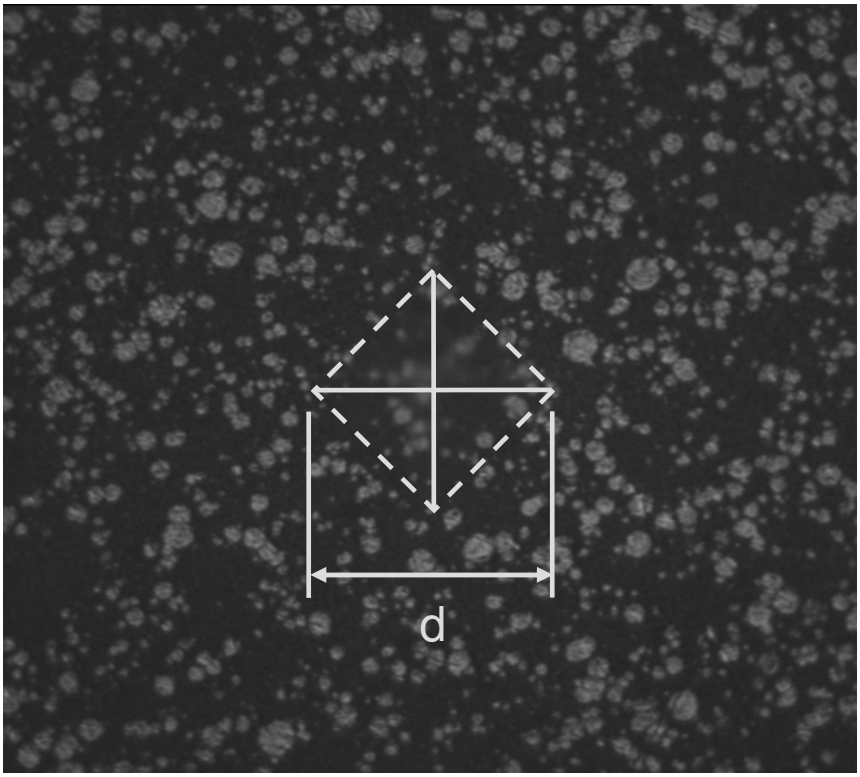

Figure 15: Geometry of Vickers microindentation hardness indent

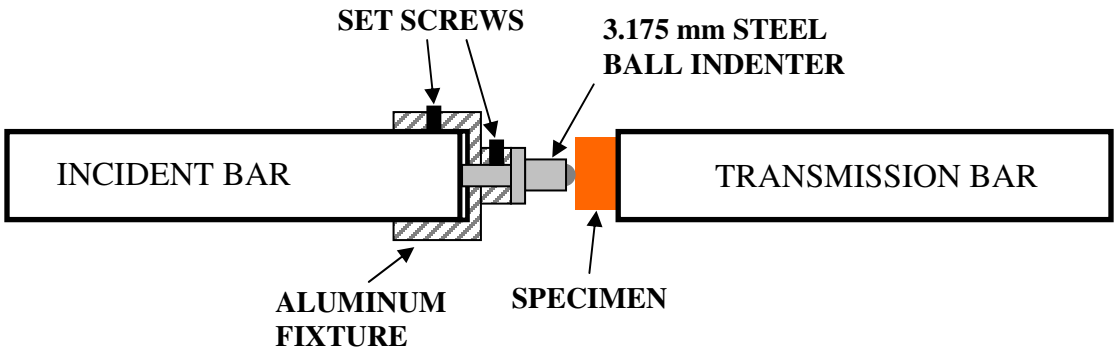

Figure 16: Schematic of dynamic indentation using the SHPB apparatus

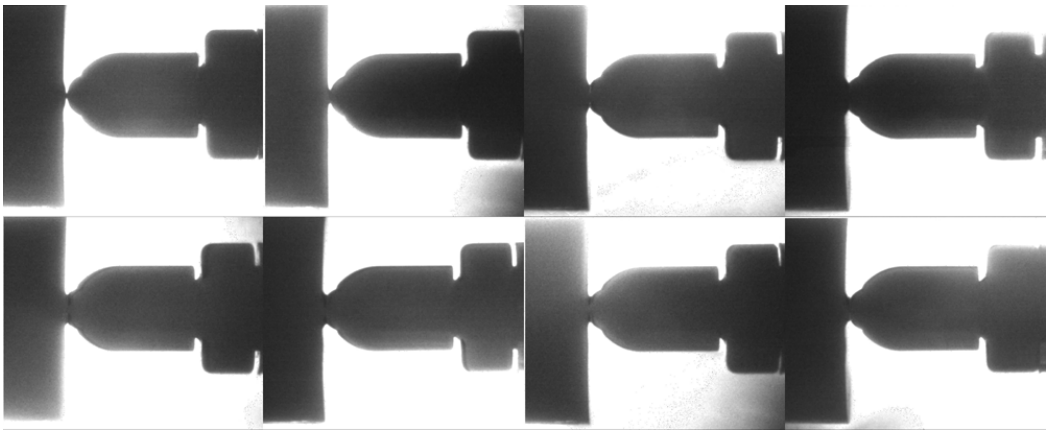

Figure 17: IMACON 200 images of dynamic Brinell hardness experiment

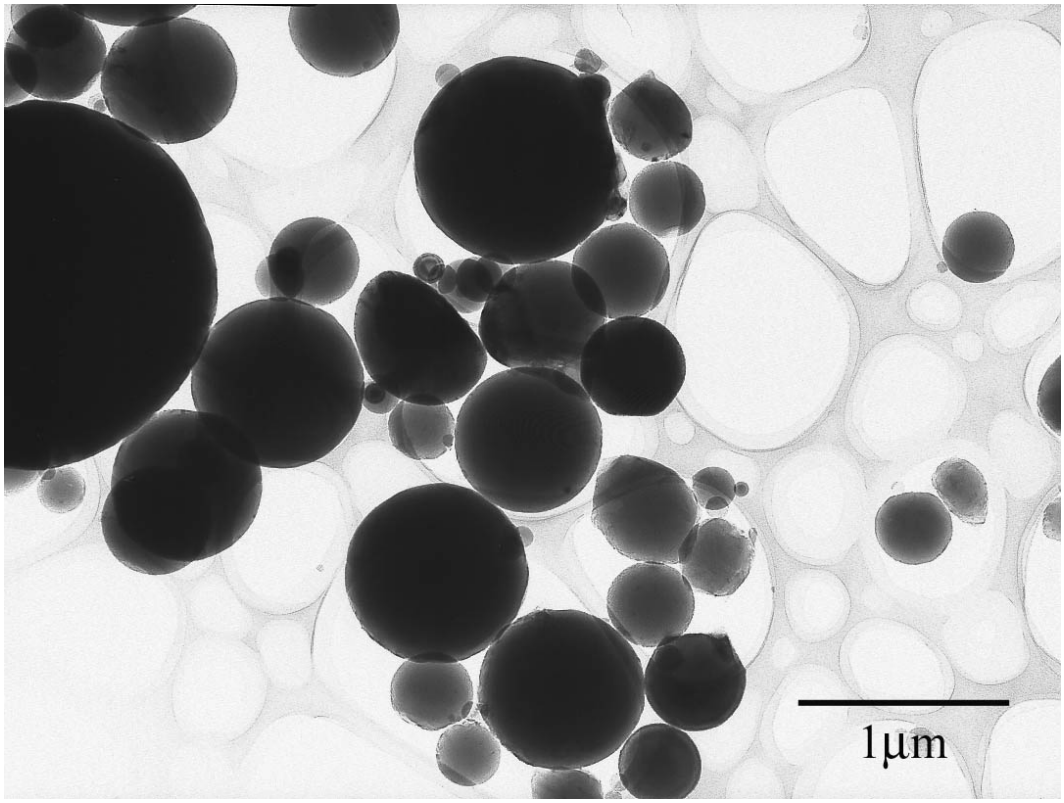

Figure 18: Transmission Electron Microscope image of aluminum particles

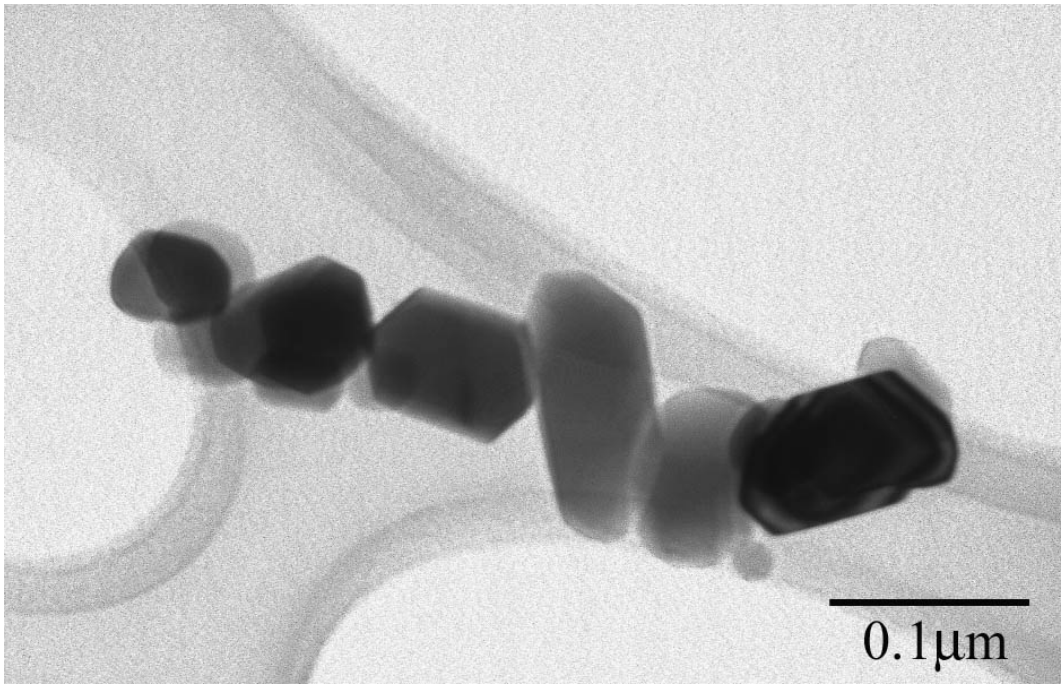

Figure 19: Transmission Electron Microscope image of Fe_2O_3 particles

Table 1: Volume and volume fraction of Al + Fe_2O_3 + Epoxy mixtures

	Volume (g/cm^3)			Volume Fraction		
Epoxy Content (%)	Epoxy	Al	Fe_2O_3	Epoxy	Al	Fe_2O_3
100	171.82	0	0	1	0	0
50	75.17	8.17	12.49	0.785	0.085	0.130
40	60.14	9.80	14.99	0.708	0.115	0.177
30	64.43	16.34	24.98	0.609	0.155	0.236
22	128.94	49.13	75.01	0.510	0.194	0.296

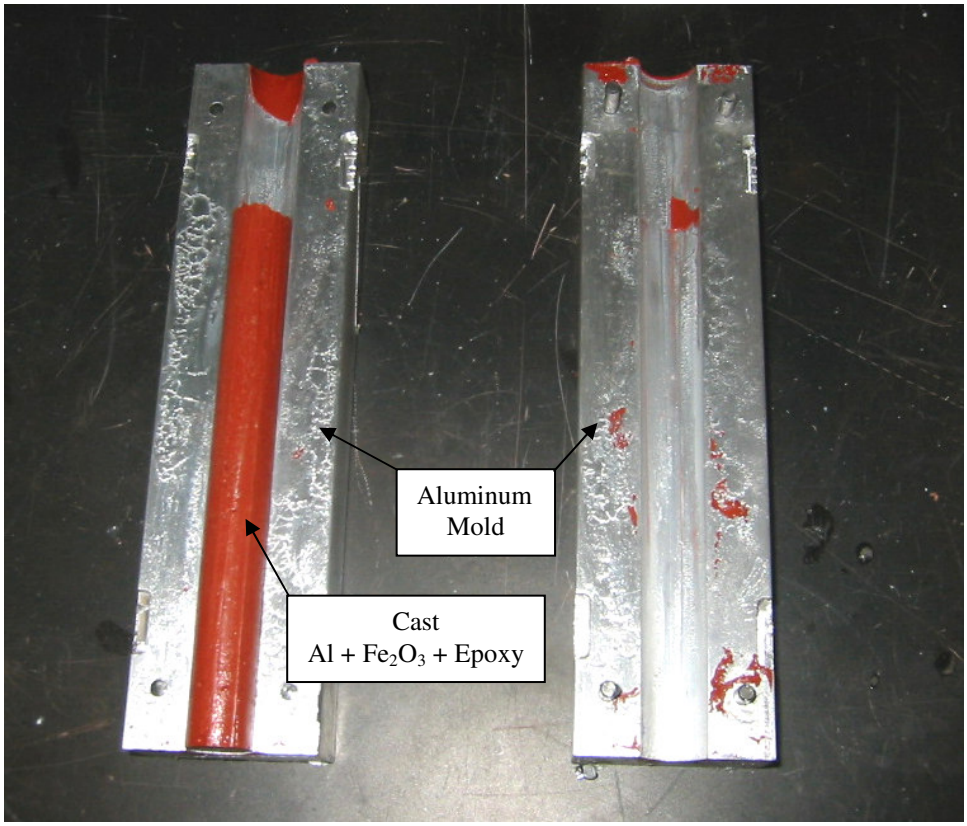

Figure 20: Al + Fe_2O_3 + Epoxy cast at The Georgia Institute of Technology

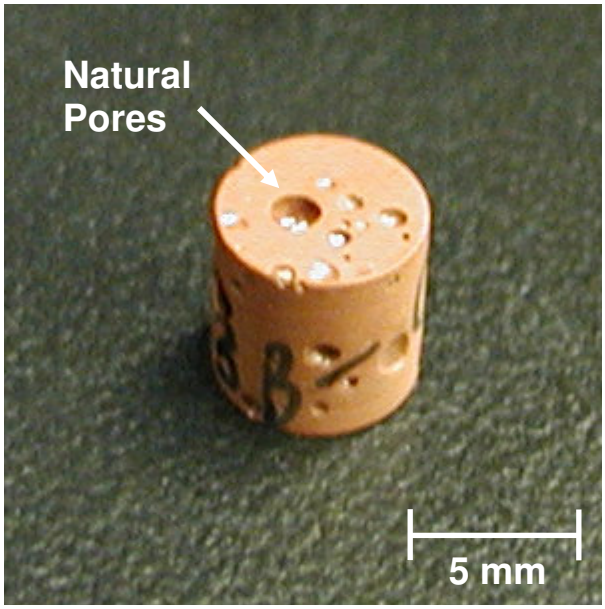

Figure 21: Naturally porous Al + Fe_2O_3 + Epoxy specimen

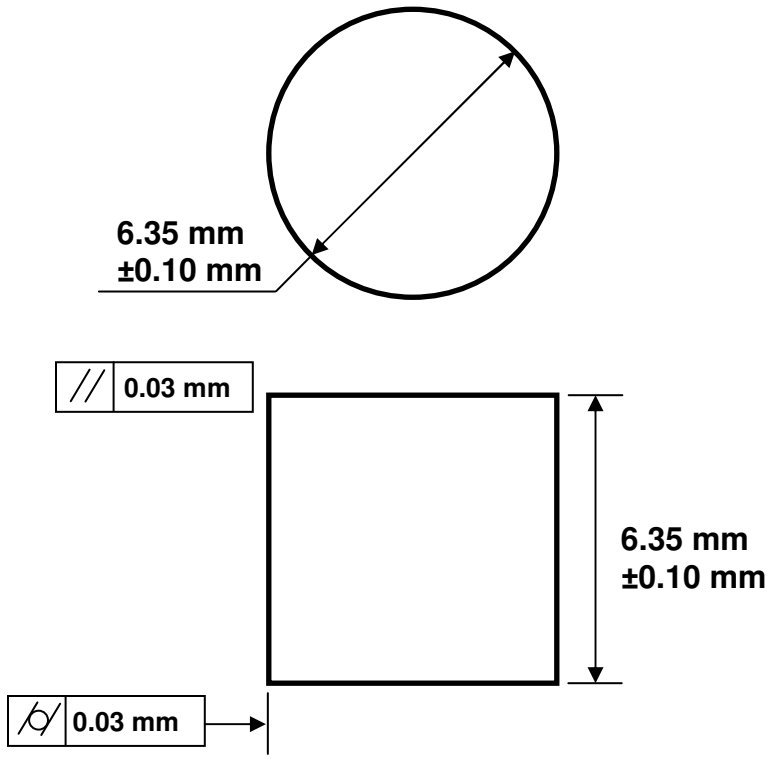

Figure 22: Al + Fe_2O_3 + Epoxy compression specimen geometry

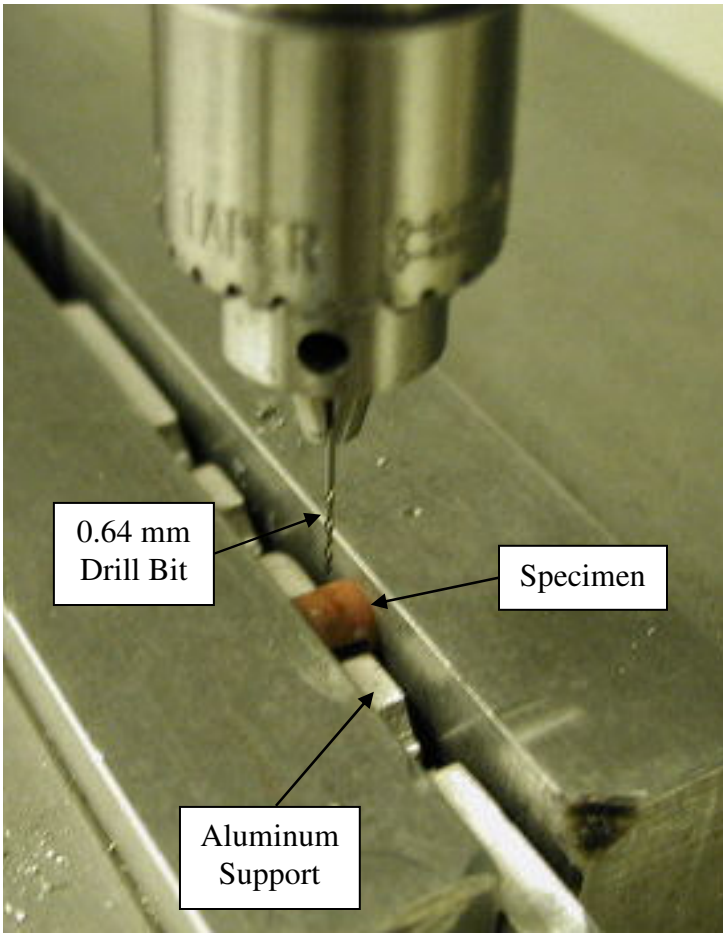

Figure 23: Method of controlling void content in Al + Fe_2O_3 + Epoxy specimens

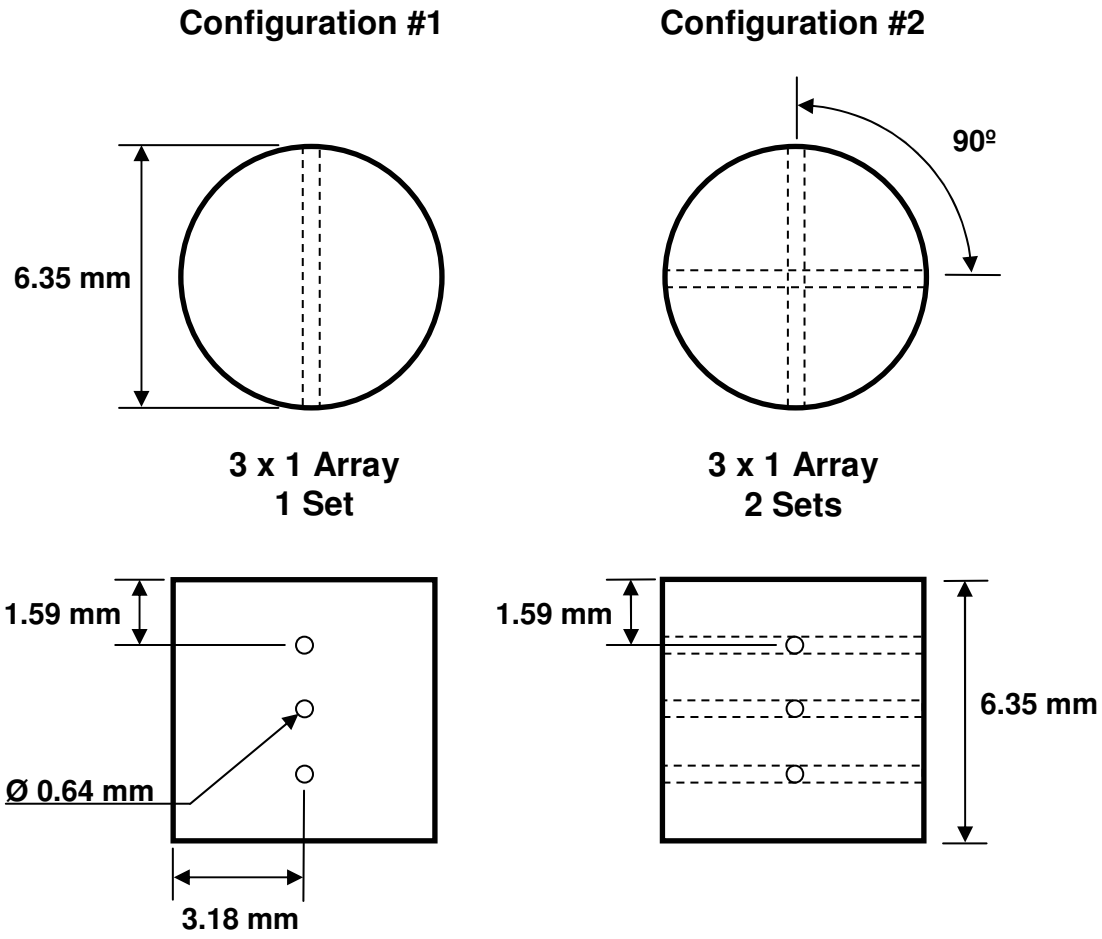

Figure 24: Al + Fe_2O_3 + Epoxy controlled porosity specimen

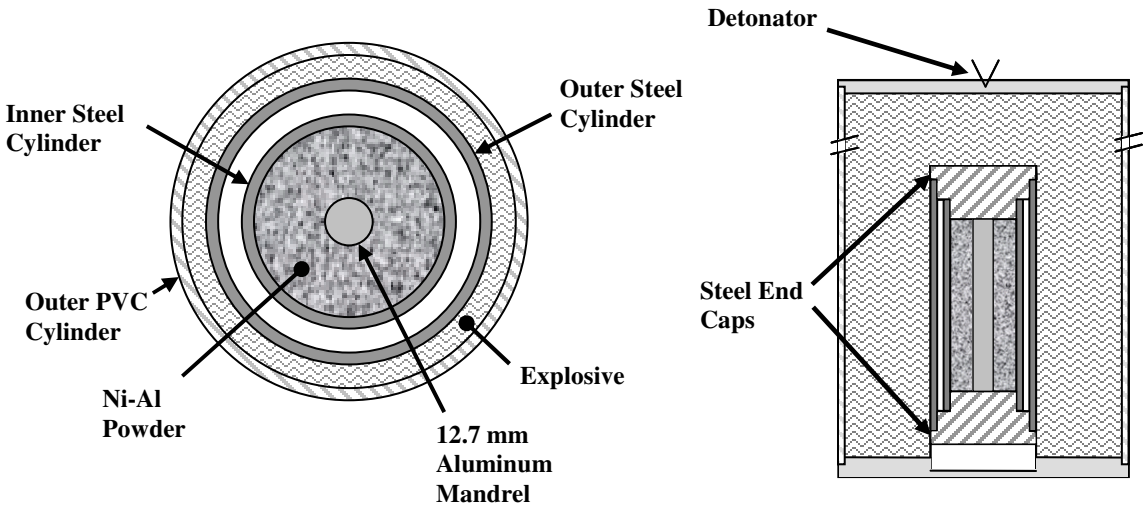

(Not drawn to scale)

Figure 25: Schematic of shock compaction setup

Figure 26: Shock compacted Ni-Al

CHAPTER III
RESULTS AND DISCUSSION

In order to investigate the mechanical behavior of two MESMs, dynamic compression tests were conducted using the SHPB apparatus in the Dynamic Properties Research Lab at the Georgia Institute of Technology. The results of these tests provide insight into the constitutive behavior of these unique materials.

3.1 Data Analysis

Data from the strain gauges are recorded by the digital oscilloscope. The two waveforms, one for each set of strain gauges, must be converted from binary to ASCII format using conversion software supplied by the oscilloscope manufacturer. A Mathcad program is used to calculate the dynamic constitutive response to high rates of loading using the converted waveforms. This program uses Equations (2.14) and (2.15) to find the strain rate-time, strain-time, stress-time, and stress-strain relations based on the data recorded on the SHPB apparatus (Appendix B).

3.2 Dynamic Constitutive Response

The dynamic constitutive response of Al + Fe_2O_3 + Epoxy at four different epoxy levels (50, 40, 30, and 22% by weight), along with 100% epoxy, and explosively densified Ni-Al are observed using the split-Hopkinson pressure bar apparatus. A summary of the material density for the specimen configurations used in this study are

summarized in Table 2. As expected, the density of the Al + Fe_2O_3 + Epoxy material increases with decreasing epoxy content. Excellent agreement between the actual density and theoretical density (which is based on a rule of mixtures approach) is found in this study; the largest variation in density being only 3.5%.

Dynamic compression tests are carried out on the specimens at strain rates on the order of 10^3 s^{-1} using the SHPB apparatus. Results from these experiments are illustrated in Figure 27 - Figure 32 and are summarized in Table 3 - Table 8. For the Al + Fe_2O_3 + Epoxy material, it is expected that the addition of the Al and Fe_2O_3 powders would result in an increase in the strength of the specimens due to the reinforcement of the matrix by the particles. As can be seen in **Error! Reference source not found.**, the strength of the mixtures does in fact increase with decreasing binder content.

Table 9 summarizes the constitutive behavior of these materials. The maximum stress achieved in the compression test increases with decreasing binder content. Due to the fact that the specimens do not fracture during the duration of loading and that the maximum stress occurs at different strains for each material, the stress achieved at 30% strain is used for the comparison of the Al + Fe_2O_3 + Epoxy specimens.

The powders act as reinforcements to the epoxy, significantly effecting the constitutive response of the Al + Fe_2O_3 + Epoxy material. In the linear loading region, the slope of the stress-strain curve increases with decreasing binder content. There is a 113% increase in the slope between the 100% Epoxy and the Al + Fe_2O_3 + 22% Epoxy specimens. Inelastic deformation is also effected by the presence of powders. The softening of the material is present in mixtures as low as Al + Fe_2O_3 + 40% Epoxy, but vanishes in mixtures with greater amounts of solids.

The soft-recovery mechanism is used for testing Ni-Al specimens to guarantee that the specimen does not fracture during the application of the load. The stress levels achieved by the Ni-Al specimens (560 MPa) are much greater than that of the Al + Fe_2O_3 + Epoxy specimens (a maximum of 397 MPa) despite being limited to approximately 10% strain. The loading slope of the Ni-Al specimens (51450 MPa) is greater than that of Al + Fe_2O_3 + Epoxy specimens (a maximum of 11400 MPa) as well.

One of the goals of this study is to aid in the design of MESMs such that the material can withstand the loading that is seen by missiles. In order to gain insight into the strength of these MESMs, dynamic compression tests of two common engineering metals, 6061-T6 Aluminum and 1045 Steel, have been conducted. The comparison of the constitutive behaviors of Al + Fe_2O_3 + 22% Epoxy, Ni-Al, 6061 Aluminum, and 1045 Steel can be seen in Figure 34. It is clear that the strength of the Al + Fe_2O_3 + Epoxy materials used in this study is still dominated by the polymer phase, and the trend shows that further reduction of the binder content will enhance the strength characteristics.

Although it has not been observed in this study, there will be a critical ratio of solids and binder that will yield maximum strength characteristics. Any further increase in solid content above this point will result in the inability of the polymer matrix to hold the solids together, resulting in the fracture of specimens. The Ni-Al specimens observed initial strength values greater than that of the 6061-T6 aluminum tested, however the lack of a binder holding the powders together resulted in the fracture of the specimens at large strains in this study. The use of the soft-recovery method limits the maximum strain to approximately 10%, preventing any comparison beyond that strain level to be made.

3.3 Work Hardening

It was observed in the stress-strain relations (**Error! Reference source not found.**) that the Al + Fe_2O_3 + Epoxy materials experienced significant levels of work hardening. The slope in the work hardening region as well as the strain at which hardening begins varied for the mixtures used in this study. The results are illustrated in Figure 35 and summarized in Table 10.

The stress-strain relations of 100% Epoxy specimens experience a region of linear elastic deformation, non-linear deformation, achieve a peak in strength, experience significant strain softening, which was followed by a slight region of work hardening. As discussed previously in Section 2.3, the strain energy exceeding the local activation energy leads to the creation of transformation sites within the matrix that leads to the deformation of polymers. The 100% Epoxy material experiences peak behavior due to the inability for the material to significantly increase the local activation energy in the regions surrounding the transformed sites, resulting in large amounts of softening. After the softening region, the material experiences significant plastic flow and experiences orientation hardening.

The Al + Fe_2O_3 + 50% Epoxy specimens experience regions of linear elastic deformation, nonlinear deformation, a slight peak, a region of strain softening, which is followed by a region of work hardening. The addition of powders into the polymer matrix aids in limiting the softening during deformation by increasing the activation energy in the regions surrounding the transformed sites. The powders increase the hardening at high levels of strain by reinforcing the epoxy matrix and assuming the load-carrying capabilities.

The Al + Fe_2O_3 + 40% Epoxy specimens experience regions of linear elastic deformation, nonlinear deformation, a slight region of strain softening, and a region of work hardening. The powders allow for the storage of strain energy, increasing the activation energy for the mixtures, which limits the number of transformation sites and reduces the nonlinearity of the stress-strain response. The increase in the activation energy within the Al + Fe_2O_3 + Epoxy mixtures can not be considered a macroscopic increase, but rather the addition of the powders to the polymer matrix in the form of reinforcement increases the required energy to form a transformation site in the polymer phase. The further increase in powders limits the softening greatly, as well as initiating the hardening region and a lower strain than that of the Al + Fe_2O_3 + 50% Epoxy specimens.

The stress-strain relations of Al + Fe_2O_3 + 30% Epoxy specimens experience regions of linear elastic deformation, nonlinear deformation, a slight region of near perfectly-plastic deformation, and a region of hardening. The powders are able to suppress the softening by acting as a reinforcement, absorbing the strain energy and limiting the transformations. The higher level of hardening, and decreased strain value at the onset of hardening, are products of the increased powder content of this mixture.

The stress-strain relations of Al + Fe_2O_3 + 22% Epoxy specimens experiences regions of linear elastic deformation and minimal nonlinear deformation, which is closely followed by a region of hardening. The significant addition of powders to this mixture leads to enhanced reinforcement, restricting the transformation of sites within the polymer, limiting the nonlinear behavior and decreasing the strain at the onset of hardening. The powders also allow for significant hardening of the material, resulting in

the maximum stress attained by any of the Al + Fe_2O_3 + Epoxy mixtures investigated. It is expected that further reduction of the binder, beyond that which is used in this study, will further enhance the work hardening effect of the Al and Fe_2O_3 particles.

3.4 Effect of Porosity on Constitutive Behavior

The effect of porosity on the dynamic constitutive response is investigated on Al + Fe_2O_3 + Epoxy specimens using the controlled porosity method. The artificial voids are created within the material by drilling holes through the specimen. The porous specimens are subjected to identical loading conditions as the fully dense specimens. Unlike the fully dense specimens, all of the controlled porosity specimens fractured during the loading duration and lost their load-carrying capabilities. The values of stress that were measured using the SHPB apparatus in these experiments represent an average stress across the specimen and do not reflect any localized high stress concentrations due to the pores.

The density of the specimens subjected to controlled porosity decreased an average of 3.1% and 6.2% for Configuration #1 and Configuration #2 (Figure 24), respectively. The densities for the specimens used in this study are summarized in Table 11. The specimens with controlled porosity achieve maximum stress states that are much lower to the corresponding fully dense specimens (Table 12).

Al + Fe_2O_3 + 50% Epoxy specimens experience the peak compressive stress at an approximate strain of 0.02 (Figure 36). The ~3% void specimens are able to maintain a certain degree of load-carrying capability up to a strain level of 0.18, while the ~6% void

specimens experience a steady decrease in load-carrying capability after the peak stress up to a strain level of 0.20.

The Al + Fe_2O_3 + 40% Epoxy specimens experience their peak compressive stress at an approximate strain of 0.04 (Figure 37). The ~3% void specimens have a steady decline in load-carrying capability from the peak stress up to a strain of 0.33, while the ~6% void specimens have an steady decrease in load-carrying capability until a strain level of 0.16, at which point two of the three specimens lose load-carrying capability.

The Al + Fe_2O_3 + 30% Epoxy specimens experience a nearly constant maximum stress until a strain of 0.15 (Figure 38). The ~3% void specimens then have a decline in load-carrying capability up to an approximate strain value of 0.25, and the ~6% void specimens show a decline in load-carrying capability up to a strain level of approximately 0.28. The Al + Fe_2O_3 + Epoxy specimens are able to maintain their load-carrying capabilities to the highest level of strain.

The Al + Fe_2O_3 + 22% Epoxy specimens experience a nearly constant maximum stress until strains of 0.15 and 0.10 for ~3% and ~6% voids, respectively (Figure 39). The ~3% void specimens show a decline in load-carrying capability up to an approximate strain value of 0.24. One of the ~6% void specimens is able to maintain a load-carrying capability until a strain level of 0.12; the other specimen lost its load-carrying capability after the peak load, which occurred at a strain of approximately 0.04.

All of the porous specimens tested fractured due to cracks initiated at the pores. During the creation of the pores in the specimens, cracks occasionally formed at the site of the pore due to drilling. These specimens were disregarded, however, visual inspections were only capable of detecting the cracks that formed on the surface of the

specimens. The presence of any internal cracks formed during the drilling of holes may have led to premature loss of load-carrying capability seen in a few of the specimens tested.

3.5 Stress Work

The ability of these materials to absorb applied energy is investigated by calculating the stress work at various levels of strain. The integration of the stress-strain curve is carried out using a program developed for Matlab (Appendix C). This post processing method is capable of producing stress work values every 1% of deformation (up to 10%) if the total straining during the experiment is less than 25%, and values every 5% of deformation (up to 50%) if the total straining during the experiment is 25% or greater.

The results from the stress work calculations for Al + Fe_2O_3 + Epoxy specimens can be found in Figure 40, Ni-Al in Figure 41, and results for both materials are summarized in Table 13. As expected, the stress work increases with decreasing binder content in the Al + Fe_2O_3 + Epoxy material. The Ni-Al specimens achieve a high state of stress work despite the low level of strain that is achieved.

The stress work is calculated for controlled porosity specimens. The introduction of porosity into Al + Fe_2O_3 + Epoxy specimens decreased the ability of the material to absorb energy (Figure 42). The average stress work values at 30% strain are summarized in Table 14. As expected, the stress work is greater in the ~3% void specimens than the ~6% void specimens, both of which are lower than the fully dense specimens. It is expected that the Al + Fe_2O_3 + 22% Epoxy specimens would possess the ability to absorb

the most energy, even when voids are present, but the material that is able to absorb the most energy is actually Al + Fe_2O_3 + 30% Epoxy. The ability for the Al + Fe_2O_3 + 30% Epoxy material to more greatly suppress the fracture of the specimens is most like attributed to the ability for the powders to withstand the applied stress while the polymer matrix is able to more readily soften at the crack tip, due to the transformation of sites occurring as a result of the increased localized stress.

3.6 Unloading Effects

Investigation into the unloading effects of a dynamic compression experiment carried out on a split-Hopkinson pressure bar is made possible through the use of the one-point method of wave separation. A program developed in Matlab (Appendix D) utilizes the one-point method to post-process the stress-strain histories of the Al + Fe_2O_3 + Epoxy material to allow for an extend view of the constitutive behavior. Based on the extended stress-strain histories for the Al + Fe_2O_3 + Epoxy material, investigation into the separation of total energy into plastic and recoverable elastic energy can be carried out. Figure 43 presents the stress-strain relations for all the Al + Fe_2O_3 + Epoxy materials, and the results are summarized in Table 15.

The slope of the loading linear region of the stress-strain curve is less than the slope of the unloading linear region for all Al + Fe_2O_3 + Epoxy materials (Figure 44). The resistance of the polymer phase to the creation of transformed sites generates back stresses within the matrix, which can cause rapid recovery in strain during unloading. The back stresses are caused by surrounding material possessing higher activation energy than the transformed sites, and during the removal of the applied load, the regions of

higher activation energy try to rapidly remove the transformed sites. The presence of the powders in the Al + Fe_2O_3 + Epoxy material will generate higher levels of back stresses, resulting in more rapid recovery of strain during unloading. In addition to the back stresses increasing the unloading slope, the rearrangement of the Al and Fe_2O_3 particles and the collapse of pores within the matrix will also increase the unloading slope.

The total work (Figure 45) was separated into the recoverable elastic work and the plastic work. With the exception of the Al + Fe_2O_3 + 40% Epoxy, the elastic work increases with decreasing binder content (Figure 46), suggesting that the Al + Fe_2O_3 + 40% Epoxy specimens may have formed cracks during the application of the load. The plastic work also increases with decreasing binder content (Figure 47), following the trend of the total work.

3.7 Dynamic Brinell Hardness

Dynamic Brinell hardness experiments are carried out on the SHPB apparatus by penetrating a steel ball indenter into the surface of Al + Fe_2O_3 + Epoxy specimens in order to characterize the dynamic indentation characteristics of the materails. High-speed digital photography is used to measure the indentation diameter; the SHPB apparatus is used to record the time-resolved force applied by the indenter, with the soft-recovery method limiting the indenter to one loading pulse of 80 μs. The measured indentation diameters and force are calculated using a Matlab program (Appendix E).

The IMACON 200 high-speed digital camera is used to obtain time-resolved diameter measurements throughout the duration of the dynamic indentation measurements. Post-indentation diameter measurements are not used due to the

possibility of rate-dependent recovery occurring in the polymer-based material, resulting in inaccurate diameter measurements. Images are captured every 25 μs through the duration of the experiments, however, only two images are found to be valid in this study. The data points are recorded at 25 μs fall within the time it takes for the stress wave to achieve equilibration within the specimen during the loading process and must be disregarded. The use of the soft-recovery method limits the duration of the experiment to 80 μs, which results in any measurement taken above 75 μs to be disregarded. The two valid images captured in this study are at 50 and 75 μs. The diameter measurements from these images, along with the corresponding load taken from the SHPB apparatus, can be used in Equation (1.3). The average dynamic Brinell hardness values and a representation of the indentation force are plotted over time in Figure 48 and summarized in Table 16. For all Al + Fe_2O_3 + Epoxy mixtures, the overall trend is a leveling off of the hardness value as the force increases. The mixtures with higher volume fractions of powders show a more level plateau compared to the mixtures with lower volume fractions, which undergo softening due to the rate-dependent polymer phase.

The value of dynamic Brinell hardness at 75 μs is closest to the point of maximum load in the experiments. This value is used to compare the hardness values among the various Al + Fe_2O_3 + Epoxy mixtures (Figure 49). The hardness of the Al + Fe_2O_3 + 22% Epoxy specimen is greatest due to the increase reinforcement provided by the powders. The trend of the dynamic Brinell hardness follows the trend of stress at 30% strain in the Al + Fe_2O_3 + Epoxy specimens closely (Figure 50).

3.8 Vickers Microindentation Hardness

To characterize the quasi-static indentation behavior of the Al + Fe_2O_3 + Epoxy mixtures used in this study, Vickers microindentation hardness experiments are carried out using a Leco MHT Series 200 apparatus. The pyramidal shaped indenter penetrates the surface of the Al + Fe_2O_3 + Epoxy specimens under an applied force of 0.050 kgf for a dwell time of 15 s. After the removal of the load, optical measurements of the indentation size are made using a 50x objective lens and the supplied Leco computer program. A total of 10 indentation tests were carried out for each material; the results of the experiments are illustrated in Figure 51 and are summarized in Table 17.

The results from the Vickers microindentation hardness values cannot be directly compared to the dynamic Brinell hardness values; however, the trend of the hardness measurements over the range of materials tested can be compared (Figure 52). The trend of the dynamic hardness experiments shows a greater increase in hardness as the volume fraction of powders increases compared to the quasi-static experiments; this trend was also observed by Subhash et al. (1999) in his study on metals. The increased resistance to indentation in the dynamic experiments indicates rate sensitivity in the Al + Fe_2O_3 + Epoxy materials.

3.9 The Hasan-Boyce Model

The compressive experimental data collected in this study is fitted to the Hasan-Boyce model (Hasan and Boyce 1995). Despite the Hasan-Boyce model being intended to describe the constitutive behavior of single-phase polymers, the data for the multi-phase polymers tested in the study have been fit in hopes to gain an understanding of the

mechanisms of deformation for these materials. Equivalent shear stress-strain relations are obtained from the stress-strain data recorded during the compression tests, and converted to true stress and strain, using $\tau = \sigma / \sqrt{3}$ and $\gamma = \sqrt{3}\varepsilon$. A Matlab program (Appendix F) is used to fit the experimental data to the Hasan-Boyce model using Equations (1.5) - (1.16), which are outlined in Section 2.3. The stress histories of 100% epoxy and the Al + Fe_2O_3 + Epoxy mixtures, which are obtained from the dynamic compression experiments conducted in this study, are used as inputs for the program. The parameters and initial conditions were originally based on those used by Lu et al. (2001) but have been modified for the different polymer system and the addition of the Al and Fe_2O_3 powders. All of the variables are calculated based on the incremental stress input, and the integration of all the rate terms are carried out incrementally using the value of Δt from the experiments.

Despite the model being intended for the fit of single-phase glassy polymers, good fits are achieved for the Al + Fe_2O_3 + Epoxy mixtures, where the Al and Fe_2O_3 particles act as particulate reinforcements for the epoxy matrix. The inclusion of powders in the matrix powders raises the local activation energy, which restricts the creation of transformation sites, and results in limited inelastic flow. The ability for the material to store the inelastic work will be enhanced with the addition of the powders as well, resulting in increased levels of work hardening.

As the volume fraction of powders increases in the materials, various model parameters evolve in order to achieve a good fit between the experimental data and the predicted behavior. Table 18 summarizes the parameters that are used to fit the experimental data to the Hasan-Boyce Model for 100% Epoxy and the Al + Fe_2O_3 +

Epoxy mixtures in this study. Figure 53 - Figure 57 compare the Hasan-Boyce model to the experimental data for pure epoxy and the Al + Fe_2O_3 + Epoxy mixtures.

The parameters used in the Hasan-Boyce model represent the physical mechanisms that are associated with the deformation of glassy polymers. Lu et al. (2001) described the effects of the parameters on modeling the constitutive behavior of a glassy polymer. ω_0, the attempt frequency, is one of the parameters used to calculate the effective frequency of shear transformations. An increase in the value of ω_0 suggests frequent formation of shear transformations within the material, resulting in pronounced softening of the material at low strains. A value of 6.05×10^{15} Hz is chosen for the pure epoxy and for the Al + Fe_2O_3 + Epoxy mixtures, to reflect the high likelihood of the creation of shear transformation sites occurring in the polymer-based material.

Another variable that is used to calculate the effective frequency of shear transformations is the pre-exponential factor, $\dot{\gamma}_0$. A decrease in the value of this term yields an increase in the value of the predicted stress at higher strains through the calculation of ω (1.12). As the volume fraction of the powders increases, the increased stress levels due to the hardening effects of the powders requires a decrease in the value of $\dot{\gamma}_0$.

The constant ξ is used in the calculation of $f(\gamma^p)$, which reflects the creation of sites with low activation energy occurs at the onset of inelastic deformation. Due to the fact that the pure polymer has a low activation energy, it can be expected that the creation of transformation sites occurs at a low strain. The addition of the powders increases the activation energy for Al + Fe_2O_3 + Epoxy mixtures, resulting in a higher value of ξ being chosen for Al + Fe_2O_3 + Epoxy mixtures compared to 100% epoxy.

$\Delta v_\tau^*(T)$ is the shear activation volume, which corresponds to the size of the inelastic shear transformation sites. λ is a parameter that controls the sensitivity of $\Delta v_\tau^*(T)$ to increases in temperature. 100% epoxy is the most likely to have transformation sites of greater volume due to the lower activation energy in the surrounding material because of the lack of powder reinforcement when compared to Al + Fe_2O_3 + Epoxy materials. $\Delta v_{\tau 0}^*$ is the initial value of the shear activation volume, and it is expected that the value of $\Delta v_{\tau 0}^*$ decreases with the increasing volume fraction of powders to reflect the decrease in the volume of the transformed sites with increasing solid content.

The evolution of a, an internal variable, represents the creation of additional regions of low activation energy due to the redistribution of the energy in the vicinity of previously transformed sites; this mainly takes place once the majority of the material has transformed. At a low value of a_0 compared to a_{eq}, the material will be able to redistribute the activation energy in the material with greater ease. Due to the fact that the Al + Fe_2O_3 + Epoxy mixtures contain higher levels of particle reinforcement, it follows that the materials will be capable of redistributing the activation energy among the solids.

β is used to represent the decline in the rate of storage of inelastic work with increasing inelastic strain. It is expected that the ability for the material to store inelastic work in the form of transformations increases with the addition of powders. This is reflected in the increasing values of β_1, β_2, and β_3 as the volume fraction of powders increases.

Table 2: Material density at different compositions

Material Makeup	Average Density (g/cm^3)	Theoretical Density (g/cm^3)	Percentage of Theoretical Density
100% Epoxy	1.185	1.164	101.8%
50% Epoxy	1.790	1.826	98.1%
40% Epoxy	2.134	2.061	103.5%
30% Epoxy	2.373	2.364	100.4%
22% Epoxy	2.642	2.670	98.0%
Ni-Al	6.770	6.804	99.5%

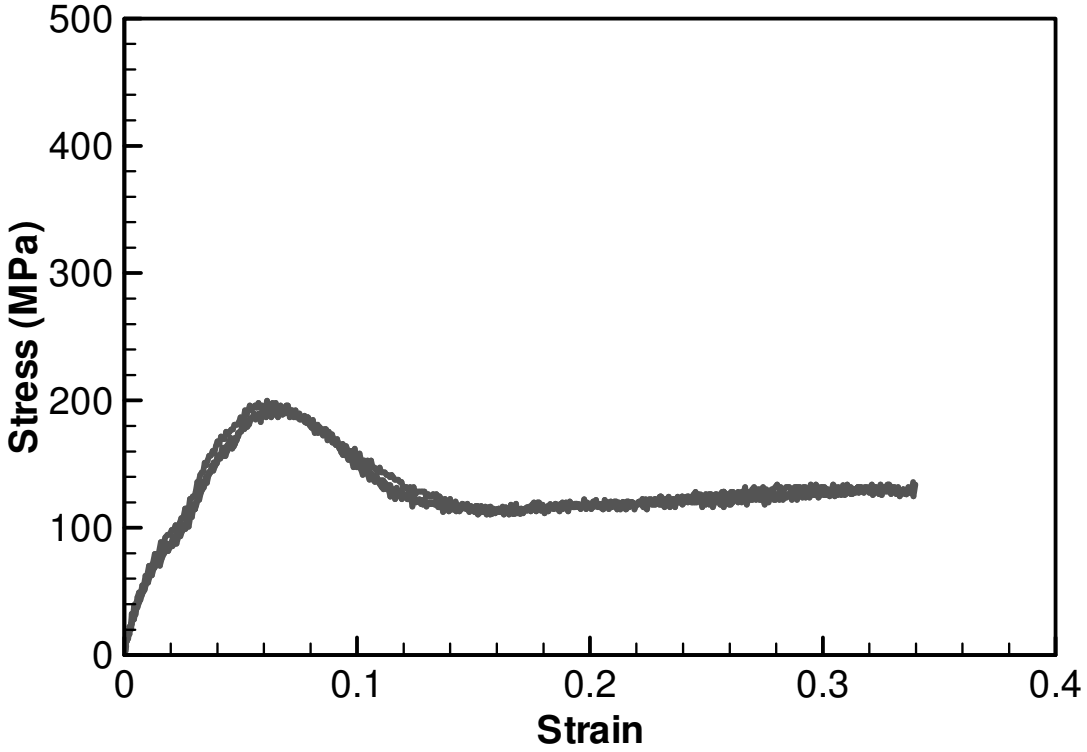

Figure 27: Stress-strain relations of 100% Epoxy

Table 3: Summary of compressive strength: 100% Epoxy

Specimen	Density (g/cm^3)	Stress at 30% Strain (MPa)	Strain Rate (s^{-1})
GT-CT-059A-10	1.188	132.1	1495
GT-CT-059A-12	1.184	129.6	1491
GT-CT-059A-13	1.183	130.2	1488

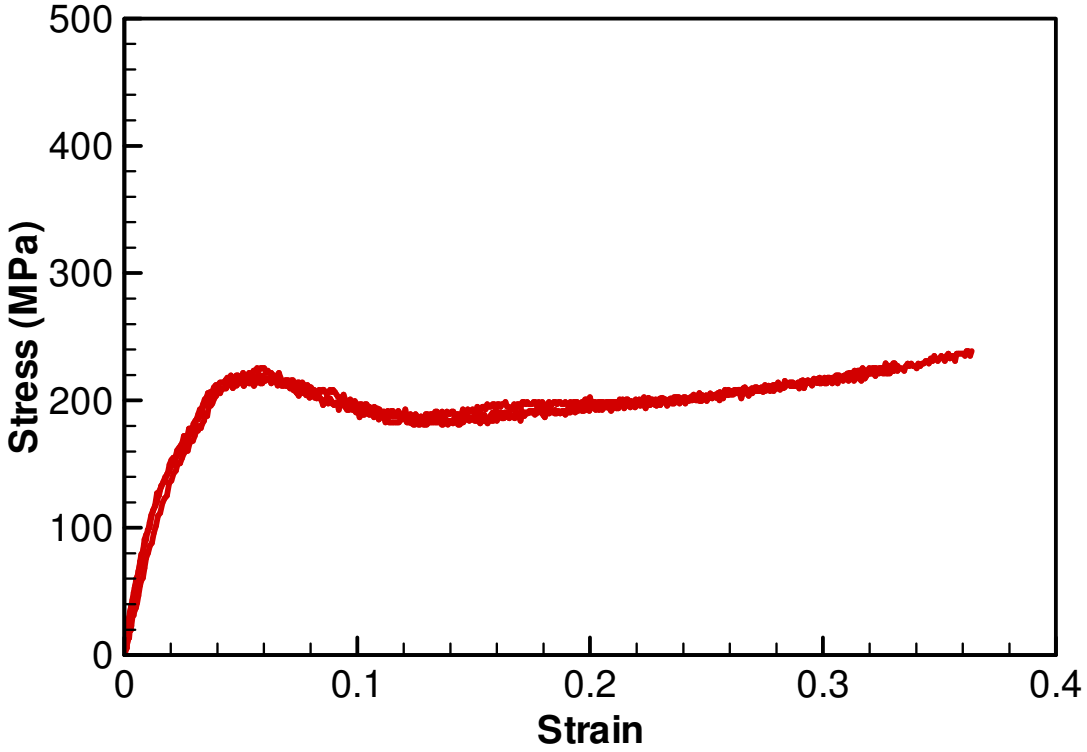

Figure 28: Stress-strain relations of Al + Fe_2O_3 + 50% Epoxy

Table 4: Summary of compressive strength: Al + Fe_2O_3 + 50% Epoxy

Specimen	Density (g/cm^3)	Stress at 30% Strain (MPa)	Strain Rate (s^{-1})
GT-CT-080A-08	1.791	216.0	1420
GT-CT-080A-09	1.790	215.6	1440
GT-CT-080A-10	1.790	215.4	1560

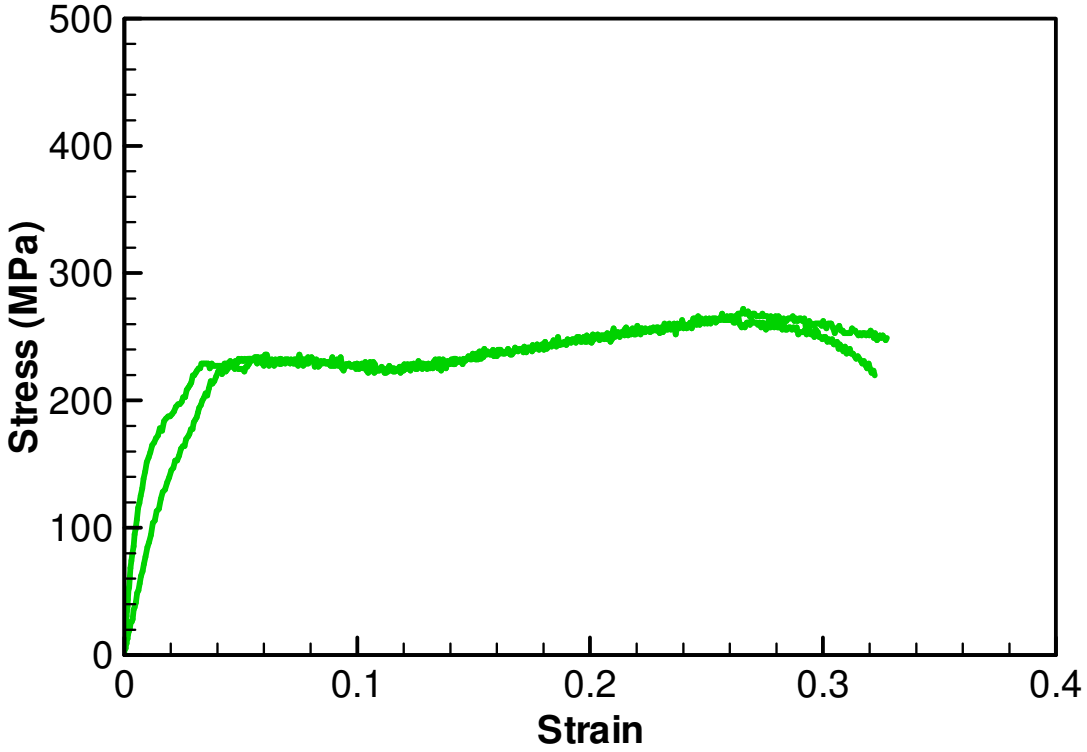

Figure 29: Stress-strain relations of Al + Fe_2O_3 + 40% Epoxy

Table 5: Summary of compressive strength: Al + Fe_2O_3 + 40% Epoxy

Specimen	Density (g/cm^3)	Stress at 30% Strain (MPa)	Strain Rate (s^{-1})
GT-CT-081A-04	2.129	262.4	1385
GT-CT-081A-05	2.139	248.0	1389

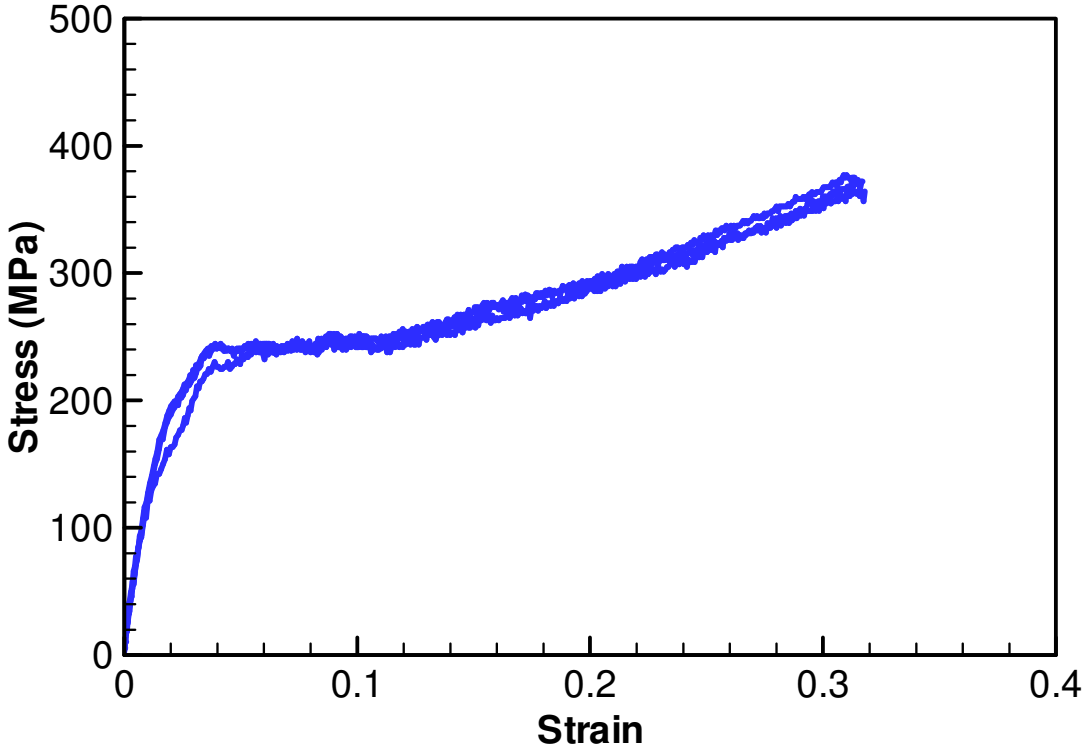

Figure 30: Stress-strain relations of Al + Fe_2O_3 + 30% Epoxy

Table 6: Summary of compressive strength: Al + Fe_2O_3 + 30% Epoxy

Specimen	Density (g/cm^3)	Stress at 30% Strain (MPa)	Strain Rate (s^{-1})
GT-CT-084A-04	2.409	360.3	1347
GT-CT-084A-05	2.329	354.6	1355
GT-CT-084A-06	2.382	365.7	1339

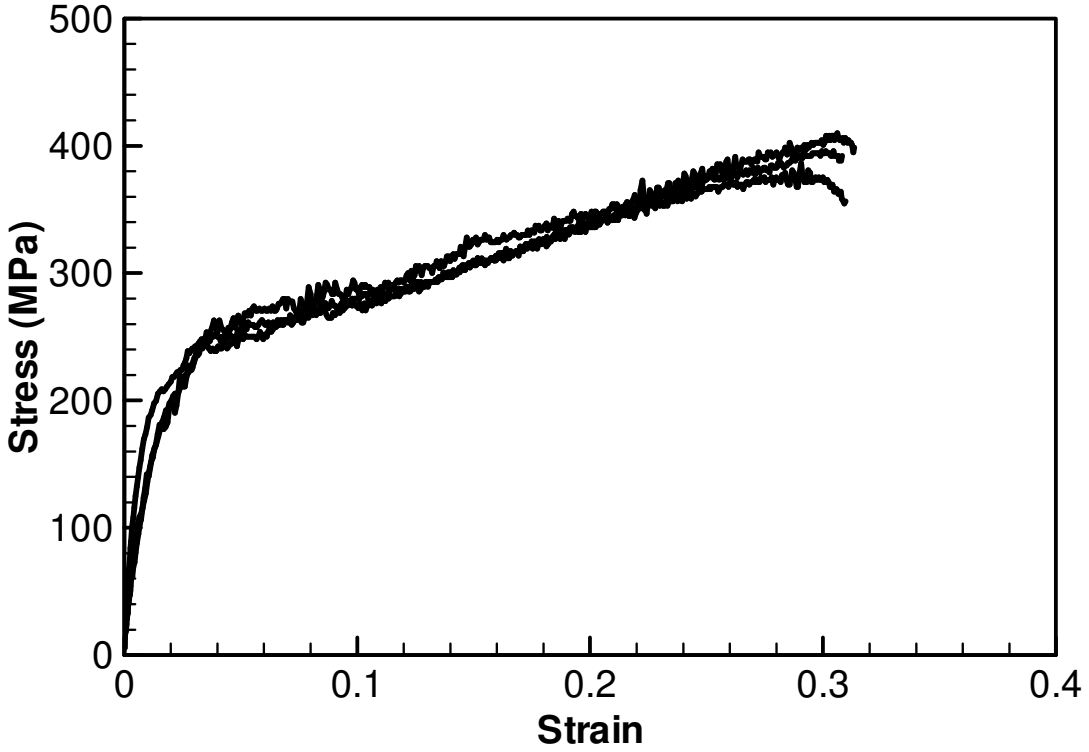

Figure 31: Stress-strain relations of Al + Fe_2O_3 + 22% Epoxy

Table 7: Summary of compressive strength: Al + Fe_2O_3 + 22% Epoxy

Specimen	Density (g/cm^3)	Stress at 30% Strain (MPa)	Strain Rate (s^{-1})
GT-CT-058B-04	2.659	395.9	1295
GT-CT-058B-05	2.634	377.4	1315
GT-CT-058B-06	2.634	400.6	1315

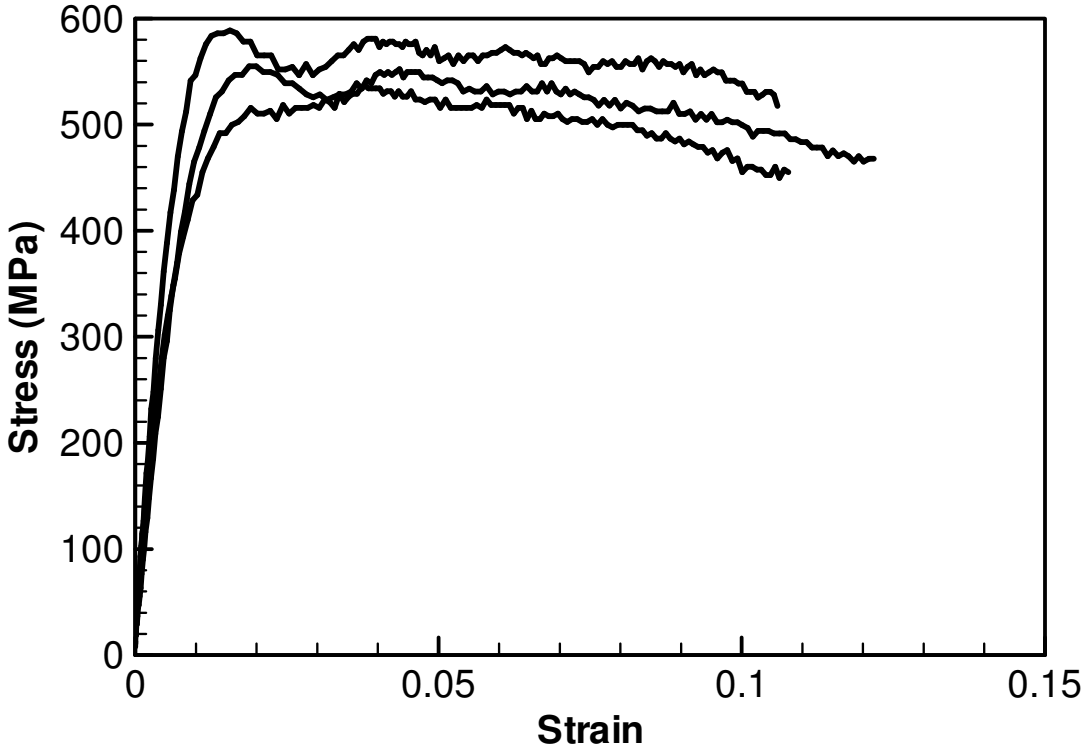

Figure 32: Stress-strain relations of Ni-Al

Table 8: Summary of compressive strength: Ni-Al

Specimen	Density (g/cm^3)	Stress at 10% Strain (MPa)	Strain Rate (s^{-1})
NM-SC-01A-03	6.758	538.7	1430
NM-SC-01A-05	6.778	455.0	1600
NM-SC-01A-07	6.775	499.4	1780

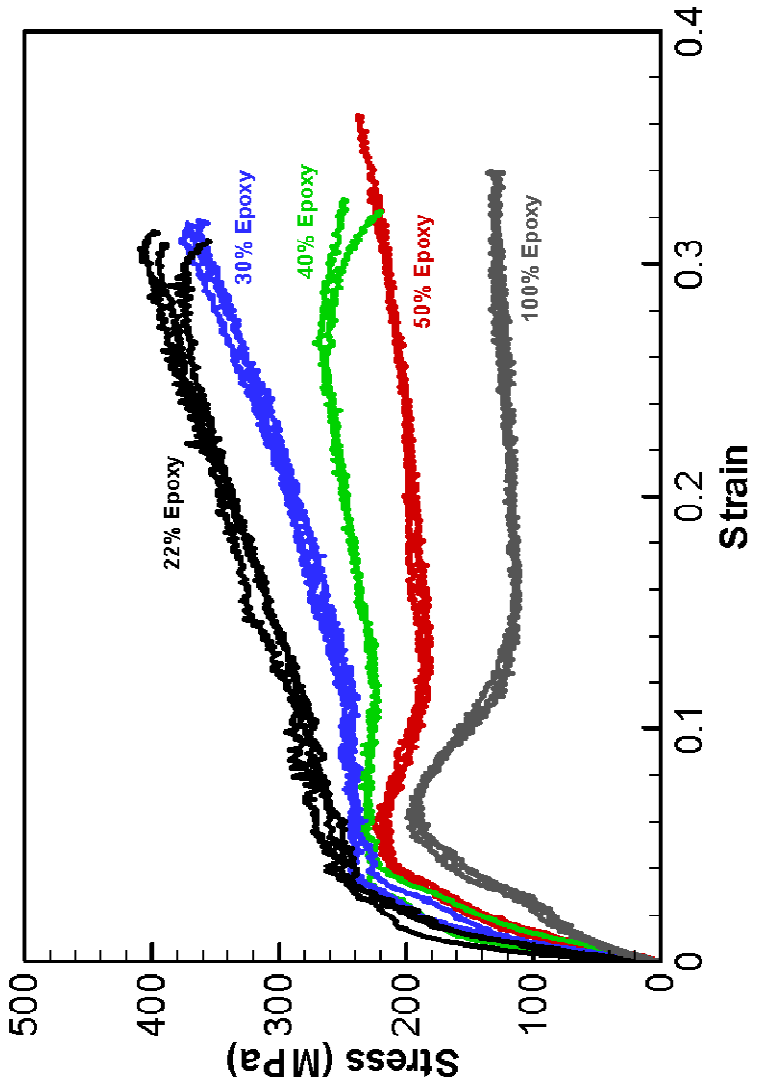

Figure 33: Summary of stress-strain relations of Al + Fe_2O_3 + Epoxy

Table 9: Summary of constitutive behavior of different material compositions

Material Makeup	Maximum Stress (MPa)	Stress at 30% Strain (MPa)	Slope of Linear Region (MPa)
100% Epoxy	196.1	130.6	5352
50% Epoxy	231.1	215.7	8103
40% Epoxy	268.5	255.2	9046
30% Epoxy	371.0	360.2	9419
22% Epoxy	396.9	391.3	11413
Ni-Al	560.2	497.7	51450

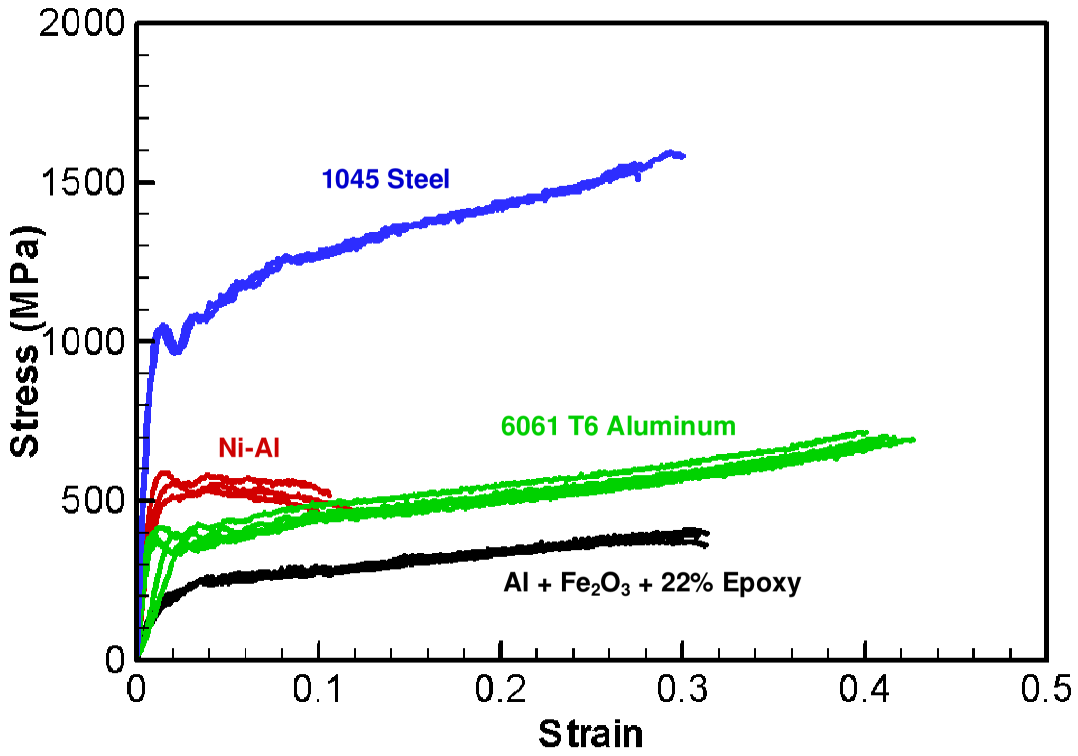

Figure 34: Comparison of constitutive behavior of MESMs and metals

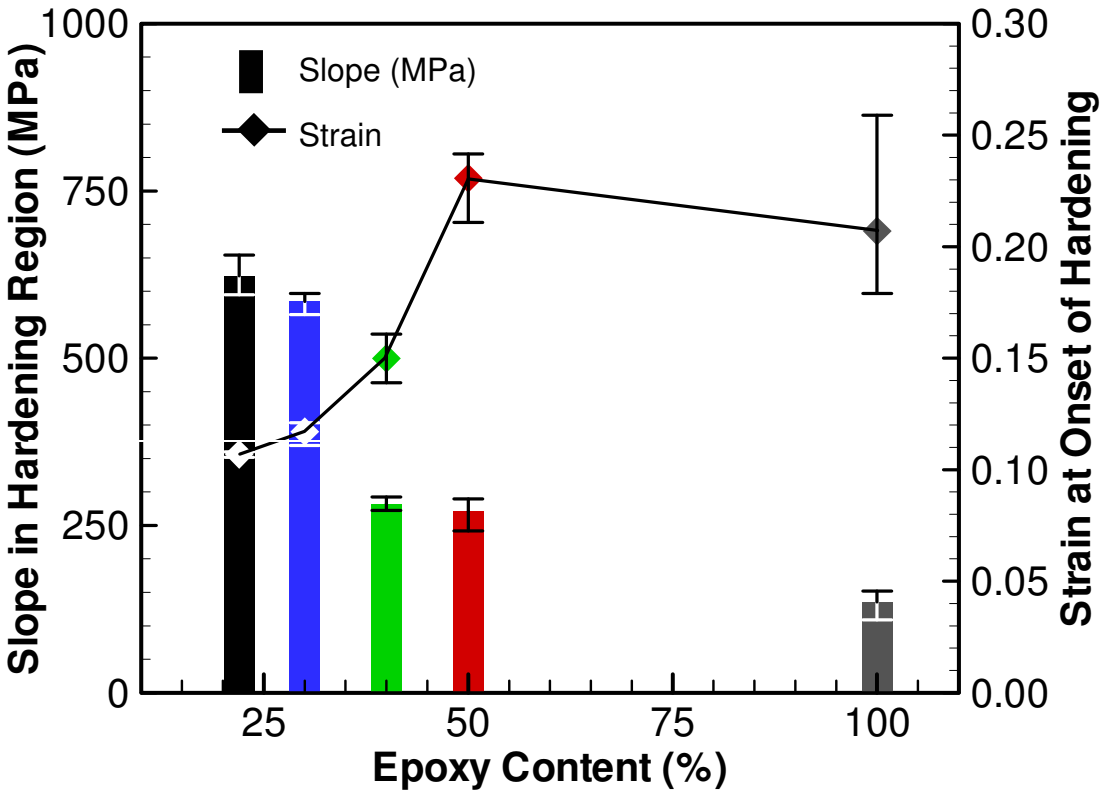

Figure 35: Slope and strain of hardening regions in Al + Fe_2O_3 + Epoxy

Table 10: Summary of work hardening: Al + Fe_2O_3 + Epoxy

Epoxy Content	Slope of Hardening Region (MPa)	Strain at Onset of Hardening	Strain at Conclusion of Hardening
100%	135.6	0.2070	0.3391
50%	271.1	0.2307	0.3431
40%	282.4	0.1499	0.2584
30%	584.7	0.1171	0.3617
22%	623.3	0.1069	0.2598

Table 11: Effect of porosity on density

	Average Density (g/cm^3)			
Porosity	50% Epoxy	40% Epoxy	30% Epoxy	22% Epoxy
Fully Dense	1.804	2.136	2.389	2.658
~3% Voids	1.755	2.075	2.314	2.587
~6% Voids	1.682	2.001	2.242	2.485

Table 12: Effect of porosity on maximum stress

	Maximum Stress (MPa)			
Porosity	50% Epoxy	40% Epoxy	30% Epoxy	22% Epoxy
Fully Dense	231.1	268.5	371.0	396.9
~3% Voids	189.1	200.4	217.7	231.9
~6% Voids	176.4	181.3	195.6	194.6

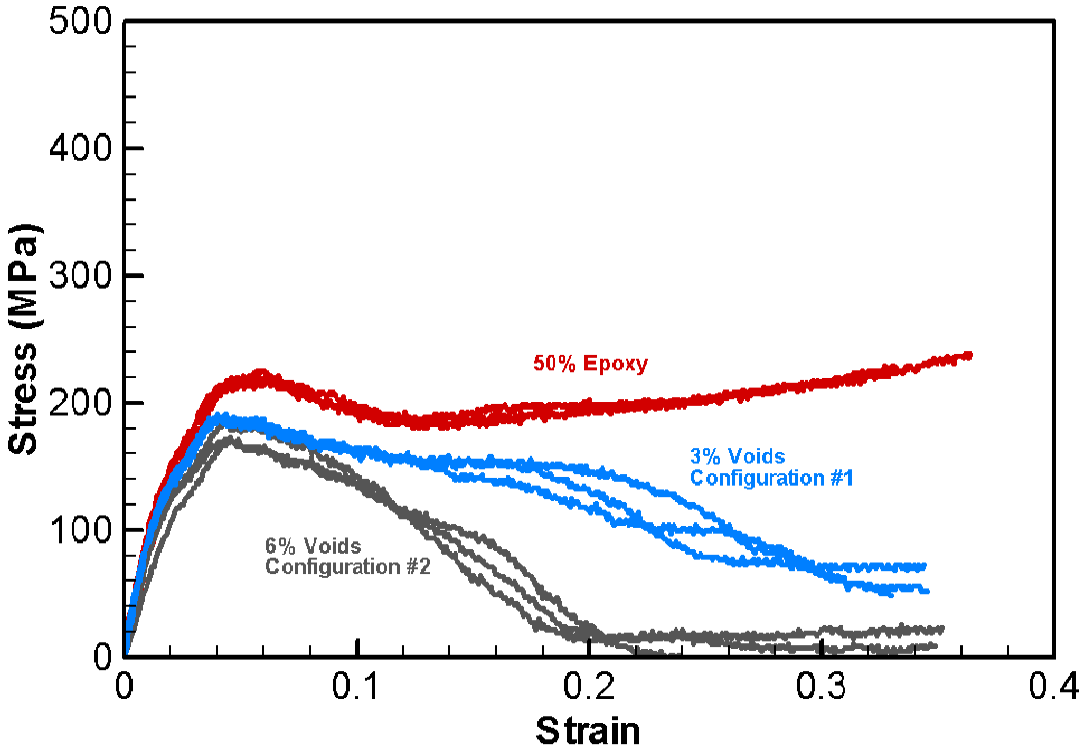

Figure 36: Effect of porosity on the stress-strain relations of Al + Fe_2O_3 + 50% Epoxy

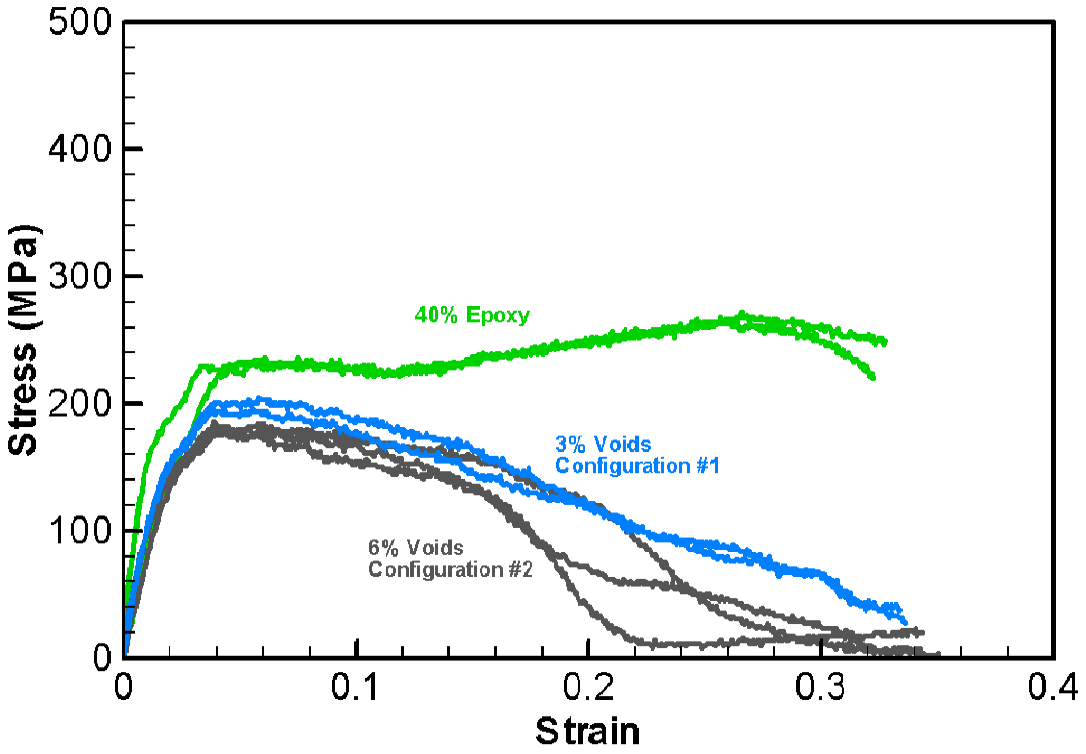

Figure 37: Effect of porosity on the stress-strain relations of Al + Fe_2O_3 + 40% Epoxy

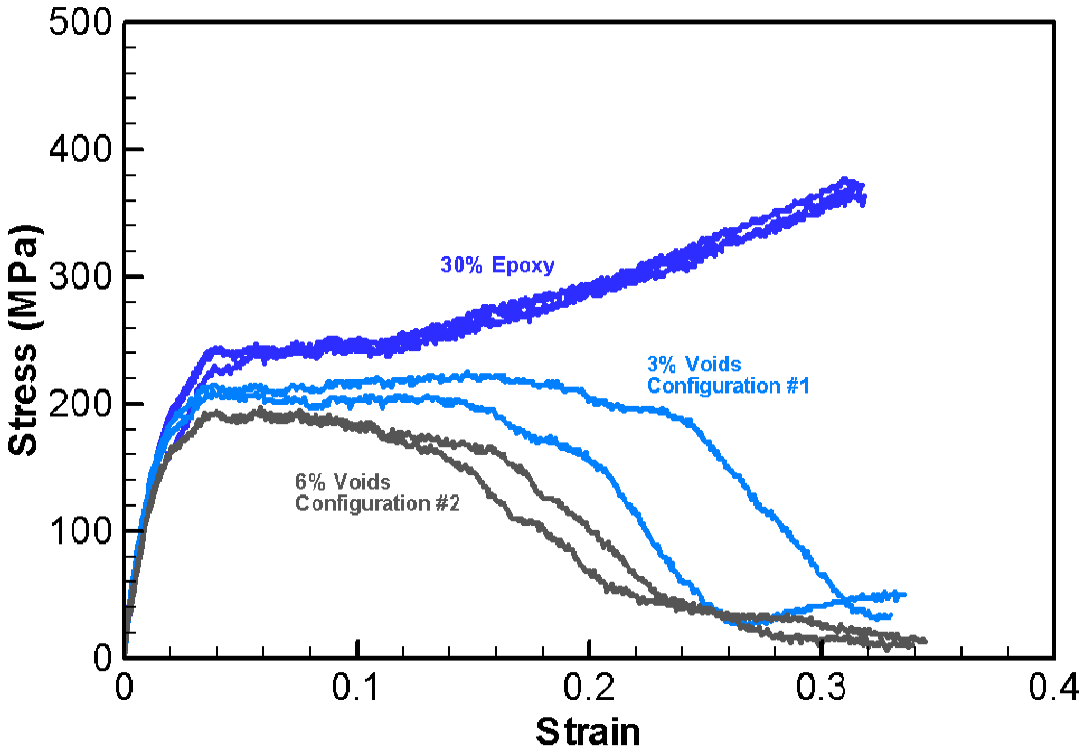

Figure 38: Effect of porosity on the stress-strain relations of Al + Fe_2O_3 + 30% Epoxy

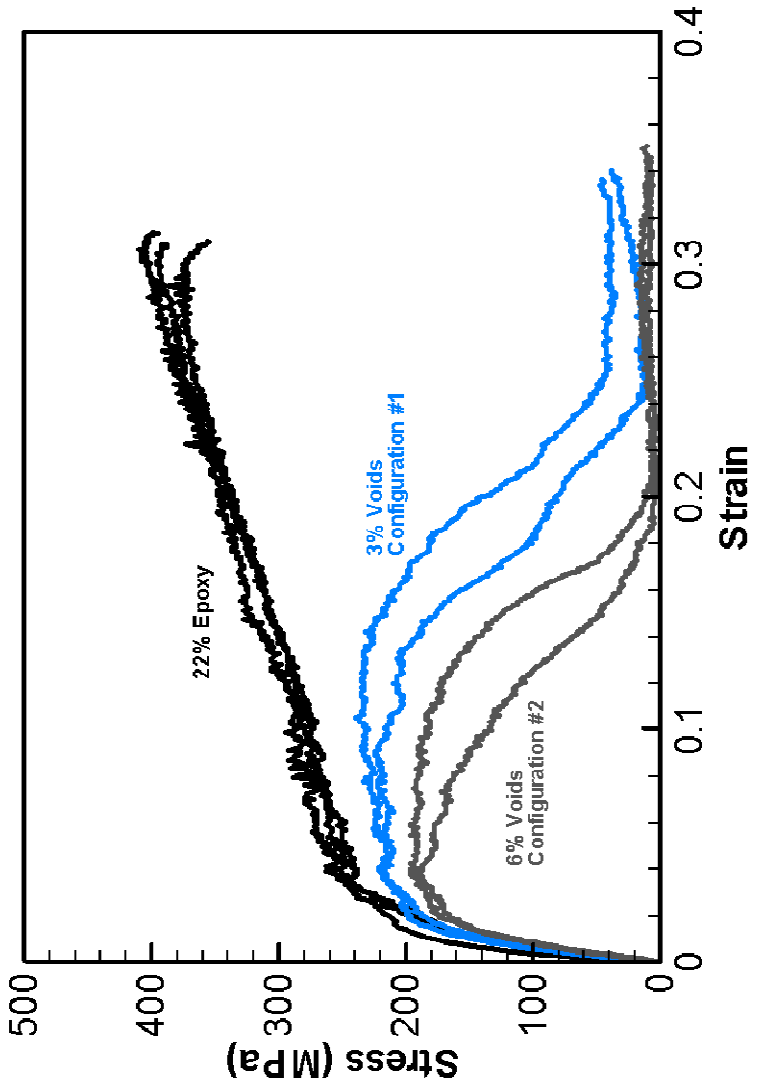

Figure 39: Effect of porosity on the stress-strain relations of Al + Fe_2O_3 + 22% Epoxy

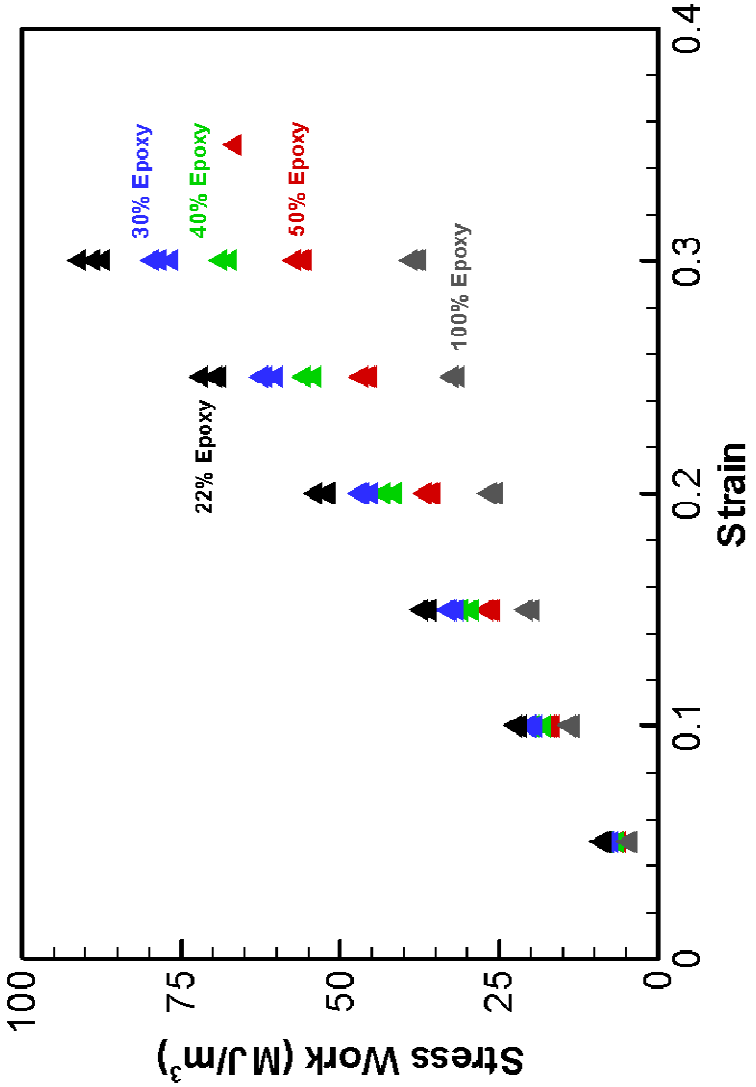

Figure 40: Stress work-strain relations for Al + Fe_2O_3 + Epoxy

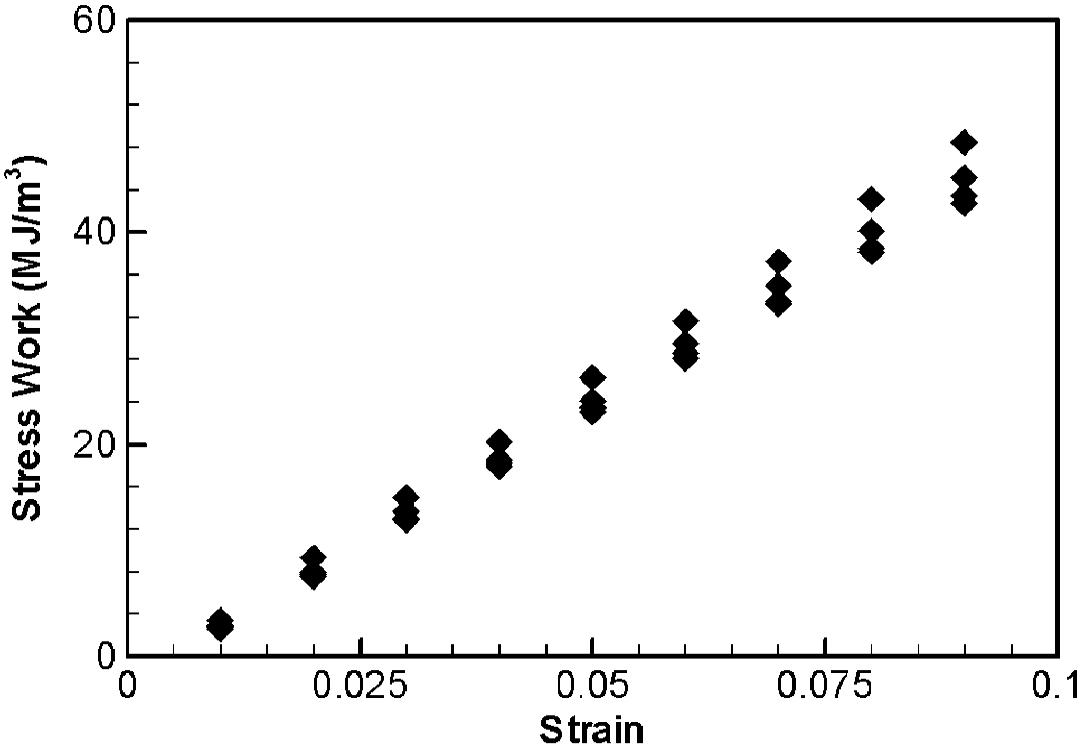

Figure 41: Stress work-strain relations for Ni-Al

Table 13: Stress work at different material compositions

	Stress Work at 30% Strain (MJ/m^3)	Total Stress Work (MJ/m^3)	Total Strain
100% Epoxy	38.1	43.7	0.3391
50% Epoxy	56.2	66.8	0.3431
40% Epoxy	68.0	75.3	0.3249
30% Epoxy	78.1	85.9	0.3167
22% Epoxy	89.0	95.3	0.3115
Ni-Al	51.0*	56.7	0.1118

*- Value taken at 10% strain

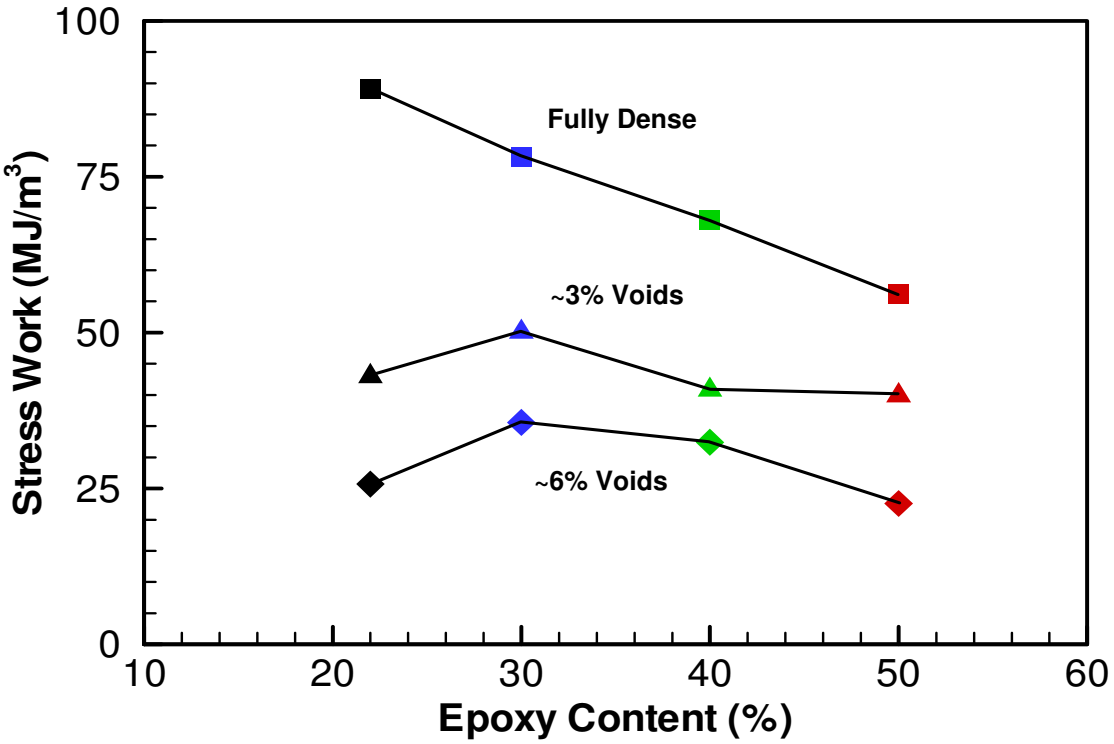

Figure 42: Effect of porosity on stress work

Table 14: Effect of porosity on stress work

	Average Stress Work at 30% Strain (MJ/m^3)			
Porosity	50% Epoxy	40% Epoxy	30% Epoxy	22% Epoxy
Fully Dense	56.2	68.0	78.1	89.0
~3% Voids	39.9	40.8	50.1	43.0
~6% Voids	22.6	32.4	35.6	25.7

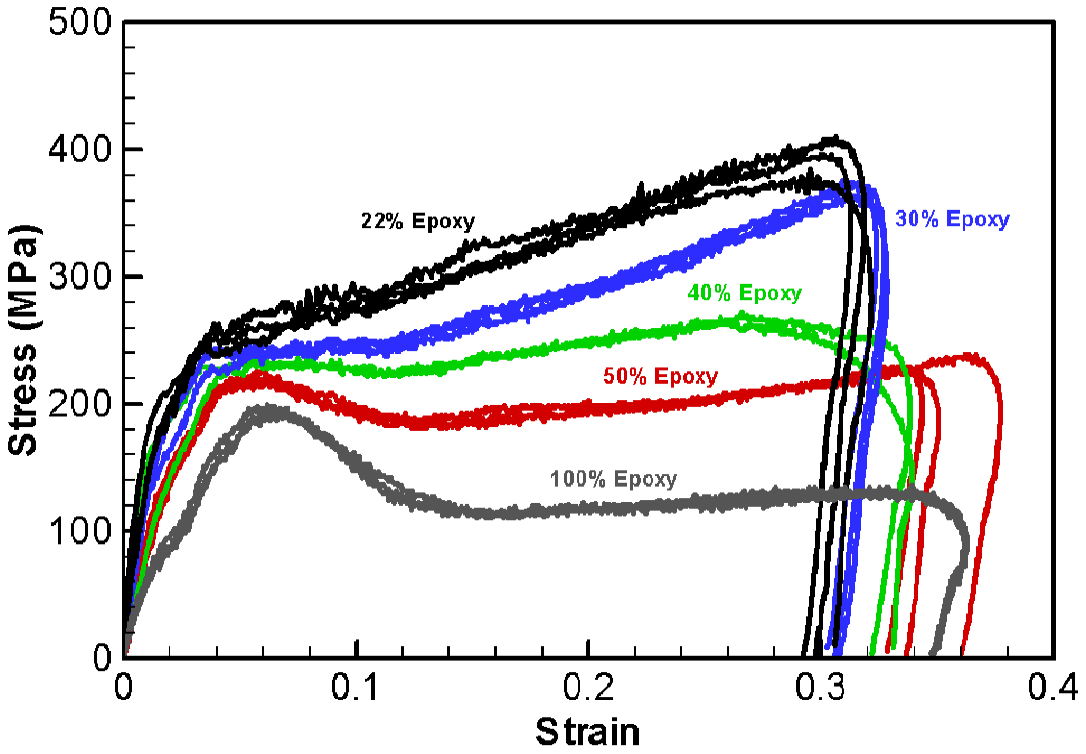

Figure 43: Unloading stress-strain relations for Al + Fe_2O_3 + Epoxy

Table 15: Summary of unloading data for Al + Fe_2O_3 + Epoxy

Epoxy Content (%)	Loading Slope (MPa)	Unloading Slope (MPa)	E_{Total}	$E_{Elastic}$	$E_{Plastic}$
100	5352	6948	46.5	0.63	45.8
50	8103	12480	69.9	1.43	68.5
40	9046	14518	78.2	1.11	77.1
30	9419	15577	89.4	3.04	86.4
22	11413	19326	97.6	3.09	94.5

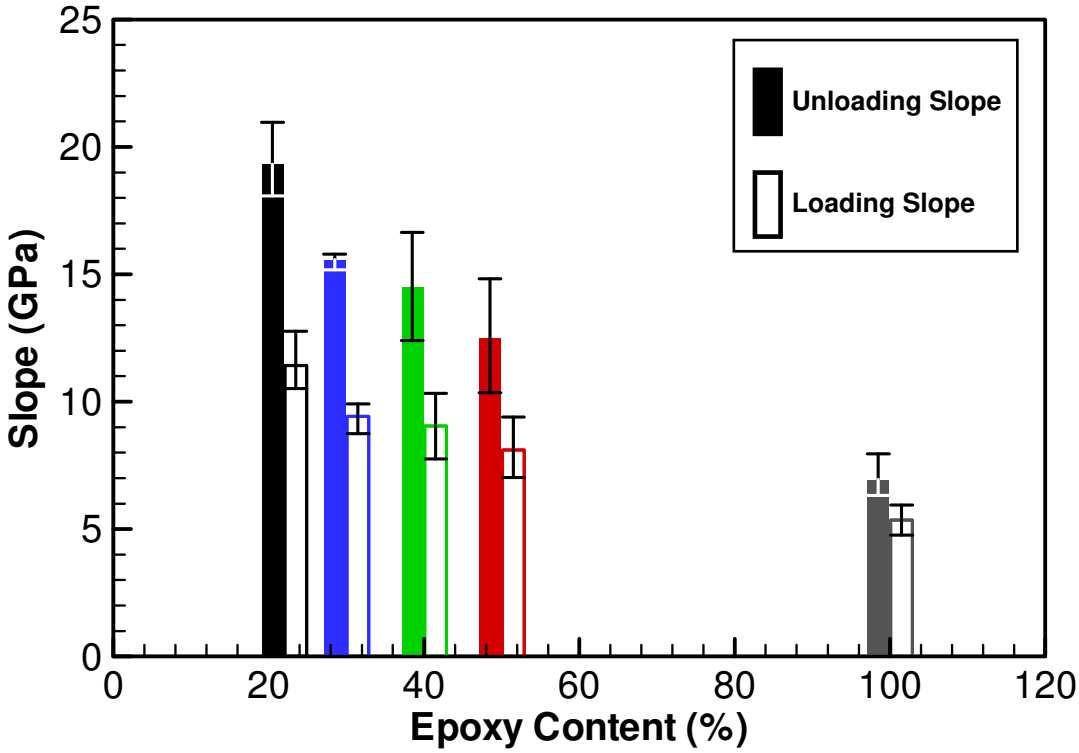

Figure 44: Unloading and loading slope for Al + Fe_2O_3 + Epoxy

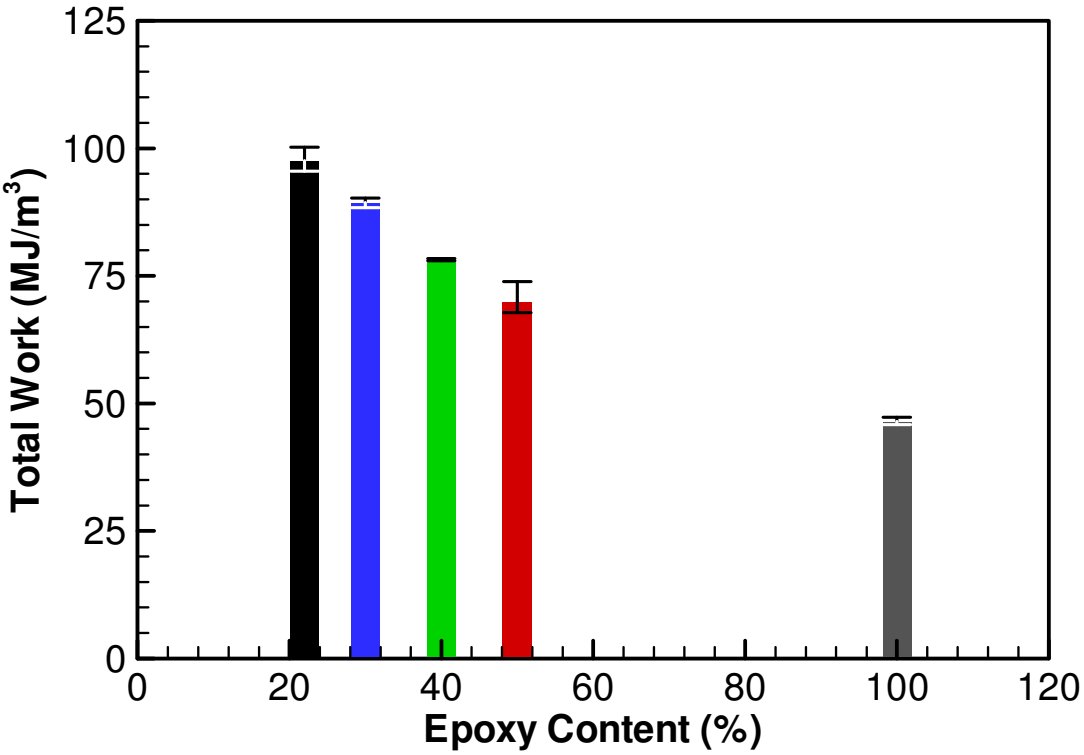

Figure 45: Total work for Al + Fe_2O_3 + Epoxy

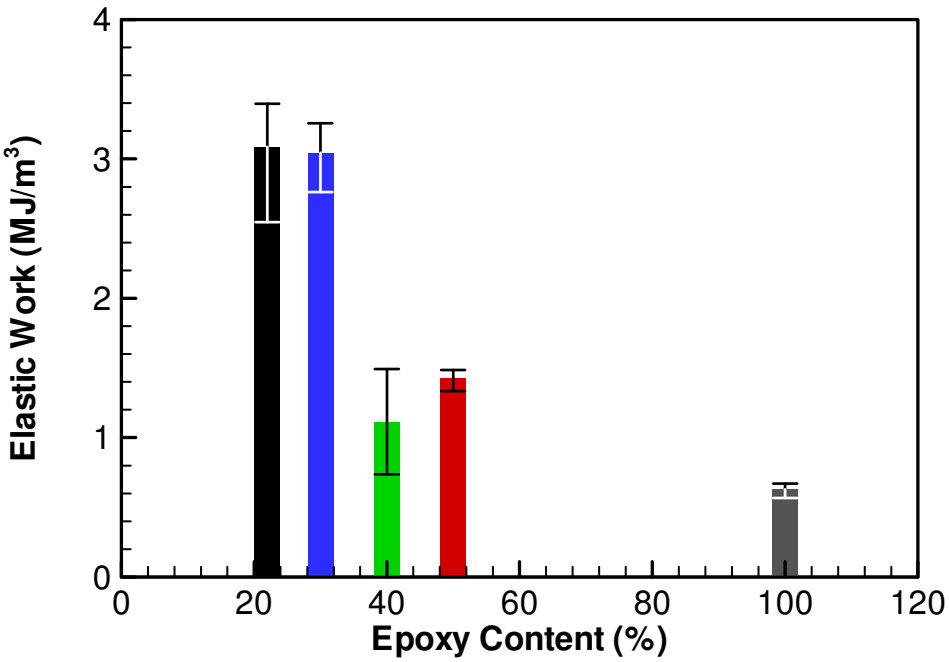

Figure 46: Elastic work for Al + Fe_2O_3 + Epoxy

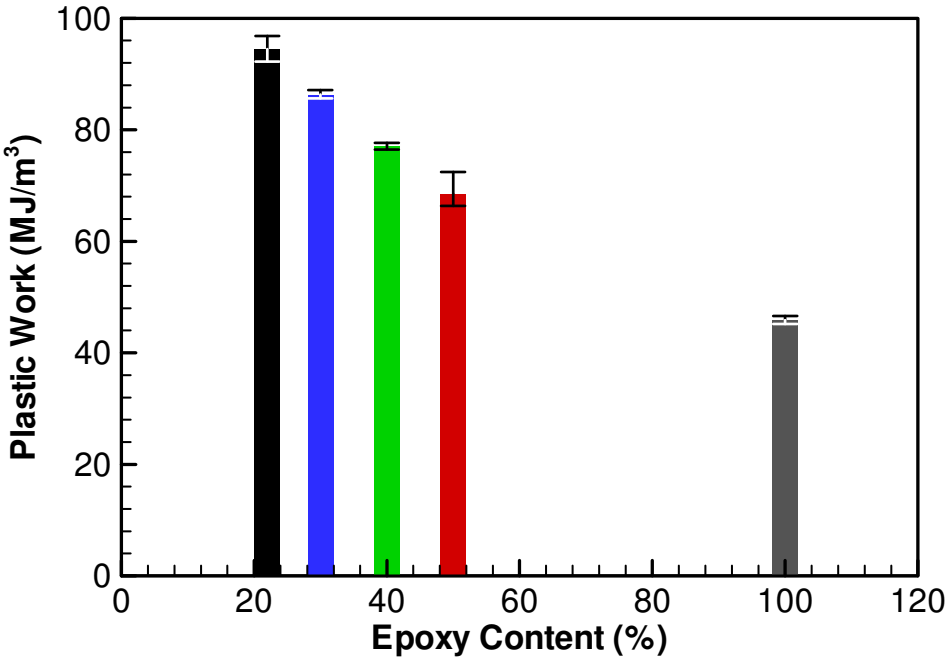

Figure 47: Plastic work for Al + Fe_2O_3 + Epoxy

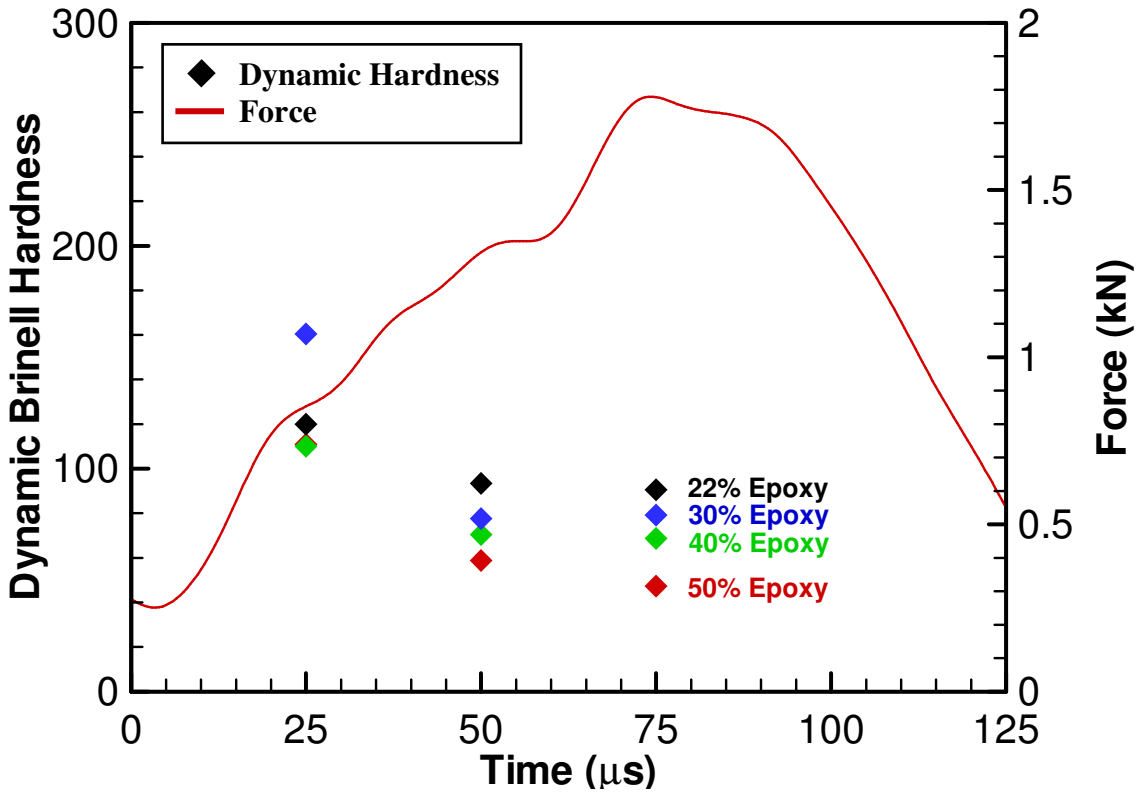

Figure 48: Average dynamic Brinell hardness-force-time relations

Table 16: Summary of dynamic Brinell hardness for Al + Fe_2O_3 + Epoxy

	Dynamic Brinell Hardness			
	50% Epoxy	40% Epoxy	30% Epoxy	22% Epoxy
50 μs	58.9	70.5	77.6	93.5
75 μs	47.3	68.8	79.1	90.6

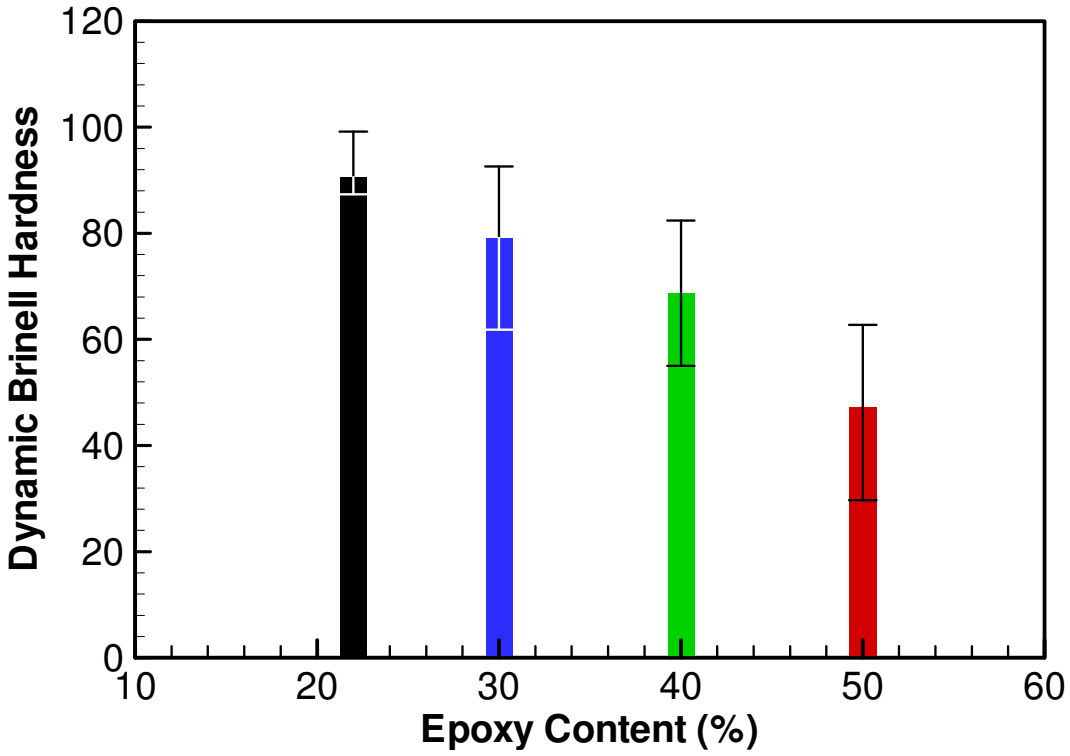

Figure 49: Dynamic Brinell hardness for Al + Fe_2O_3 + Epoxy at 75 µs

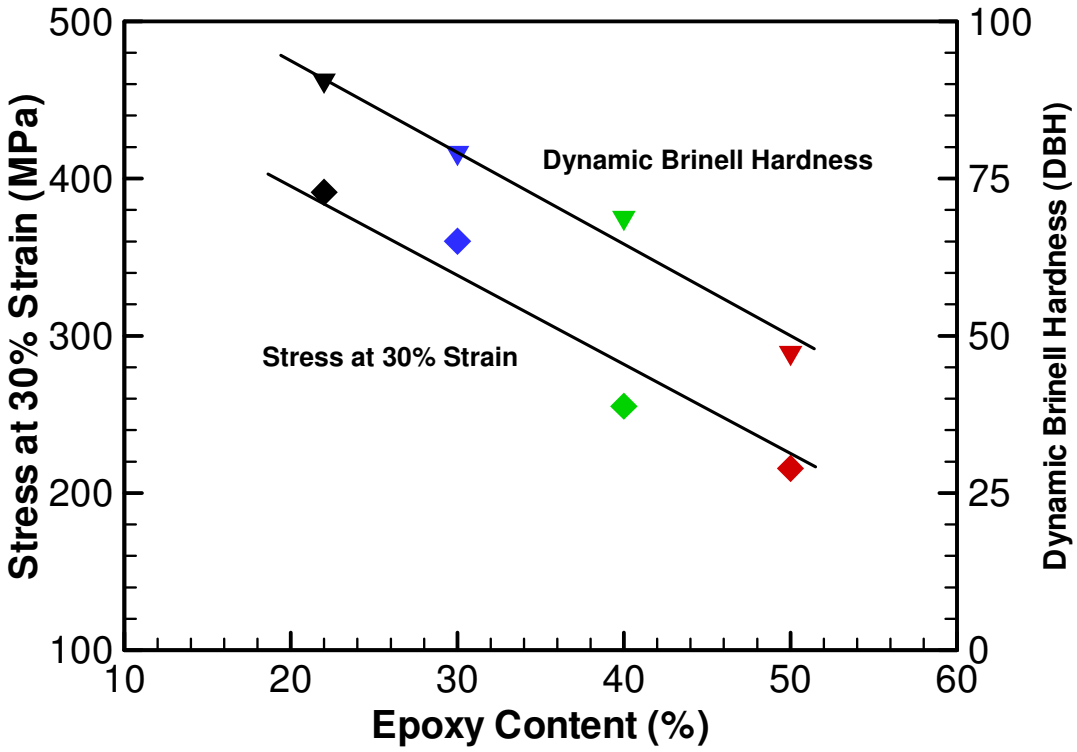

Figure 50: Stress at 30% strain and dynamic Brinell hardness trends for Al + Fe_2O_3 + Epoxy

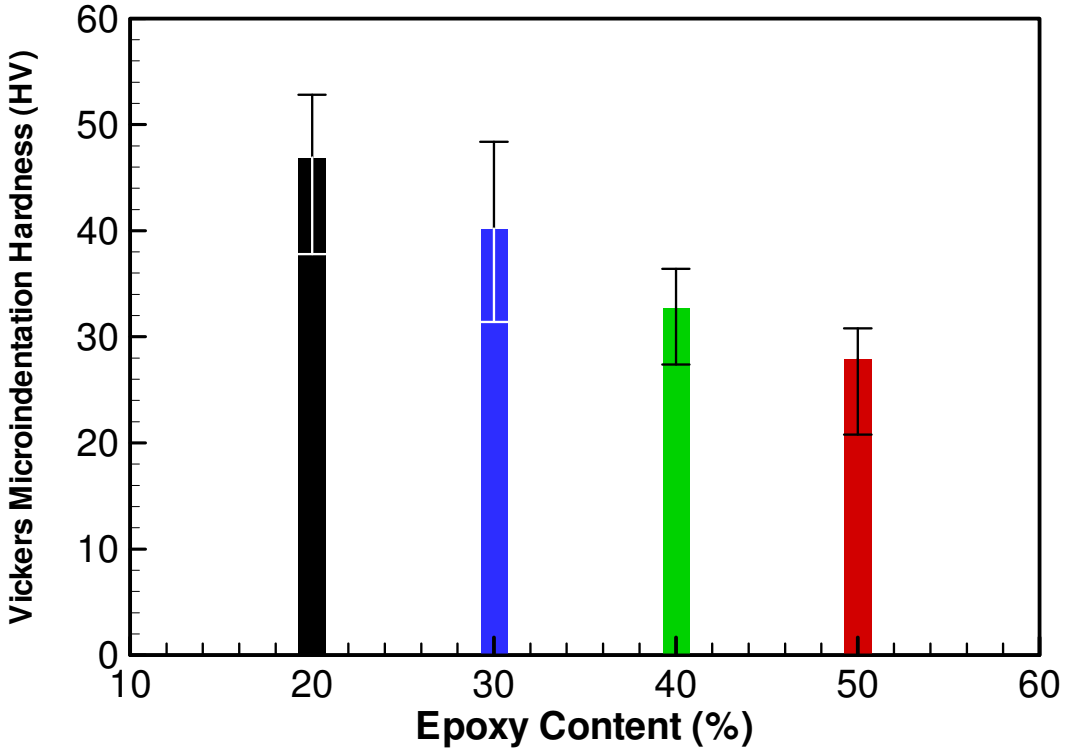

Figure 51: Vickers microindentation hardness for Al + Fe_2O_3 + Epoxy

Table 17: Summary of Vickers microindentation hardness for Al + Fe_2O_3 + Epoxy

Material Makeup	Average HV
50% Epoxy	27.9
40% Epoxy	32.7
30% Epoxy	40.2
20% Epoxy	46.9

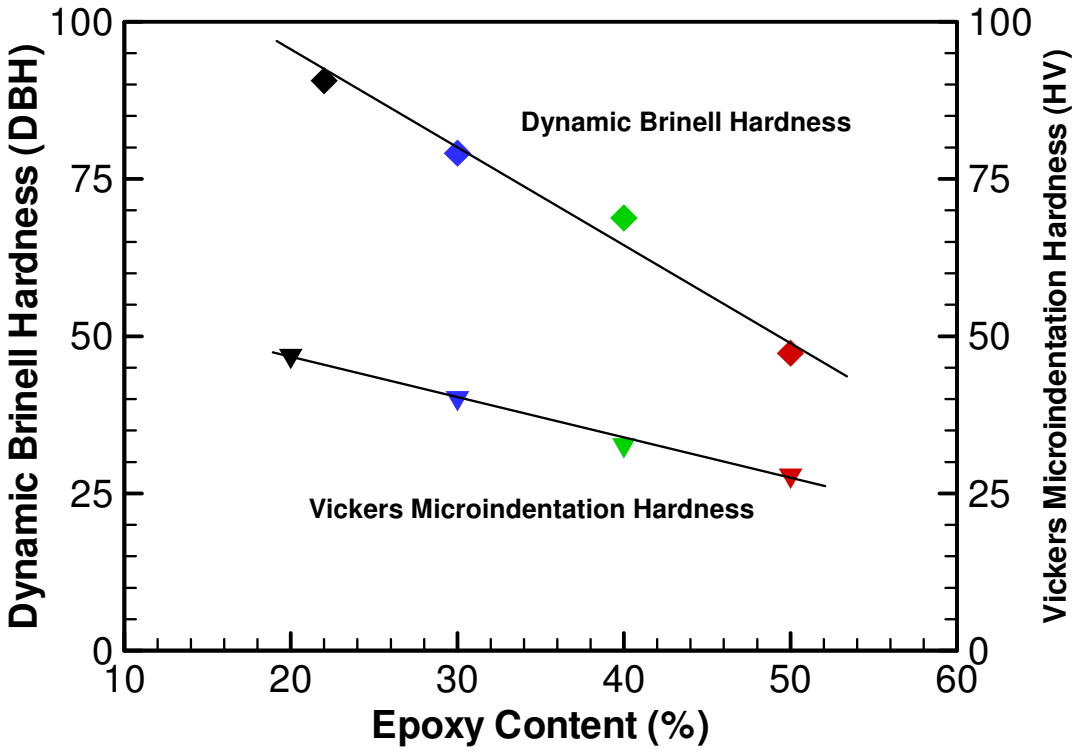

Figure 52: Dynamic and quasi-static hardness trends for Al + Fe_2O_3 + Epoxy

Table 18: Summary of parameters used for fitting of the Hasan-Boyce Model

	100%	50%	40%	30%	22%
ω_0 (Hz)	6.05×10^{15}	6.05×10^{15}	6.05×10^{15}	6.05×10^{15}	6.05×10^{15}
$\dot{\gamma}_0$ (s^{-1})	4.35×10^{16}	2.30×10^{16}	2.00×10^{16}	1.50×10^{16}	1.45×10^{16}
ξ	5	50	50	50	50
λ ($Å^3$/K)	1.45	2.0	2.0	2.0	2.0
α_{eq}^{-1} (eV^{-1})	1.87	1.87	1.87	1.87	1.87
a_{eq} (eV)	0.800	0.800	0.800	0.800	0.800
β_1	90	260	280	300	310
β_2	500	800	1000	1000	1100
β_3	900	1500	3000	5250	7000
$\Delta v_{\tau 0}^{*}$ ($Å^3$)	19.5	30.0	25.0	19.0	19.0
α_0^{-1} (eV^{-1})	1	1	1	1	1
a_0 (eV)	0.530	0.529	0.529	0.525	0.522
S_0 (eV)	-0.001	-0.001	-0.001	-0.001	-0.001

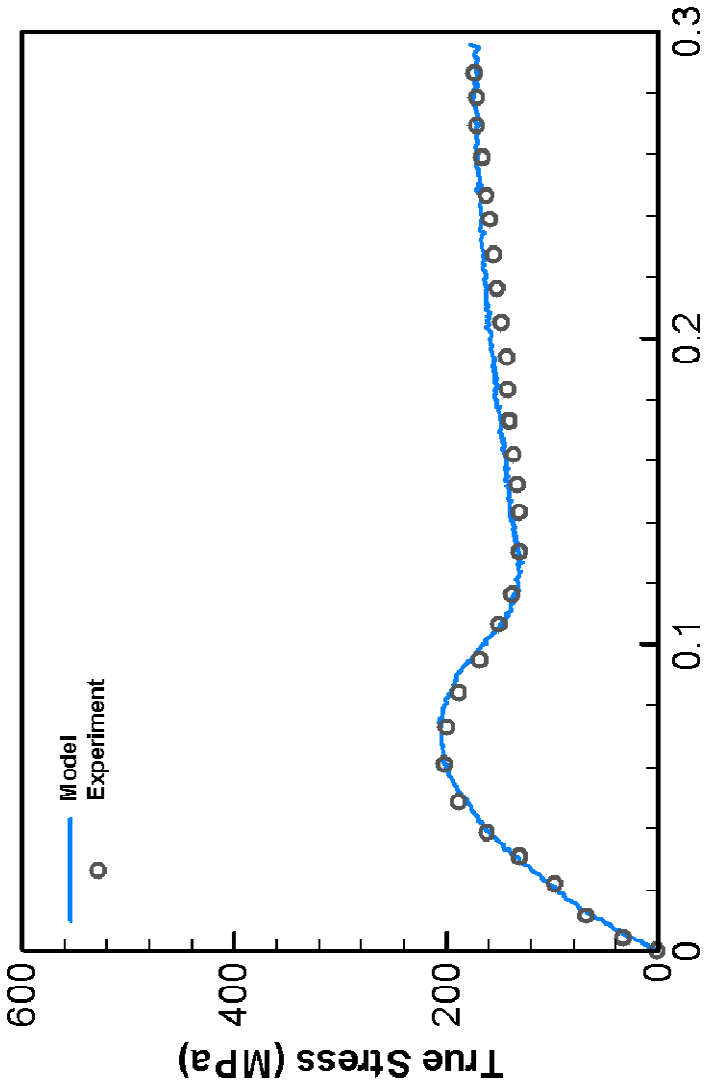

Figure 53: Comparison of Hasan-Boyce Model to 100% Epoxy experimental data

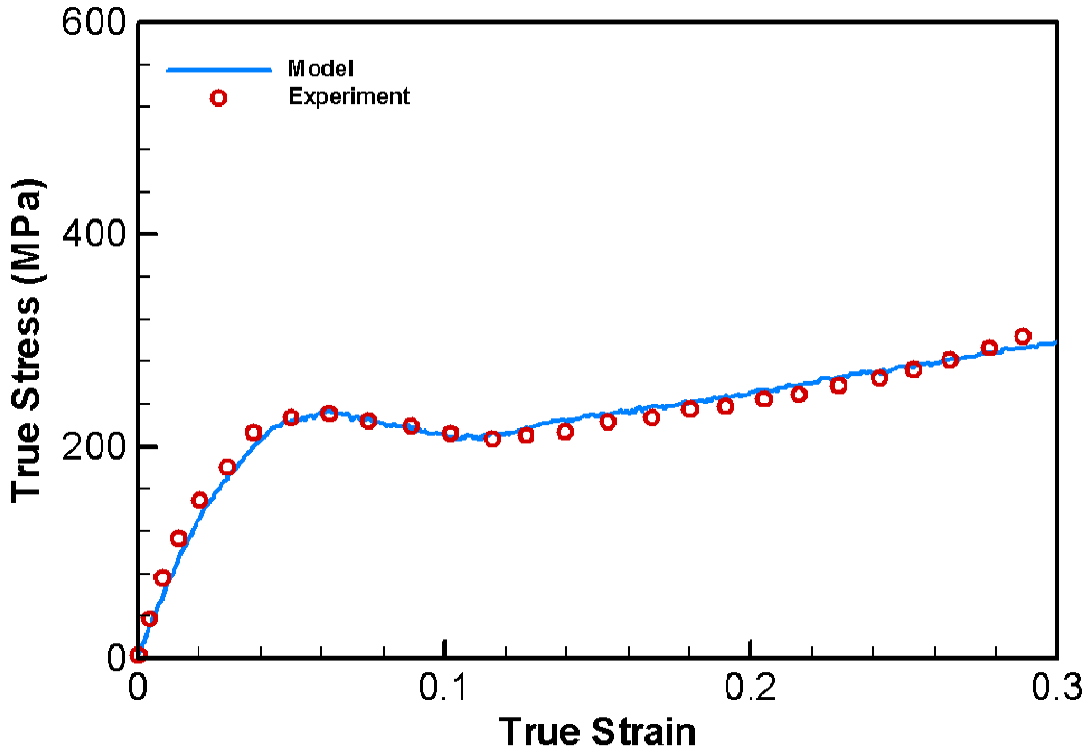

Figure 54: Comparison of Hasan-Boyce Model to Al + Fe_2O_3 + 50% Epoxy experimental data

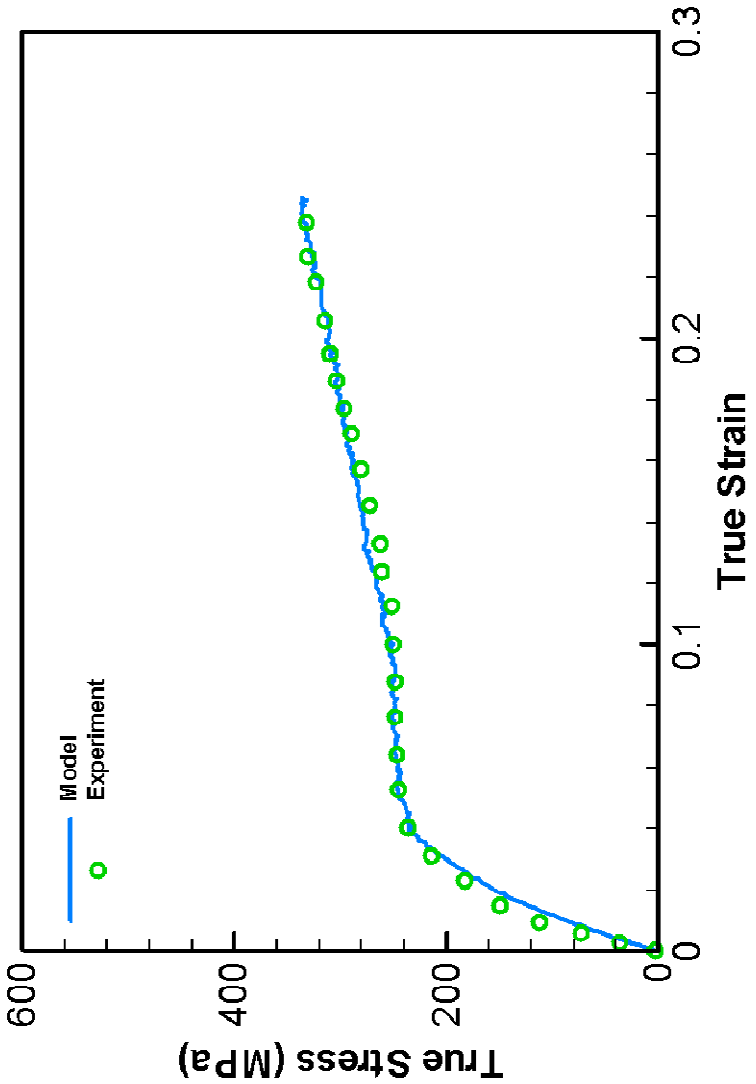

Figure 55: Comparison of Hasan-Boyce Model to Al + Fe_2O_3 + 40% Epoxy experimental data

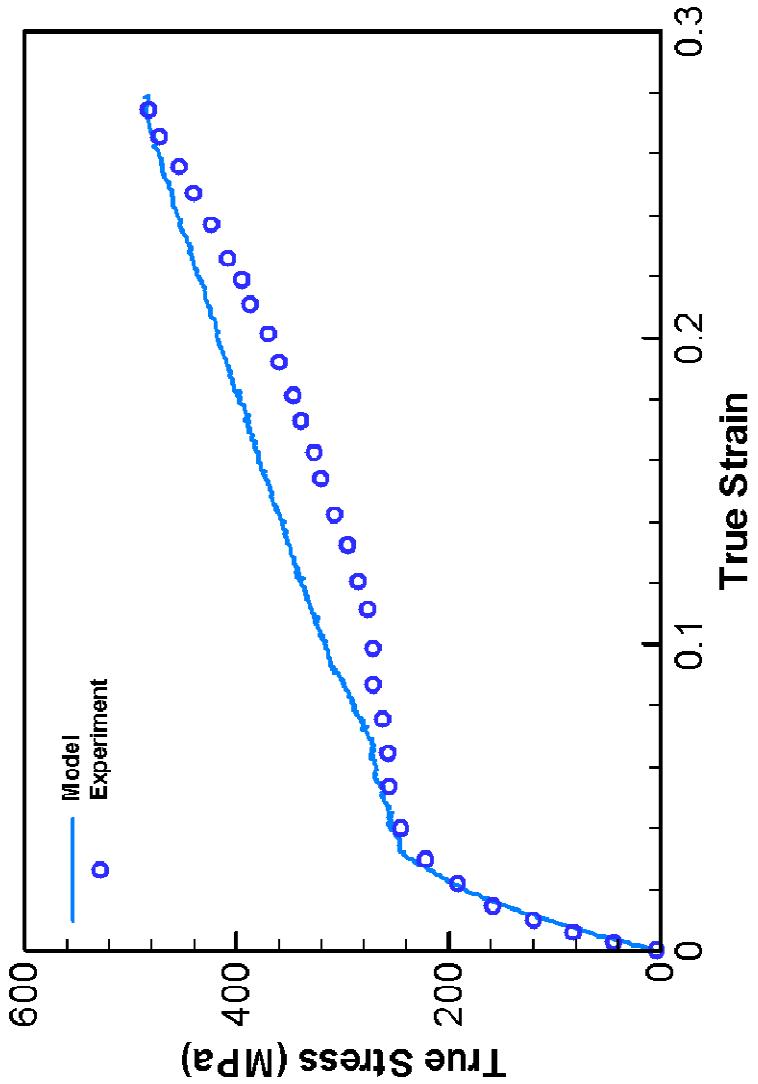

Figure 56: Comparison of Hasan-Boyce Model to Al + Fe_2O_3 + 30% Epoxy experimental data

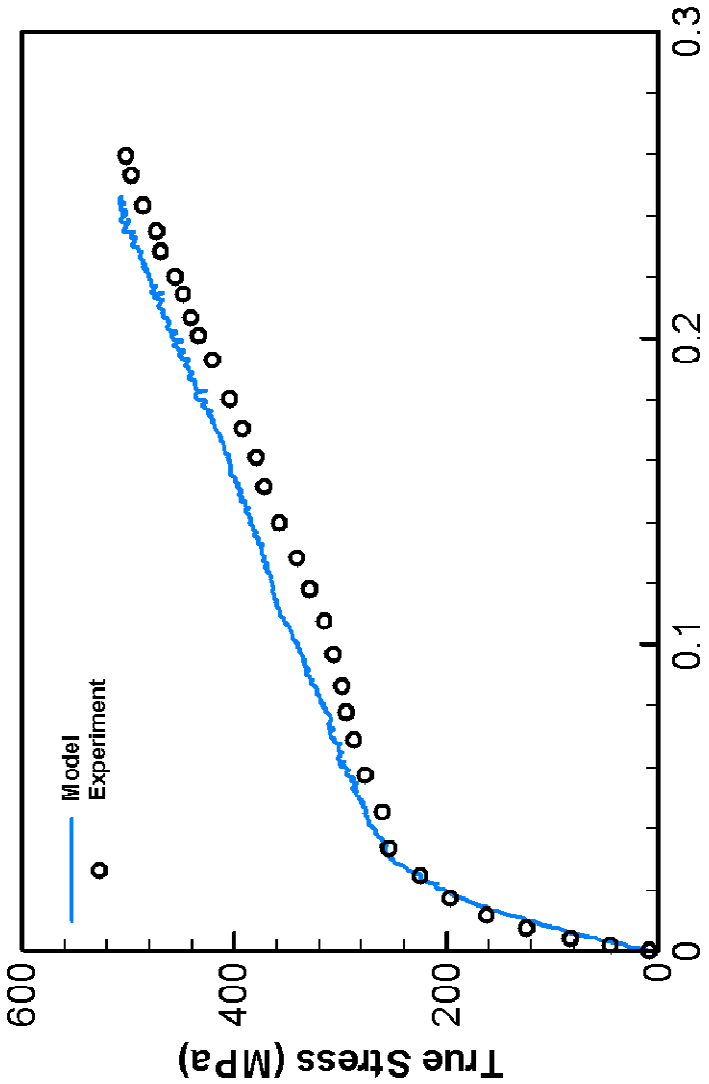

Figure 57: Comparison of Hasan-Boyce Model to Al + Fe_2O_3 + 22% Epoxy experimental data

CHAPTER IV
CONCLUSIONS AND RECOMMENDATIONS

4.1 Conclusions

In this study, the constitutive behavior of two MESMs was investigated in the intermediate strain rate regime. Al + Fe_2O_3 + Epoxy cast specimens along with shock compacted Ni-Al specimens were tested in compression using a split-Hopkinson pressure bar apparatus at strain rates on the order of 10^3 s^{-1}.

The Ni-Al specimens were subjected to a single loading pulse with the use of the soft-recovery method. The results of the experiments showed that the Ni-Al specimens experienced stress levels 25% higher than the strongest of the Al + Fe_2O_3 + Epoxy materials, but could only withstand low levels of strain (~10%) prior to fracture.

Results of the dynamic compression experiments on Al + Fe_2O_3 + Epoxy material revealed that deformation is dominated by the polymer phase. Pure epoxy is ductile in nature, with elastic-plastic hardening, softening, and perfectly plastic stages of deformation. The Al and Fe_2O_3 particles, when added to the epoxy, acted as particulate reinforcement to the matrix. Increasing the volume fraction of powders in the epoxy resulted in the vanishing of the softening phenomena and an increase in the work hardening effect. As a result, the stress work shows an increasing trend with the increase in volume fraction of powders.

The introduction of pores into Al + Fe_2O_3 + Epoxy specimens produced a negative effect on the strength characteristics. Stress concentrations in the regions

surrounding the pores generated high stress levels compared to the applied stress, which led to the formation and propagation of cracks, and subsequent fracture under the applied load.

Investigation into the unloading characteristics of the Al + Fe_2O_3 + Epoxy specimens revealed that back stresses within the polymer phase results in an unloading slope that is greater than the loading slope. Increased activation energy, a result of the presence of powders in the matrix, generates larger back stresses, increasing the difference between the unloading and loading slopes. The separation of the stress-strain curve into the loading and unloading portions allowed for the quantification of the plastic work and recoverable elastic work. As the binder content of the Al + Fe_2O_3 + Epoxy material decreased, the elastic work, slope of the loading, and slope of the unloading portions of the stress-strain curve increased.

Dynamic hardness measurements show that the hardness of Al + Fe_2O_3 + Epoxy materials increased with increasing volume fraction of powders. The trend of the increase is similar to the increase in stress at 30% strain for the mixtures. The quasi-static Vickers microindentation tests showed an increase in hardness with increasing volume content; however the rate of increase was less than that of the dynamic tests, displaying the strain rate dependence of the material.

The experimental results of 100% Epoxy and the Al + Fe_2O_3 + Epoxy specimens were fitted to the Hasan-Boyce model, which uses a distribution of activation energies to characterize the energy barrier of localized shear transformations. Based on the parameters that were fitted to pure epoxy and the mixtures, the increase in the volume fraction of powders points to an increase activation energy, decrease in the formation of

transformed sites, the redistribution of applied strain energy, and enhanced storage of inelastic work. These findings suggest that increasing the volume fraction of powders in the material will not only aid in the reinforcement of the polymer matrix, but will also aid in preventing the creation of transformation sites through an increase in the activation energy, resulting in a stronger material.

Based on the results of this study, it is determined that a further decrease in the binder content will not only result in enhanced strength characteristics, but can also increase the overall reactivity of the energetic material through more intimate contact between the reactive constituents.

4.2 Recommendations

The objective of this research was to characterize the mechanical response of two energetic structural materials under dynamic compression. During the course of this research, certain improvements in the testing methods have been noted to attempt to improve the results. The following recommendations are made to provide guidance for future work and the characterization of the mechanical response of energetic structural materials.

Based on the results of this study, a further increase in the volume fractions of powders will result in an increase in strength characteristics. From a synthesis standpoint, this may prove to be difficult, but further modifications to the synthesis procedure should be explored. This study was unable to point out the critical ratio of powders and epoxy that will yield maximum strength characteristics for the Al + Fe_2O_3 + Epoxy mixture. At this point, any further reduction of polymer binder will decrease the strength

characteristics due to the inability to properly provide a structural matrix for the powders, providing the best compromise between strength and energetic functionalities of the material.

The investigation to the thermal output of the Al + Fe_2O_3 + Epoxy materials during dynamic loading would be of interest. Even though the stress levels achieved on the SHPB apparatus are not sufficient enough to initiate reaction within the material, it would be beneficial to study the thermal output of the material due to the rapid loading applied by the SHPB apparatus. Li and Lambros (2001) investigated the thermal output of a polymer that was subjected to dynamic compressive loading. The use of a high speed infrared (IR) radiation detector allowed for the measurements of fast rise times and taking multi-point measurements. The results of the thermal output measurements can then be compared to the theoretical thermal output from the modified Hasan-Boyce model (Lu et al. 2001).

For future dynamic Brinell hardness experiments, the inter-frame time used on the IMACON 200 camera should be reduced from the 25 μs time used in this investigation. Despite the entire duration of the load lasting approximately 150 μs, only the application of the load, which lasts approximately 75 μs, is of interest. A reduction in the inter-frame time will also allow for more data points to be collected using the time-resolved dynamic Brinell hardness method.

To fully understand the Al + Fe_2O_3 + Epoxy material characteristics, specimens of smaller diameter should be tested to promote failure upon the application of the first loading pulse. The fully dense specimens used in this study had a 6.35 mm diameter, and did not fail during the application of the first load.

APPENDIX A
MATERIAL SYNTHESIS PROCEDURE AND MIXTURE SHEETS

A.1 Synthesis Procedure for Al + Fe_2O_3 + Epoxy

Prior to the synthesis of Al + Fe_2O_3 + Epoxy material, the aluminum molds, powders, and epoxy resin must be prepared. The surfaces of the aluminum molds are cleaned using acetone, and a thin layer of mold release is spread over all surfaces of the molds that the epoxy will come into contact with. The two halves of the molds are pressed together, and the bottom end and sides are sealed with high-temperature foil tape. The molds are preheated at 100ºC for at least an hour prior to the mixture being poured into them. The Al and Fe_2O_3 powders and epoxy resin used in the mixture are preheated in the oven as well to allow for evaporation of any moisture that may be present and decreasing the viscosity of the resin.

The material synthesis process starts with measuring out a portion of the aluminum powder into a disposable plastic beaker on a scale. The proper amount of EPON 826 resin is then added to the beaker. A special blender is attached to a drill and is used to mix the aluminum powder and the resin. It is important to mix the mixture such that there is homogeneous mixture of the aluminum within the resin. At this time, a portion of the Fe_2O_3 powder is added, and it is mixed again until the Fe_2O_3 is properly dispersed. This process is repeated until all predetermined portions of powders have been added and properly mixed into the epoxy. Next, if Toluene is going to be used, it is added at 5% of the weight of the solid powders. Finally, the Diethanolamine hardener is

added to the beaker. At lower binder contents, the viscosity of the mixture can become very high, making it difficult to achieve a homogeneous material. Heating the mixture between the addition of the portions of powders, the addition of Tolune, and the addition of the DEA hardener decreases the viscosity of the mixture.

The mixture can now be degassed prior to being poured into the molds. Degassing is done in a glass desiccator, with vacuum being pulled by an external pump; a vacuum gauge is used to measure the vacuum level within the desiccator. As vacuum is applied to the material in the plastic beaker, air bubbles are pulled out from within the material. By opening the valve to atmospheric pressure the material collapses back into the beaker. This process is repeated until a vacuum of 7.5×10^{-3} Pa (1 torr) is reached. The epoxy can now be poured into the molds that have already been prepared and heated in the oven at 100ºC for at least one hour. The molds can now be placed into the oven that is set to 100ºC for 24 hours to cure.

After the material has cured, the molds are removed from the oven and taken apart. The rods are removed from the molds and cleaned off using acetone. The molds are designed to be oversized (15.9 and 22.2 mm) so they can be machined to an exact diameter. This is done using a lathe in the Mechanical Engineering Machine Shop at the Georgia Institute of Technology. Once the rods are machined down to the correct diameter, then a linear precision saw with a diamond-tipped cutting blade is used to cut the specimens. The blade is set to run at 1250 revolutions per minute (rpm) and the linear feed rate is set at 0.25 inches per minute (in/min). The specimens are cut at a length of approximately 0.5 mm (0.02 in) above the desired specimen length. The ends of the specimens are polished on a rotating sander using 2400 grit paper. A steel cylinder with

an oversized hole is used to contain the specimen during sanding, and it ensures that the faces of the cylindrical specimens are perpendicular to the wall. The densities of the specimens are measured by the Archimedes' water immersion technique using a scale and density kit.

The subsequent sections contain the mixture sheets used to create the Al + Fe_2O_3 + Epoxy and 100% Epoxy specimens used in this study.

A.2 Al + Fe_2O_3 + 50% Epoxy Mixture Sheet

Date: 5/18/2004

Makeup: Al + Fe_2O_3 + 50% Epoxy + 5% Toluene

	Lot #	Date
EPON 826:	DMDL0027	4/14/2004
Aluminum:	03-4106	5/5/2004
Fe_2O_3:	897168	5/10/2004
DEA:	08412PB	5/10/2004
Toluene:	I24N01	4/21/2004

Sample ID	**Dimensions**
GT-CT-080A	5/8" Diameter
GT-CT-080B	5/8" Diameter

Wt %	Material	Mass (g)	Actual Mass (g)
0.9231	Epon 826	80.8	80.8
0.2526	Al	22.1	7.3+7.6+7.2 = 22.1
0.7474	Fe_2O_3	65.4	21.8+21.8+21.8 = 65.4
0.05xsolid	Toluene	4.4	4.4
0.0769	DEA	6.7	6.7

	Time Out	Time In
1. Mix Al, Fe_2O_3, Epon 826 and place in oven		11:32 (5/18)
2. Mix Toluene and place back in oven	13:23 (5/18)	13:27 (5/18)
3. Mix DEA and place back in oven	13:35 (5/18)	13:38 (5/18)
4. Degas and place back in oven	14:12 (5/18)	14:17 (5/18)

Degas Time: 4 min **Vacuum Level:** 1.6 torr

5. Mixture poured in molds and in the oven	14:22 (5/18)	14:23 (5/18)

Comments: Mixed in powder in 3 steps
Used spatula to mix powders for first and second step
Used blender to mix before & after addition of toluene & DEA
Flowed and degassed well
Poured into molds well
Avg. cure temperature: ~100ºC
8:15 (5/19) molds opened, placed back in oven

A.3 Al + Fe_2O_3 + 40% Epoxy Mixture Sheet

Date: 5/18/2004

Makeup: Al + Fe_2O_3 + 40% Epoxy + 5% Toluene

	Lot #	Date
EPON 826:	DMDL0027	4/14/2004
Aluminum:	03-4106	5/5/2004
Fe_2O_3:	897168	5/10/2004
DEA:	08412PB	5/10/2004
Toluene:	I24N01	4/21/2004

Sample ID	**Dimensions**
GT-CT-081A	5/8" Diameter
GT-CT-081B	5/8" Diameter

Wt %	Material	Mass (g)	Actual Mass (g)
0.9231	Epon 826	64.6	64.6
0.2526	Al	26.5	8.9+9.1+8.5 = 26.5
0.7474	Fe_2O_3	78.5	26.1+25.9+26.5 = 78.5
0.05xsolid	Toluene	5.3	5.3
0.0769	DEA	5.4	5.4

	Time Out	Time In
1. Mix Al, Fe_2O_3, Epon 826 and place in oven		13:22 (5/18)
2. Mix Toluene and place back in oven	14:08 (5/18)	14:12 (5/18)
3. Mix DEA and place back in oven	14:38 (5/18)	14:40 (5/18)
4. Degas and place back in oven	15:56 (5/18)	16:02 (5/18)

Degas Time: 7 min **Vacuum Level:** 2.0 torr

5. Mixture poured in molds and in the oven	16:33 (5/18)	16:38 (5/18)

Comments: Mixed in powder in 3 steps
Placed in oven between 2nd & 3rd mixing step
Used spatula to mix powders for first and second step
Used blender to mix before & after addition of toluene & DEA
Degassed only to 2.0 torr
First rod poured well, second did not
→ Should place mixture back in oven after pouring 1st rod
Avg. cure temperature: ~100ºC
8:45 (5/19) molds opened, placed back in oven

A.4 Al + Fe_2O_3 + 30% Epoxy Mixture Sheet

Date: 5/19/2004

Makeup: Al + Fe_2O_3 + 30% Epoxy + 5% Toluene

	Lot #	Date
EPON 826:	DMDL0027	4/14/2004
Aluminum:	03-4106	5/5/2004
Fe_2O_3:	897168	5/10/2004
DEA:	08412PB	5/10/2004
Toluene:	I24N01	4/21/2004

Sample ID	**Dimensions**
GT-CT-084A	5/8" Diameter
GT-CT-084B	5/8" Diameter

Wt %	Material	Mass (g)	Actual Mass (g)
0.9231	Epon 826	69.2	69.2
0.2526	Al	44.2	11.1+10.9+11.0+11.2 = 44.2
0.7474	Fe_2O_3	130.8	32.7+32.9+34.6+30.6 = 130.8
0.05xsolid	Toluene	8.8	8.8
0.0769	DEA	5.8	5.8

	Time Out	Time In
1. Mix Al, Fe_2O_3, Epon 826 and place in oven		19:00 (5/19)
2. Mix Toluene and place back in oven	13:21 (5/20)	13:24 (5/20)
3. Mix DEA and place back in oven	14:27 (5/20)	14:31 (5/20)
4. Degas and place back in oven	15:02 (5/20)	15:09 (5/20)
Degas Time: 6 min **Vacuum Level:** 3.0 torr		
5. Mixture poured in molds and in the oven	15:39 (5/20)	15:41 (5/20)

Comments: Mixed 1st & 2nd sets of powder, put in oven at 11:11 (5/19)
Mixed 3rd & 4th Al & 3rd Fe2O3 @ 17:00 (5/19) in oven 17:25
Mixed 4th Fe2O3 in oven 19:00 (5/19)
Use blender to mix in all steps, left blender in oven with mix.
Degassed only to 3.0 torr
Avg. cure temperature: ~100ºC
10:26 (5/20) molds opened, back in oven
17:34 (5/23), put molds in small oven (~90ºC)
→ Shut power off to slow cool
Placed mixture back in oven after pouring first rod (~20 minutes)
→ 2nd rod still did not pour well

A.5 Al + Fe_2O_3 + 22% Epoxy Mixture Sheet

Date: 2/4/2004

Makeup: Al+Fe_2O_3+22% Epoxy+5% Toluene

	Lot #	Date
EPON 826:	Unknown	11/22/2003
Aluminum:		
Fe_2O_3:		
DEA:	Unknown	11/22/2003
Toluene:		

Sample ID	Dimensions
GT-CT-058B	7/8" Diameter
GT-CT-058D	5/8" Diameter

Wt %	Material	Mass (g)	Actual Mass (g)
0.9231	Epon 826	138.5	138.6
0.2526	Al	132.7	38.2+19.8+18.3+18.8+18.9+18.9 = 132.9
0.7474	Fe_2O_3	392.1	112.1+56.0+56.0+56.6+56.1+56.0 = 392.8
0.05xsolid	Toluene	29.5	0+0+0+14.9+0+14.9 = 29.8
0.0769	DEA	11.5	0+0+0+0+0+0+11.5 = 11.5

	Time Out	Time In
1. Mix Al, Fe_2O_3, Epon 826 and place in oven		
2. Mix Toluene and place back in oven		
3. Mix DEA and place back in oven		
4. Degas and place back in oven		

Degas Time: **Vacuum Level:**

5. Mixture poured in molds and in the oven		

Comments: Blender remained in mixture during heating

A.6 100% Epoxy Mixture Sheet

Date: 2/18/014

Makeup: 100% Epoxy

	Lot #	Date
EPON 826:	Unknown	11/22/2003
Aluminum:		
Fe_2O_3:		
DEA:	Unknown	11/22/2003
Toluene:		

Sample ID	Dimensions
GT-CT-059A	5/8" Diameter
GT-CT-059B	5/8" Diameter

Wt %	Material	Mass (g)	Actual Mass (g)
0.9231	Epon 826	184.6	184.6
0.2526	Al	0.0	0
0.7474	Fe2O3	0.0	0
0.05xsolid	Toluene	0.0	0
0.0769	DEA	7.7	15.4

Time Out	Time In

1. Mix Al, Fe_2O_3, Epon 826 and place in oven
2. Mix Toluene and place back in oven
3. Mix DEA and place back in oven
4. Degas and place back in oven

Degas Time: **Vacuum Level:**

5. Mixture poured in molds and in the oven

Comments:

APPENDIX B
MATHCAD: DYNAMIC CONSTITUTIVE RESPONSE ANALYSIS

DATA FROM TEST EXPERIMENT PERFORMED ON 6/20/2004
Specimen: GT-CT-080A-08

$V_e := 30 \cdot volt$ Exitation Voltage

$P := 100 \cdot psi$ Gun Pressure

$P = 6.8948 \cdot 10^5 \cdot Pa$

$D_o := 0.75 \cdot in$ Bar Diameter

$D := .2490 \cdot in$ Specimen Diameter

$L := .2545 \cdot in$ Specimen Length

$I := READPRN(DAT1)$ Read Experimental Data

$O := READPRN(DAT2)$

$n := rows(I)$

$n = 4000$

$usec := \frac{sec}{10^6}$

$i := 0 .. (n - 1)$ Number of Data points

$Time_i := I_{i,1} \cdot sec$ Define the time variable as :

$Time_i$

$V_i := I_{i,0} \cdot volt$ Define the impact-bar bridge voltage reading as:

V_i

$Vo_i := O_{i,0} \cdot volt$ Define the output-bar bridge voltage reading as:

Vo_i

Calculate the average voltage recorded by the osciliscope prior to the triggering event

$r := 0 .. 100$ Data Points Prior to Triggering

$V_{395} = 9.6 \cdot 10^{-5} \cdot volt$

$ave_i := \frac{\sum V_r}{101}$

$ave_i = 9.7267 \cdot 10^{-5} \cdot volt$ Average input- bar bridge reading

$ave_o := \frac{\sum Vo_r}{101}$

$ave_o = -1.9802 \cdot 10^{-4} \cdot volt$ Average output- bar bridge reading

Correct the oscillicope readings for the non zero initial voltage reading.

$VC_i := I_{i,0} \cdot volt - ave_i$ Corrected input-bar voltage

$VoC_i := O_{i,0} \cdot volt - ave_o$ Corrected output-bar voltage

Plot the corrected voltage readings versus time

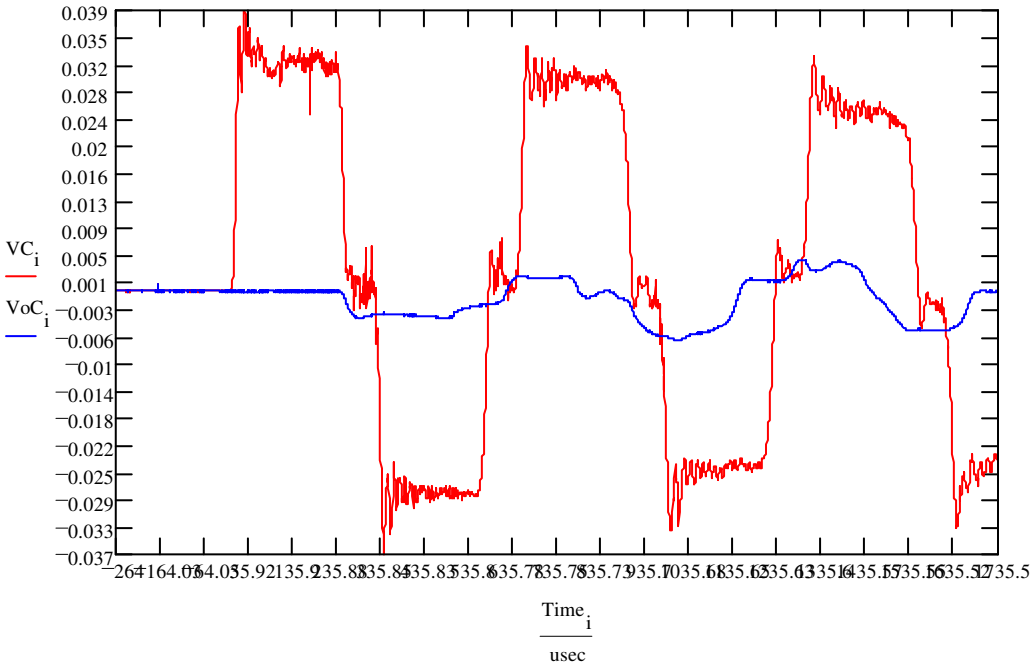

Calculate the Strain Measured by the Strain Gauges

$f := 2.04$ Strain Gauge Factor

$GPa := Pa \cdot 10^9$

$\varepsilon_{i_i} := \frac{2 \cdot VC_i}{f \cdot V_e}$ Defines strain for the impact-bar gauge

$\varepsilon_{t_i} := \frac{2 \cdot VoC_i}{f \cdot V_e}$ Defines strain for the output-bar gauge

Calculate the wave speed in the Hopkinson bar

$E := 200 \cdot GPa$ Young's Modulus

$\rho := 8100 \frac{kg}{m^3}$ Mass Density

$C_o := \sqrt{\frac{E}{\rho}}$

$C_o = 4969.0399 \frac{m}{sec}$

Incident Pulse Duration:

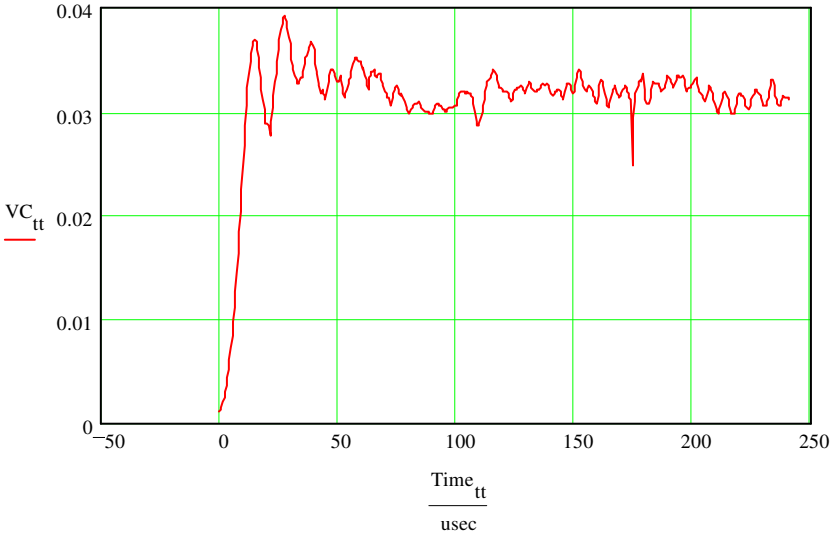

Specimen Stress calculation

Plot the Voltage Output (Transmitted Wave)

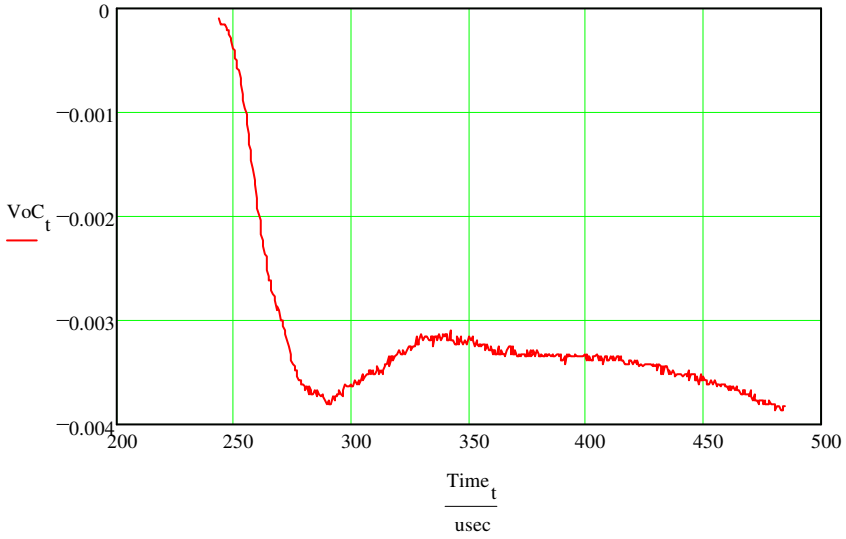

$A_o := \frac{\pi \cdot D_o^2}{4}$ Hopkinson Bar Cross sectional area

$A_o = 2.8502 \cdot 10^{-4}\ \cdot m^2$

$A := \frac{\pi \cdot D^2}{4}$ Specimen Cross sectional area

$A = 3.1416 \cdot 10^{-5}\ \cdot m^2$

$MPa := Pa \cdot 10^6$

Calculate specimen Stress from Transmitted Wave

$$\sigma_t := -E \cdot \frac{A_o}{A} \cdot \varepsilon_t$$

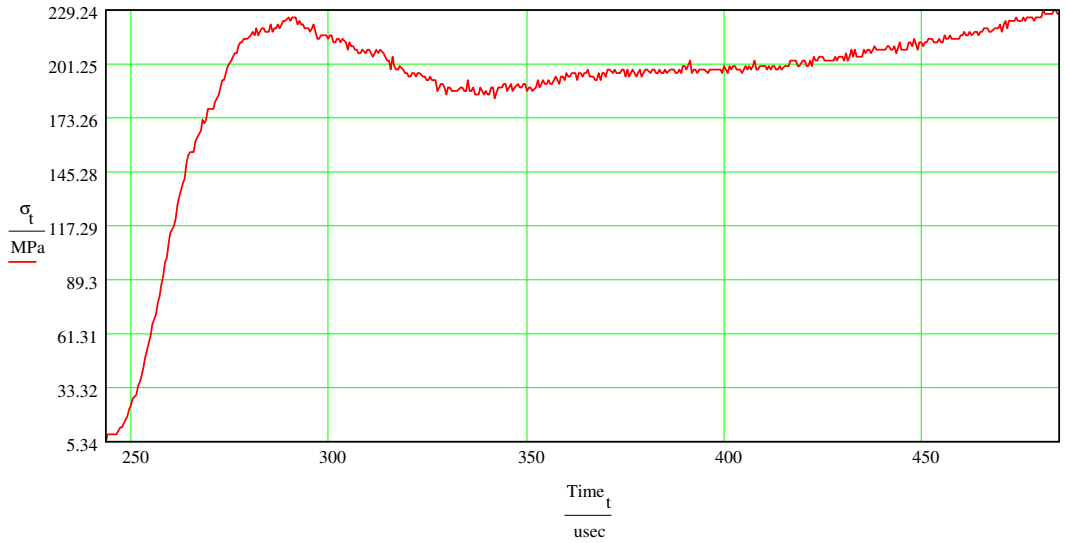

Duration of Reflected Wave:

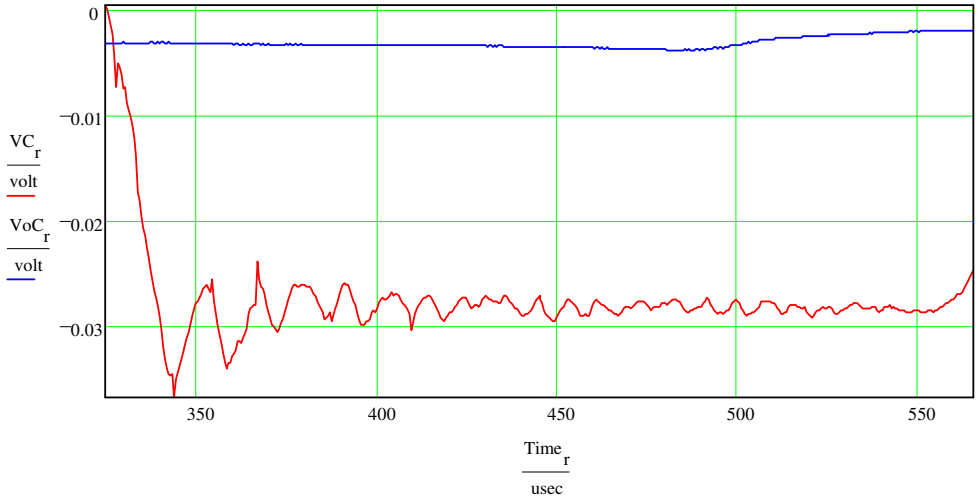

Calculate Strain Rate in sample:

$$\varepsilon dot_{jj} := \frac{-2 \cdot C_o}{L} \cdot \left(\varepsilon i_{jj+q} \right)$$

$$\varepsilon dot2_{jj} := \frac{C_o}{L} \cdot \left[\left(\varepsilon i_{jj+wb} - \varepsilon i_{jj+q} \right) - \varepsilon t_{jj+w} \right]$$

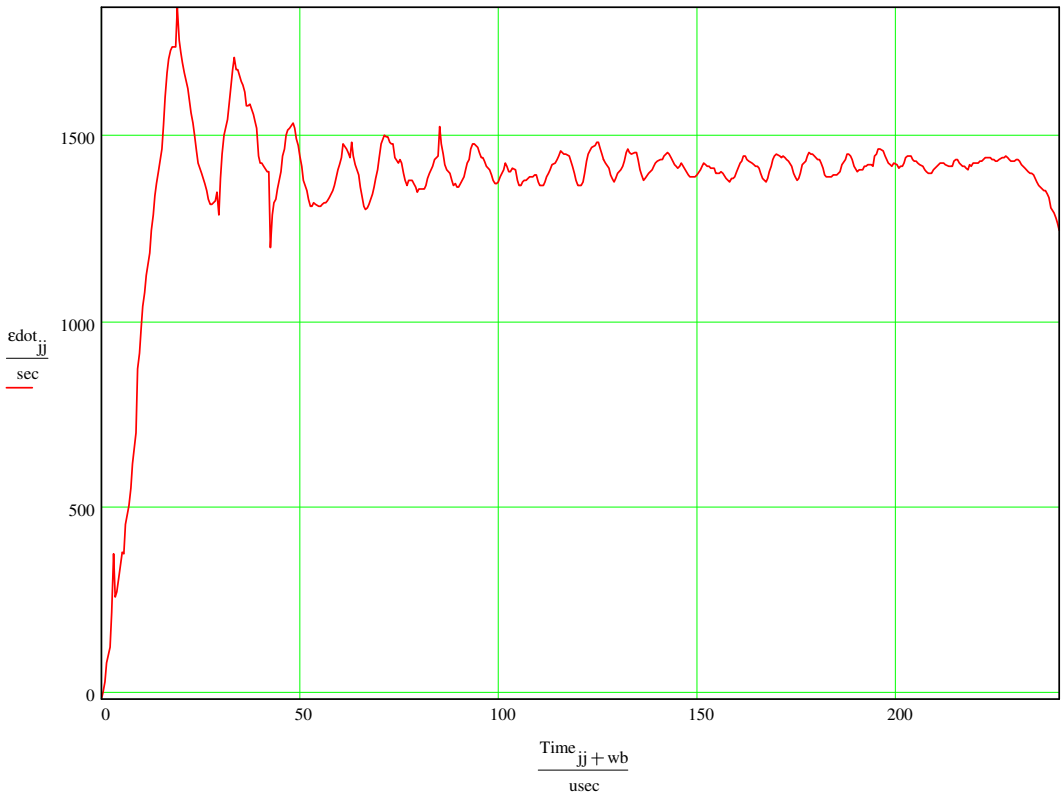

$$\varepsilon dot_r := \frac{-2 \cdot C_o}{L} \cdot \left(\varepsilon i_r \right)$$

Calculate Strain from Strain Rate in Sample:

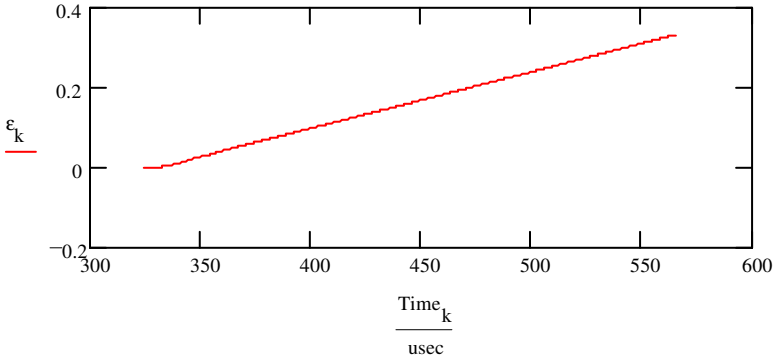

Plot Stress vs. Strain in sample:

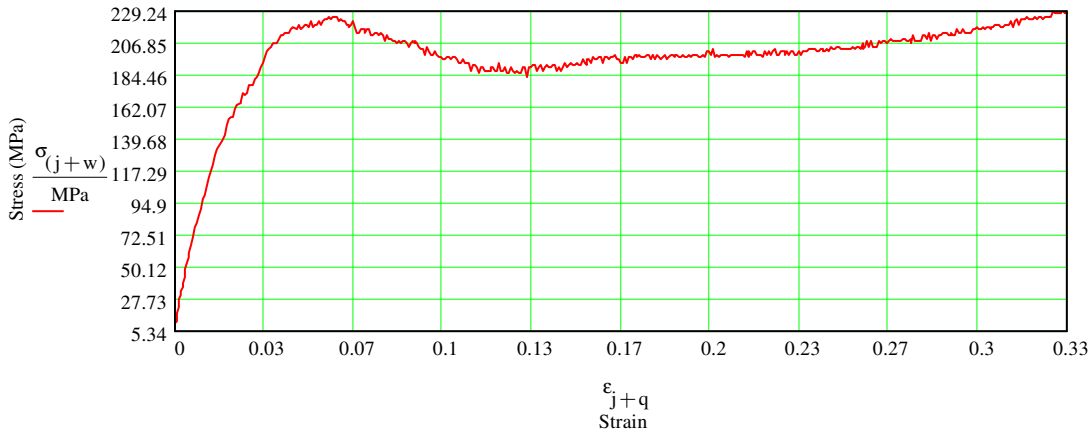

$ss_j := \frac{\sigma_{(j+w)}}{MPa}$

$straint_{k,0} := \frac{Time_k}{usec}$

$strainra_{r,1} := \frac{\epsilon dot_r}{\left(\frac{1}{sec}\right)}$

$st_j := \varepsilon_{j+q}$

$strainra_{r,0} := \frac{Time_r}{usec}$

$Dat_{j,1} := ss_j$

$Dat_{j,0} := st_j$

$straint_{k,1} := \varepsilon_k$

$WRITEPRN(strainrate) := strainra$

$WRITEPRN(stress\_strain) := Dat$

$WRITEPRN(strain) := straint$

$ss1_{j,1} := \frac{\sigma incident_j}{MPa}$

$ss1_{j,0} := \frac{Time_{j+wb}}{usec}$

$D1_{j,0} := st_j$

$D1_{j,1} := ss1_{j,1}$

$ss2_{j,1} := \frac{\sigma transmitter_j}{MPa}$

$ss2_{j,0} := \frac{Time_{j+wb}}{usec}$

$D2_{j,0} := st_j$

$D2_{j,1} := ss2_{j,1}$

$$ss3_{j,1} := \frac{\sigma_{ave_j}}{MPa}$$

$$ss3_{j,0} := \frac{Time_{j+wb}}{usec}$$

$$D3_{j,0} := st_j$$

$$D3_{j,1} := ss3_{j,1}$$

WRITEPRN(stime_incident) := ss1

WRITEPRN(ss_incident) := D1

WRITEPRN(stime_trans) := ss2

WRITEPRN(ss_trans) := D2

WRITEPRN(stime_ave) := ss3

WRITEPRN(ss_ave) := D3

APPENDIX C
MATLAB: STRESS WORK ANALYSIS CODE

This program is used to calculate the stress work of dynamic compressive experiments conducted in this study. The input for the program is the "stress_strain.prn" file, which is an output of the Mathcad program described in Appendix B, the gas gun pressure (psi), and the confinement condition of the experiment. The output is a plot of the stress-strain curve with the stress work results displayed in this figure (Figure 58). The "Data" variable complies the gas gun pressure, maximum strain value, maximum stress value, total stress work, and stress work at various strain levels into one matrix that can be imported into a graphics program or a database of experimental results.

```
format
%Set working directory to directory with tests
cd('C:\Documents and Settings\nitinp\My Documents\Research\GT-CT-059AB');

%Loads the incident bar waveform using a dialog box
[file,dirpath] = uigetfile('stress_strain.prn','Choose stress_strain.prn');
wholefilepath = [dirpath file];
stress_strain = load(wholefilepath);

%Set working directory back to Matlab's working directory
cd('C:\MATLAB6p5\work');

S = file;

%Cut extension off of "file"
file2 = num2str(file);
w = length(file2) - 4;
file_name = file2(1,1:w);
disp(file_name)
```

```
%Cut extension off of "wholefilepath"
wholefilepath1 = num2str(wholefilepath);
w = length(wholefilepath1) - 4;
wholefilepath2 = wholefilepath1(1,1:w);

%Find Shot Number
t = length(file_name);
r1 = file_name(1,t-1:t);
q = str2num(r1);

Input Gas Gun Pressure
PSI = input('psi= ','s');

Input Confinement condition
confinement_input = input('Unconfined (Enter "u") or Confined (Enter "c"): ','s');
switch lower(confinement_input)
   case 'u'
      confinement = 'Unconfined';
   case 'c'
      confinement = 'Confined';
end

%Loads the file into the program and breaks up the columns
strain = stress_strain(:,1);
stress = stress_strain(:,2);

%Finds maximum strain, stress and length of file
[x,k] = max(strain);       %x is the value of max strain and k is the index of max strain
j1 = max(stress);          %j1 is the value of max stress
l_s = length(strain);      %l is the length of the strain column

%Find the total energy
Total_energy = trapz(strain,stress);

if x < 0.25   %If max strain is less than 25%

   s = strain*1000;    %Changes the strain values into integers
   w = int2str(s);     %Changes the s vector into a vector of strings
   s = str2num(w);     %Changes the w vector into a vector of numbers
   j = s(l_s,1);       %Finds the last number in the s vector

    if j > 10          %Calculates the energy up to 1% strain
      one = find(s == 10);
      one = one(1,1);
      one1 = strain(1:one,1);
```

```
    one2 = stress(1:one,1);
    Strain_one = trapz(one1,one2);
end

    if j > 20          %Calculates the energy up to 2% strain
    two = find(s == 20);
    two = two(1,1);
    two1 = strain(1:two,1);
    two2 = stress(1:two,1);
    Strain_two = trapz(two1,two2);
end

    if j > 30          %Calculates the energy up to 3% strain
    three = find(s == 30);
    three = three(1,1);
    three1 = strain(1:three,1);
    three2 = stress(1:three,1);
    Strain_three = trapz(three1,three2);
end

if j > 40              %Calculates the energy up to 4% strain
    four = find(s == 40);
    four = four(1,1);
    four1 = strain(1:four,1);
    four2 = stress(1:four,1);
    Strain_four = trapz(four1,four2);
end

if j >= 50             %Calculates the energy up to 5% strain
    five = find(s == 50);
    five = five(1,1);
    five1 = strain(1:five,1);
    five2 = stress(1:five,1);
    Strain_five = trapz(five1,five2);
end

    if j >= 60         %Calculates the energy up to 6% strain
    six = find(s == 60);
    six = six(1,1);
    six1 = strain(1:six,1);
    six2 = stress(1:six,1);
    Strain_six = trapz(six1,six2);
end

    if j >= 70         %Calculates the energy up to 7% strain
    seven = find(s == 70);
```

```
        seven = seven(1,1);
        seven1 = strain(1:seven,1);
        seven2 = stress(1:seven,1);
        Strain_seven = trapz(seven1,seven2);
    end

    if j >= 80              %Calculates the energy up to 8% strain
        eight = find(s == 80);
        eight = eight(1,1);
        eight1 = strain(1:eight,1);
        eight2 = stress(1:eight,1);
        Strain_eight = trapz(eight1,eight2);
    end

        if j >= 90          %Calculates the energy up to 9% strain
        nine = find(s == 90);
        nine = nine(1,1);
        nine1 = strain(1:nine,1);
        nine2 = stress(1:nine,1);
        Strain_nine = trapz(nine1,nine2);
    end

    if j >= 100          %Calculates the energy up to 10% strain
        ten = find(s == 100);
        ten = ten(1,1);
        ten1 = strain(1:ten,1);
        ten2 = stress(1:ten,1);
        Strain_ten = trapz(ten1,ten2);
    end
end

if x >= 0.25   %If max strain is greater than 25%
    s = strain*100;
    w = int2str(s);
    s = str2num(w);
    j = s(l_s,1);

    if j >= 5          %Calculates the energy up to 5% strain
        five = find(s == 5);
        five = five(1,1);
        five1 = strain(1:five,1);
        five2 = stress(1:five,1);
        Strain_five = trapz(five1,five2);
    end

    if j >= 10          %Calculates the energy up to 10% strain
```

```
    ten = find(s == 10);
    ten = ten(1,1);
    ten1 = strain(1:ten,1);
    ten2 = stress(1:ten,1);
    Strain_ten = trapz(ten1,ten2);
end

if j >= 15          %Calculates the energy up to 15% strain
    fifteen = find(s == 15);
    fifteen = fifteen(1,1);
    fifteen1 = strain(1:fifteen,1);
    fifteen2 = stress(1:fifteen,1);
    Strain_fifteen = trapz(fifteen1,fifteen2);
end

if j >= 20          %Calculates the energy up to 20% strain
    twenty = find(s == 20);
    twenty = twenty(1,1);
    twenty1 = strain(1:twenty,1);
    twenty2 = stress(1:twenty,1);
    Strain_twenty = trapz(twenty1,twenty2);
end

if j >= 25          %Calculates the energy up to 25% strain
    twentyfive = find(s == 25);
    twentyfive = twentyfive(1,1);
    twentyfive1 = strain(1:twentyfive,1);
    twentyfive2 = stress(1:twentyfive,1);
    Strain_twentyfive = trapz(twentyfive1,twentyfive2);
end

if j >= 30          %Calculates the energy up to 30% strain
    thirty = find(s == 30);
    thirty = thirty(1,1);
    thirty1 = strain(1:thirty,1);
    thirty2 = stress(1:thirty,1);
    Strain_thirty = trapz(thirty1,thirty2);
end

if j >= 35          %Calculates the energy up to 35% strain
    thirtyfive = find(s == 35);
    thirtyfive = thirtyfive(1,1);
    thirtyfive1 = strain(1:thirtyfive,1);
    thirtyfive2 = stress(1:thirtyfive,1);
    Strain_thirtyfive = trapz(thirtyfive1,thirtyfive2);
end
```

```
    if j >= 40          %Calculates the energy up to 40% strain
        forty  = find(s == 40);
        forty = forty(1,1);
        forty1 = strain(1:forty,1);
        forty2 = stress(1:forty,1);
        Strain_fourty = trapz(forty1,forty2);
    end

    if j >= 45          %Calculates the energy up to 45% strain
        fortyfive  = find(s == 45);
        fortyfive = fortyfive(1,1);
        fortyfive1 = strain(1:fortyfive,1);
        fortyfive2 = stress(1:fortyfive,1);
        Strain_fourtyfive = trapz(fortyfive1,fortyfive2);
    end

    if j >= 50          %Calculates the energy up to 50% strain
        fifty = find(s == 50);
        fifty = fifty(1,1);
        fifty1 = strain(1:fifty,1);
        fifty2 = stress(1:fifty,1);
        Strain_fifty = trapz(fifty1,fifty2);
    end
end

%Ablsolute value of Strain Vectors
strain = abs(strain);

%Plot the Stress vs. Strain, Loading, and Unloading
clf
plot(strain,stress), title('Stress vs. Strain'), xlabel('Strain'), ylabel('Stress (MPa)')
axis_strain = 1.1*x;
axis_stress = 1.1*j1;
axis([0 axis_strain 0 axis_stress]);

%Display boxes on figure with information
uicontrol('string', 'Specimen ID', 'position',[390 225 100 25]);
uicontrol('string', file_name, 'position',[490 225 100 25]);
uicontrol('string', 'PSI', 'position',[390 200 100 25]);
uicontrol('string', PSI, 'position',[490 200 100 25]);
uicontrol('string', 'Confinement', 'position',[390 175 100 25]);
uicontrol('string', confinement, 'position',[490 175 100 25]);
uicontrol('string', 'Max Strain', 'position',[390 150 100 25]);
uicontrol('string', x, 'position',[490 150 100 25]);
uicontrol('string', 'Max Stress', 'position',[390 125 100 25]);
```

```
uicontrol('string', j1, 'position',[490 125 100 25]);
uicontrol('string', 'Total Energy', 'position',[390 100 100 25]);
uicontrol('string', Total_energy, 'position',[490 100 100 25]);

P = str2num(PSI);

%Displays Energy information for given strain values if strain is less than 25%
if x < 0.25
   if j >= 10
      uicontrol('string', 'Energy 1%', 'position',[600 225 70 25]);
      uicontrol('string', Strain_one, 'position',[670 225 70 25]);
      Data = [P, x, j1, Total_energy, Strain_one, -10, -10, -10, -10, -10, -10, -10, -10, -10];
   end
   if j >= 20
      uicontrol('string', 'Energy 2%', 'position',[600 200 70 25]);
      uicontrol('string', Strain_two, 'position',[670 200 70 25]);
      Data = [P, x, j1, Total_energy, Strain_one, Strain_two, -10, -10, -10, -10, -10, -10, -
10, -10];
   end
   if j >= 30
      uicontrol('string', 'Energy 3%', 'position',[600 175 70 25]);
      uicontrol('string', Strain_three, 'position',[670 175 70 25]);
      Data = [P, x, j1, Total_energy, Strain_one, Strain_two, Strain_three, -10, -10, -10, -
10, -10, -10, -10];
   end
   if j >= 40
      uicontrol('string', 'Energy 4%', 'position',[600 150 70 25]);
      uicontrol('string', Strain_four, 'position',[670 150 70 25]);
      Data = [P, x, j1, Total_energy, Strain_one, Strain_two, Strain_three, Strain_four, -10,
-10, -10, -10, -10, -10];
   end
   if j >= 50
      uicontrol('string', 'Energy 5%', 'position',[600 125 70 25]);
      uicontrol('string', Strain_five, 'position',[670 125 70 25]);
      Data = [P, x, j1, Total_energy, Strain_one, Strain_two, Strain_three, Strain_four,
Strain_five, -10, -10, -10, -10, -10];
   end
   if j >= 60
      uicontrol('string', 'Energy 6%', 'position',[750 225 70 25]);
      uicontrol('string', Strain_six, 'position',[820 225 70 25]);
      Data = [P, x, j1, Total_energy, Strain_one, Strain_two, Strain_three, Strain_four,
Strain_five, Strain_six, -10, -10, -10, -10];
   end
    if j >= 70
      uicontrol('string', 'Energy 7%', 'position',[750 200 70 25]);
      uicontrol('string', Strain_seven, 'position',[820 200 70 25]);
```

```
      Data = [P, x, j1, Total_energy, Strain_one, Strain_two, Strain_three, Strain_four,
Strain_five, Strain_six, Strain_seven, -10, -10, -10];
   end
  if j >= 80
      uicontrol('string', 'Energy 8%', 'position',[750 175 70 25]);
      uicontrol('string', Strain_eight, 'position',[820 175 70 25]);
      Data = [P, x, j1, Total_energy, Strain_one, Strain_two, Strain_three, Strain_four,
Strain_five, Strain_six, Strain_seven, Strain_eight, -10, -10];
   end
   if j >= 90
      uicontrol('string', 'Energy 9%', 'position',[750 150 70 25]);
      uicontrol('string', Strain_nine, 'position',[820 150 70 25]);
      Data = [P, x, j1, Total_energy, Strain_one, Strain_two, Strain_three, Strain_four,
Strain_five, Strain_six, Strain_seven, Strain_eight, Strain_nine, -10];
   end
   if j >= 100
      uicontrol('string', 'Energy 10%', 'position',[750 125 70 25]);
      uicontrol('string', Strain_ten, 'position',[820 125 70 25]);
      Data = [P, x, j1, Total_energy, Strain_one, Strain_two, Strain_three, Strain_four,
Strain_five, Strain_six, Strain_seven, Strain_eight, Strain_nine, Strain_ten];
   end
end

%Displays Energy information for given strain values if strain is greater than 25%
if x >= 0.25
   if j >= 5
      uicontrol('string', 'Energy 5%', 'position',[600 225 70 25]);
      uicontrol('string', Strain_five, 'position',[670 225 70 25]);
      Data = [P, x, j1, Total_energy, Strain_five, -10, -10, -10, -10, -10, -10, -10, -10, -
10];
   end
   if j >= 10
      uicontrol('string', 'Energy 10%', 'position',[600 200 70 25]);
      uicontrol('string', Strain_ten, 'position',[670 200 70 25]);
      Data = [P, x, j1, Total_energy, Strain_five, Strain_ten, -10, -10, -10, -10, -10, -10, -
10, -10];
   end
    if j >= 15
      uicontrol('string', 'Energy 15%', 'position',[600 175 70 25]);
      uicontrol('string', Strain_fifteen, 'position',[670 175 70 25]);
      Data = [P, x, j1, Total_energy, Strain_five, Strain_ten, Strain_fifteen, -10, -10, -10, -
10, -10, -10, -10];
   end
  if j >= 20
      uicontrol('string', 'Energy 20%', 'position',[600 150 70 25]);
      uicontrol('string', Strain_twenty, 'position',[670 150 70 25]);
```

```
        Data = [P, x, j1, Total_energy, Strain_five, Strain_ten, Strain_fifteen, Strain_twenty,
-10, -10, -10, -10, -10, -10];
    end
     if j >= 25
        uicontrol('string', 'Energy 25%', 'position',[600 125 70 25]);
        uicontrol('string', Strain_twentyfive, 'position',[670 125 70 25]);
        Data = [P, x, j1, Total_energy, Strain_five, Strain_ten, Strain_fifteen, Strain_twenty,
Strain_twentyfive, -10, -10, -10, -10, -10];
    end
   if j >= 30
        uicontrol('string', 'Energy 30%', 'position',[750 225 70 25]);
        uicontrol('string', Strain_thirty, 'position',[820 225 70 25]);
        Data = [P, x, j1, Total_energy, Strain_five, Strain_ten, Strain_fifteen, Strain_twenty,
Strain_twentyfive, Strain_thirty, -10, -10, -10, -10];
    end
   if j >= 35
        uicontrol('string', 'Energy 35%', 'position',[750 200 70 25]);
        uicontrol('string', Strain_thirtyfive, 'position',[820 200 70 25]);
        Data = [P, x, j1, Total_energy, Strain_five, Strain_ten, Strain_fifteen, Strain_twenty,
Strain_twentyfive, Strain_thirty, Strain_thirtyfive, -10, -10, -10];
    end
    if j >= 40
        uicontrol('string', 'Energy 40%', 'position',[750 175 70 25]);
        uicontrol('string', Strain_fourty, 'position',[820 175 70 25]);
        Data = [P, x, j1, Total_energy, Strain_five, Strain_ten, Strain_fifteen, Strain_twenty,
Strain_twentyfive, Strain_thirty, Strain_thirtyfive, Strain_fourty, -10, -10];
    end
     if j >= 45
        uicontrol('string', 'Energy 45%', 'position',[750 150 70 25]);
        uicontrol('string', Strain_fourtyfive, 'position',[820 150 70 25]);
        Data = [P, x, j1, Total_energy, Strain_five, Strain_ten, Strain_fifteen, Strain_twenty,
Strain_twentyfive, Strain_thirty, Strain_thirtyfive, Strain_fourty, Strain_fourtyfive, -10];
    end
   if j >= 50
        uicontrol('string', 'Energy 50%', 'position',[750 125 70 25]);
        uicontrol('string', Strain_fifty, 'position',[820 125 70 25]);
        Data = [P, x, j1, Total_energy, Strain_five, Strain_ten, Strain_fifteen, Strain_twenty,
Strain_twentyfive, Strain_thirty, Strain_thirtyfive, Strain_fourty, Strain_fourtyfive,
Strain_fifty];
    end
end

%The Master Data Matrix compiles all the information into one matrix that
%can be copied into Excel or Tecplot
master_data(q,:) = Data;
```

```
%Save Plot as *.fig in folder with *.prn file (to avoid saving figure, comment figure)
saveas(gcf, wholefilepath2, 'fig')

%Print Plot (to print, uncomment command)
%orient landscape
%print

%Close Figure (to close figure, uncommment command)
%close

%Clear Figure (to clear figure at end, uncomment command)
%clf
```

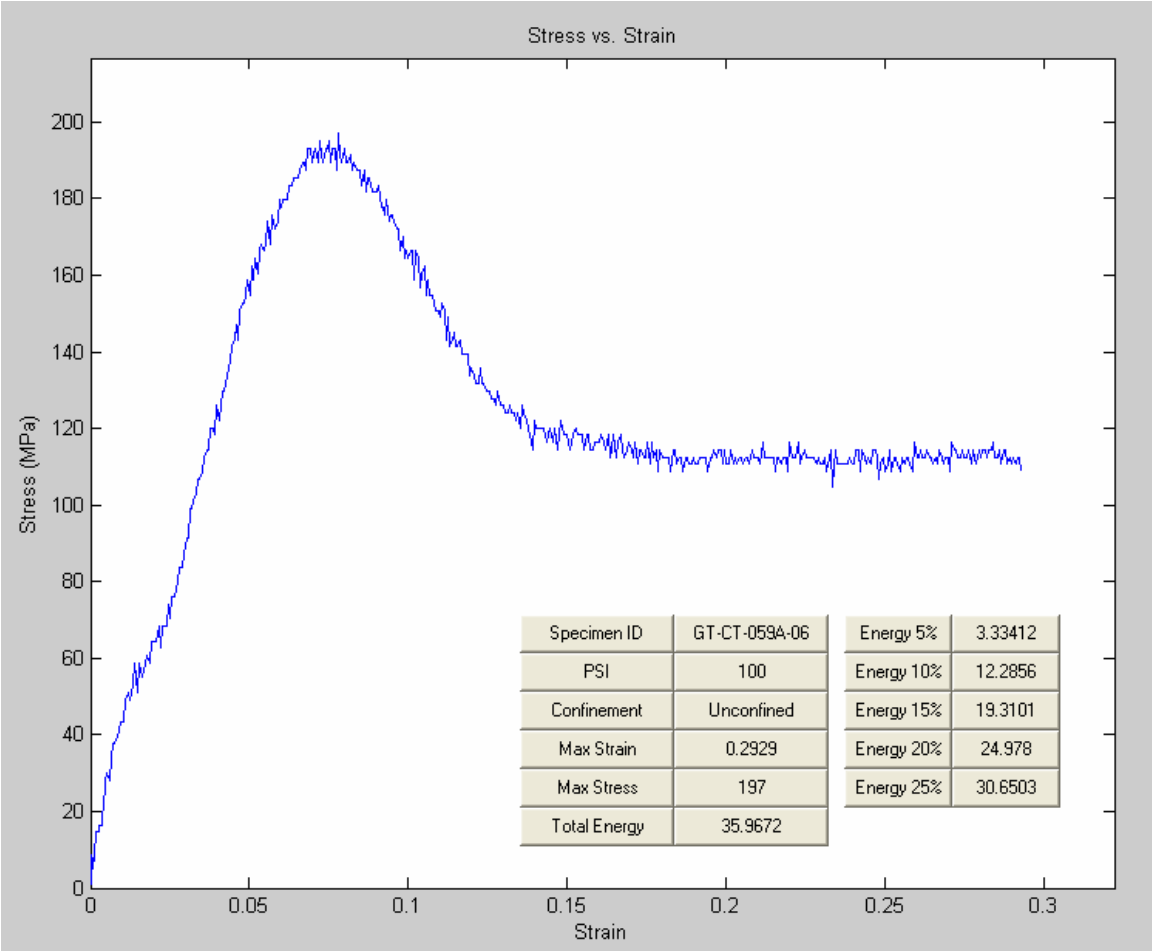

Figure 58: Output figure from stress work Matlab program

APPENDIX D
MATLAB: WAVE CORRECTION FOR UNLOADING ANALYSIS CODE

This program employs the one-point method of wave separation to allow for the extended analysis of the SHPB experiments from this study. The input for this program is the first of the two converted waveforms collected by the oscilloscope. The output figure contains the extended stress-strain, stress-time, and strain-time relations in addition to the total stress work, elastic work, and plastic work calculated values (Figure 59). An output filed named "tecplot_data.dat" is created in the same directory as the input waveform; it contains the extended stress and strain values for the experiment.

```
format
clear data
clear stress
clear strain
clear b
clear estart

%Set working directory to directory with test files
cd('C:\Documents and Settings\nitinp\My Documents\tests\GT-CT-084A\');

%Loads the incident bar waveform using a dialog box
[file_i,dirpath] = uigetfile('WAVE####.flt','Choose incident bar waveform');
wholefilepath_i = [dirpath file_i];
waveform_i = dlmread(wholefilepath_i);

%Set working directory back to Matlab's working directory
cd('C:\MATLAB6p5\work');

%Finds the Specimen Name
specimen_name = wholefilepath_i(1,64:76);
disp(specimen_name)
```

```
%Loads the transmission bar waveform based on wave number
wave = file_i(1,1:4);
file_number1 = file_i(1,5:8);
file_number1 = str2num(file_number1);
file_number = file_number1 + 1;
file_number = num2str(file_number);
ext = file_i(1,9:12);
file_t = [wave file_number ext];
wholefilepath_t = [dirpath file_t];
waveform_t = dlmread(wholefilepath_t);
waveform_t = -waveform_t;

%Loads the file into the program and breaks up the columns
voltage_unzeroed_i = waveform_i(:,1);
voltage_unzeroed_t = waveform_t(:,1);
time1 = waveform_i(:,2);
time0 = time1 * 10^6;

%Find the average zero value
zero_voltage_i = voltage_unzeroed_i(1:101);
zero_i = mean(zero_voltage_i);
zero_voltage_t = voltage_unzeroed_t(1:101);
zero_t = mean(zero_voltage_t);

%Zero the voltage
voltage_i = voltage_unzeroed_i - zero_i;
voltage_t = voltage_unzeroed_t - zero_t;

%Calculate the strain in the pressure bars due to the stress wave
wave_strain_i = (2*voltage_i)/(2.05*30);     %Strain gage factor is 2.05 and exitation
voltage is 30V
wave_strain_t = (2*voltage_t)/(2.05*30);

% Young's Modulus of Pressure Bar (MPa)
E = 200000;

%Pressure bar diameter = 0.75in = 19.05mm
A_bar = (pi * 0.01905^2)/4;

%Wave speed in the bar material (m/s)
C = 4969.0399;

%Input the Specimen number
shot = specimen_name(1,12:13);
shot = str2num(shot);
```

```
%Input the Specimen diameter in inches
specimen_dia = input('Specimen Diameter (in): ');
specimen_dia = specimen_dia*0.0254;        %Convert to meters
A_specimen = (pi * specimen_dia^2)/4;      %Cross-Sectional Area of specimen

%Input the Specimen length in inches
specimen_length = input('Specimen Length (in): ');
specimen_length = specimen_length*0.0254;   %Convert to meters

index_stress = input('Start Time of Transmitted Wave (us): ');
index_strainrate = input('Start Time of Reflected Wave (us): ');

% Calculate the Stress in the specimen
stress0 = E * (A_bar/A_specimen) * wave_strain_t;

stress_time(:,1) = time0;
stress_time(:,2) = stress0;

stress_start1 = find(time0 > index_stress);
stress_start = stress_start1(1,1) - 1;

stress1 = stress0(stress_start:stress_start+640,1);  %Clean loading data
stress2 = stress0(stress_start+641:stress_start+784,1);  %Data affected by tensile wave
stress3 = stress0(stress_start:stress_start+143,1);  %Beginning portion of loading pulse
stress4 = stress2 - stress3;    %Removing affect of tensile pulse

zero = find(stress4 <= 0);      %Finds value where stress reaches zero

stress5 = stress4(1:zero-1,1);
index = length(stress5);
index2 = 641 + index;

stress(1:641,1) = stress1;
stress(642:index2,1) = stress5;

index3 = stress_start + index2;
time = time0(stress_start:index3-1,1);

%--------
%Calculates the Strain based on the reflected wave in the incident bar
%--------
strainrate_start1 = find(time0 > index_strainrate);
strainrate_start = strainrate_start1(1,1) - 1;
```

```
strainrate = (-2*C*wave_strain_i)/(specimen_length);
edot = strainrate(strainrate_start:strainrate_start-1+index2,1);
time_edot = time1(strainrate_start:strainrate_start-1+index2,1);
inc = length(time_edot);
format long
area = (time_edot(2:inc) - time_edot(1:inc-1)) .* ((edot(2:inc)+ edot(1:inc-1)))./2;
efinish = cumsum(area);
estart(1)=0;
for b = 1:length(time_edot)-1
   estart(b+1) = efinish(b);
   strain = estart';
end

time_edot1 = time_edot * 10^6;

figure(1)
clf     %Clears figure(1) if open

%Creates plot of Stress vs. Strain, Stress vs. Time, Strain vs. Time
subplot(2,2,1), plot(strain,stress,'r'), title('Stress vs. Strain'), xlabel('Strain'), ylabel('Stress
(MPa)')
subplot(2,2,2), plot(time,stress), title('Stress vs. Time'), xlabel('Time (\mus)'),
ylabel('Stress (MPa)')
subplot(2,2,3), plot(time_edot1,strain), title('Strain vs. Time'), xlabel('Time (\mus)'),
ylabel('Strain')

%--------
%Calculates the Stress Work based on the Stress vs. Strain plot
%--------

[x,k] = max(strain);        %x is the value of max strain and k is the index of max strain
j1 = max(stress);           %j1 is the value of max stress
l_s = length(strain);       %l_s is the length of the strain column

loading_energy = trapz(strain(1:k,1),stress(1:k,1));           %Find loading energy
unloading_energy = trapz(strain(k+1:l_s,1),stress(k+1:l_s,1));  %Find unloading energy
total_energy = trapz(strain,stress);                           %Find total energy

%Displays energy values on plot
uicontrol('string', 'Specimen', 'position',[600 295 100 25]);
uicontrol('string', specimen_name, 'position',[725 295 100 25]);
uicontrol('string', 'Total Energy', 'position',[600 260 100 25]);
uicontrol('string', total_energy, 'position',[725 260 100 25]);
uicontrol('string', 'Loading Energy', 'position',[600 225 100 25]);
uicontrol('string', loading_energy, 'position',[725 225 100 25]);
uicontrol('string', 'Unloading Energy', 'position',[600 190 100 25]);
```

```
uicontrol('string', unloading_energy, 'position',[725 190 100 25]);

%Saves loading data into matrix using shot number as row number
Data = [loading_energy, unloading_energy, total_energy];
master_data(shot,:) = Data

%Write output file 'tecplot_data.dat' with columns of Time, Stress, and Strain into same
directory as waveform file
data(:,1) = time;          %Time vector for Stress
data(:,2) = stress;        %Stress
data(:,3) = time_edot1;    %Time vector for Strain
data(:,4) = strain;        %Strain
ext = ('.dat');
output_filename = [dirpath specimen_name ext];
dlmwrite(output_filename,data,'\t');

%Save a copy of the figure into same directory as waveform file
output_figurename = ('matlab_figure.fig');
output_figure = [dirpath output_figurename];
saveas(gcf, output_figure, 'fig');

% Print Plot (to print, uncomment command)
% orient landscape
% print
```

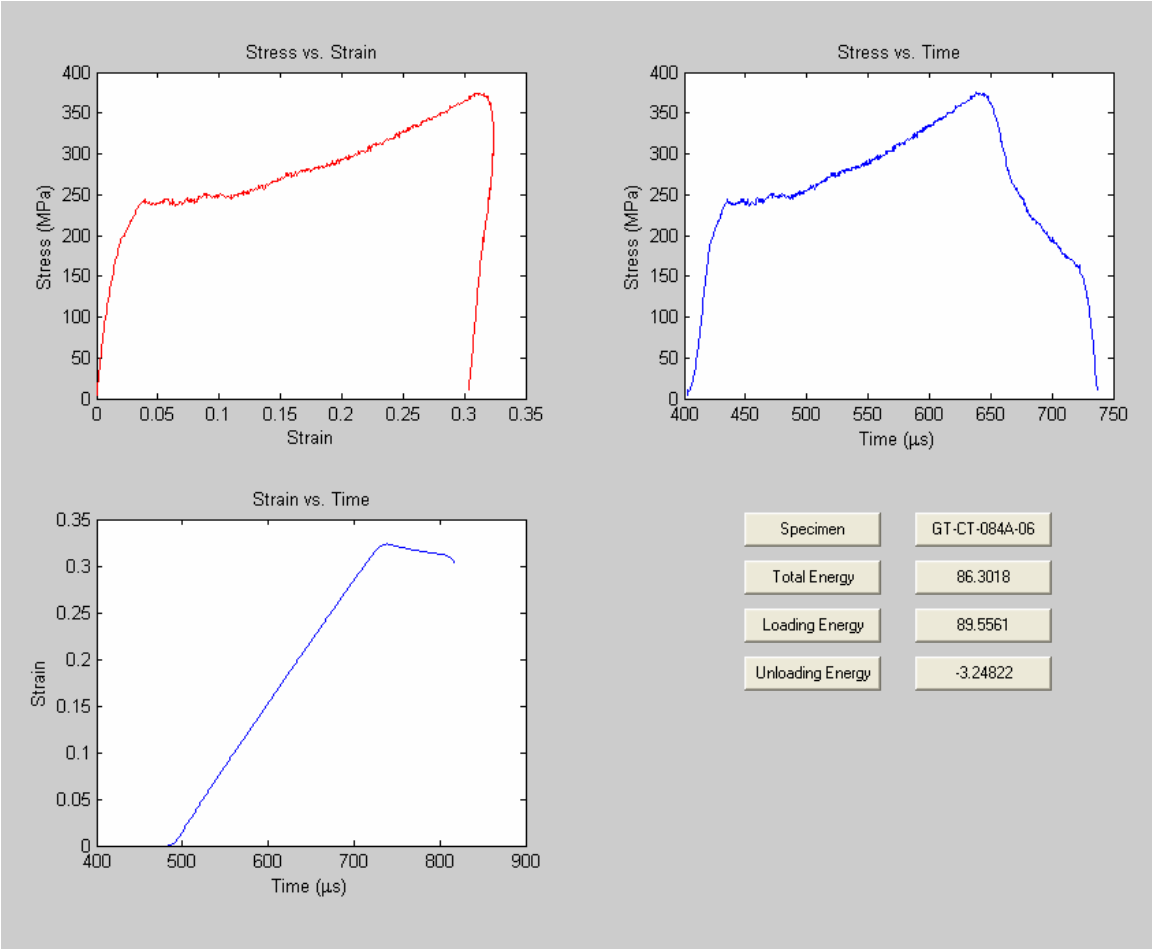

Figure 59: Output figure from the unloading analysis Matlab program

APPENDIX E
MATLAB: DYNAMIC HARDNESS ANALYSIS CODE

This program calculates the dynamic Brinell hardness for the specimens in this study. The inputs for this program are the first of the two converted waveforms collected by the oscilloscope and the "dh_data.m" file, which is a tabulation of the time-resolved diameter measurements from the high-speed digital camera. The program contains four graphical inputs for the beginning and ending of the incident wave, the beginning of the reflected wave, and the beginning of the transmission wave (Figure 60). Figure 61 is a plot of the interface force measured by the SHPB apparatus. The other outputs of this program are files that contain information of the dynamic Brinell hardness values and the force-time relations.

```
format
clear

%Set working directory to directory with tests
cd('C:\Documents and Settings\nitinp\My Documents\tests\Dynamic Hardness\06-15-
04\');
%Loads the incident bar waveform using a dialog box
[file_i,dirpath] = uigetfile('WAVE####.flt','Choose incident bar waveform');
wholefilepath_i = [dirpath file_i];
waveform_i = dlmread(wholefilepath_i);

%Set working directory back to Matlab's working directory
cd('C:\MATLAB6p5\work');

%Loads Dynamic Hardness data, a .m file created using Excel calculations
load dh_data.m;
```

```
%Displays folder name
 x= dirpath(1,79:85);
 y = dirpath(1,87:92);
filename = [x, '-', y];
disp(filename)

%Extracts data from dh_data.m file
test_number = input('Which Dynamic Hardness test? ');
diameter = dh_data(:,test_number);

%Loads the transmission bar waveform based on wave number
wave = file_i(1,1:4);
file_number1 = file_i(1,5:8);
file_number1 = str2num(file_number1);
file_number = file_number1 + 1;
file_number = num2str(file_number);
ext = file_i(1,9:12);
file_t = [wave file_number ext];
wholefilepath_t = [dirpath file_t];
waveform_t = dlmread(wholefilepath_t);

%Loads the file into the program and breaks up the columns
voltage_unzeroed_i = waveform_i(:,1);
voltage_unzeroed_t = waveform_t(:,1);
time1 = waveform_i(:,2);
time0 = time1 * 10^6;

%Find the average zero value
zero_voltage_i = voltage_unzeroed_i(1:101);
zero_i = mean(zero_voltage_i);
zero_voltage_t = voltage_unzeroed_t(1:101);
zero_t = mean(zero_voltage_t);

%Zero the voltage
voltage_i = voltage_unzeroed_i - zero_i;
voltage_t = voltage_unzeroed_t - zero_t;

%Input the Excitation Voltage
Ve_i = 30; Ve_t = 30;

%Calculate the strain in the pressure bars due to the stress wave
wave_strain_i = (2*voltage_i)/(2.05*Ve_i);     %Strain gage factor is 2.05 and exitation
voltage is 30V
wave_strain_t = (2*voltage_t)/(2.05*Ve_t);

% Young's Modulus of Pressure Bar (MPa)
```

```
E = 200e9;

%Pressure bar diameter = 0.75in = 19.05mm
A_bar = (pi * 0.01905^2)/4;

%Wave speed in the bar material (m/s)
C = 4969.0399;

%Diameter of indenter
D = 3.175;

%Transmitted Wave
figure(1), clf
plot(time0(800:2500,1), voltage_t(800:2500,1), 'b'), title('Transmitted Pulse -- Voltage vs.
Time'), xlabel('Time (us)'), ylabel('Voltage (V)');
[coord_xxx, coord_yyy] = ginput(1);
coord_xxx1 = coord_xxx(1);
rdcoord_xxx1 = round(coord_xxx1);

%Find the index of the start and end of the Transmitted Pulse
idxxx1 = find(time0 == rdcoord_xxx1);
idxxx2 = idxxx1 + 400;
index_duration = idxxx2 - idxxx1;

%Creates Transmitted Wave
e_t = wave_strain_t(idxxx1:idxxx2,1);

%Calculate the Force (N) at the Transmission Bar/Specimen interface
P_t = E *  A_bar * (-e_t);

dh_time = [25; 50; 75; 100; 125; 150; 175];

%Find value of force at 25, 50, 75 ... us using indexes from time
Force (1,1) = P_t(51);
Force (2,1) = P_t(101);
Force (3,1) = P_t(151);
Force (4,1) = P_t(201);
Force (5,1) = P_t(251);
Force (6,1) = P_t(301);
Force (7,1) = P_t(351);

%Time of impact
idx_time = find(time0 == 0.5);
idx_time = idx_time - 1;
time_impact = time0(idx_time:idx_time+index_duration);
time_impact(1,1) = 0;
```

```
%Interface Forces
figure(2), clf
hold on
plot(time_impact,P_t), title('Interface Force vs. Time'), xlabel('Time (us)'), ylabel('Force
(N)');
hold off

%Find the Max Force from the Transmission Bar Force (95% of Force (kN))
max_force = max(P_t)*.95*10^-3;
format short g
max_force_N = max_force*10^3
format

%Dynamic Hardness
DH = 0.102*((2*Force)./(pi*D.*(D-(D.^2-diameter.^2).^0.5)));

%Write Dynamic Hardness output file
data(:,1) = dh_time;              %Time (every 25 us)
data(:,2) = DH;                   %Dynamic Hardness
data(:,3) = Force;                %Force every 25 us (kN)
data(:,4) = diameter;             %Diameter of indentation (mm)

dirpath2 = dirpath(1,1:86);
ext = ('.dat');
output_filename = [dirpath2 filename ext];
dlmwrite(output_filename,data,'\t');

%Write Force vs. Time output file
data2(:,1) = time_impact;         %Total Time
data2(:,2) = P_t*10^-3;           %Transmission Bar Force (kN)
format short g
data2(1,3) = max_force;

file = ('Force vs. Time Data');
ext = ('.dat');
output_filename = [dirpath file ext];
dlmwrite(output_filename,data2,'\t');
```

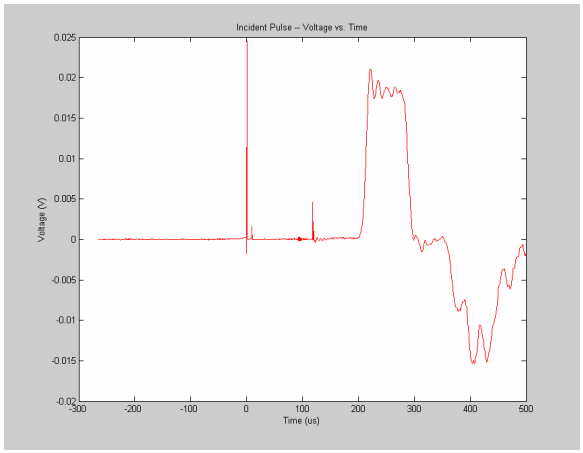

(a)

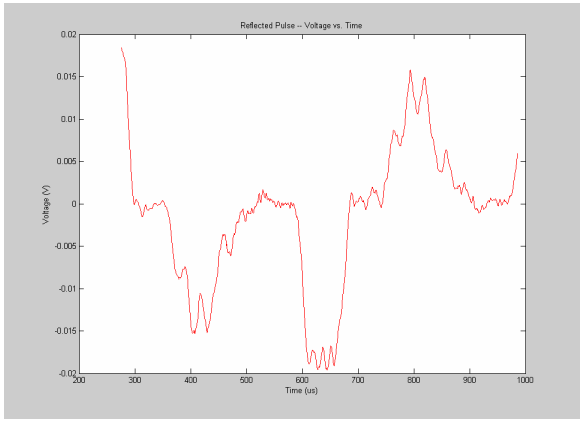

(b)

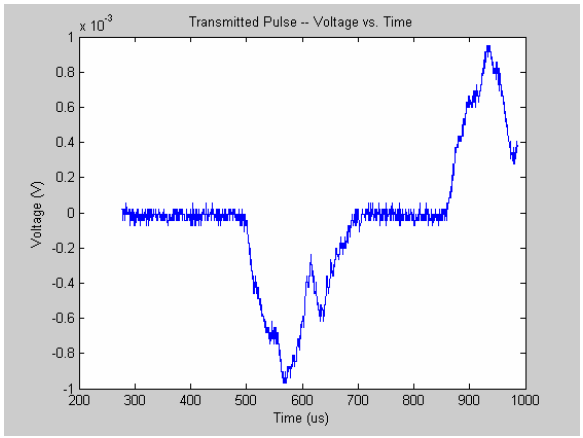

(c)

Figure 60: Experimental waveforms for the (a) incident wave, (b) reflected wave, and (c) transmitted wave

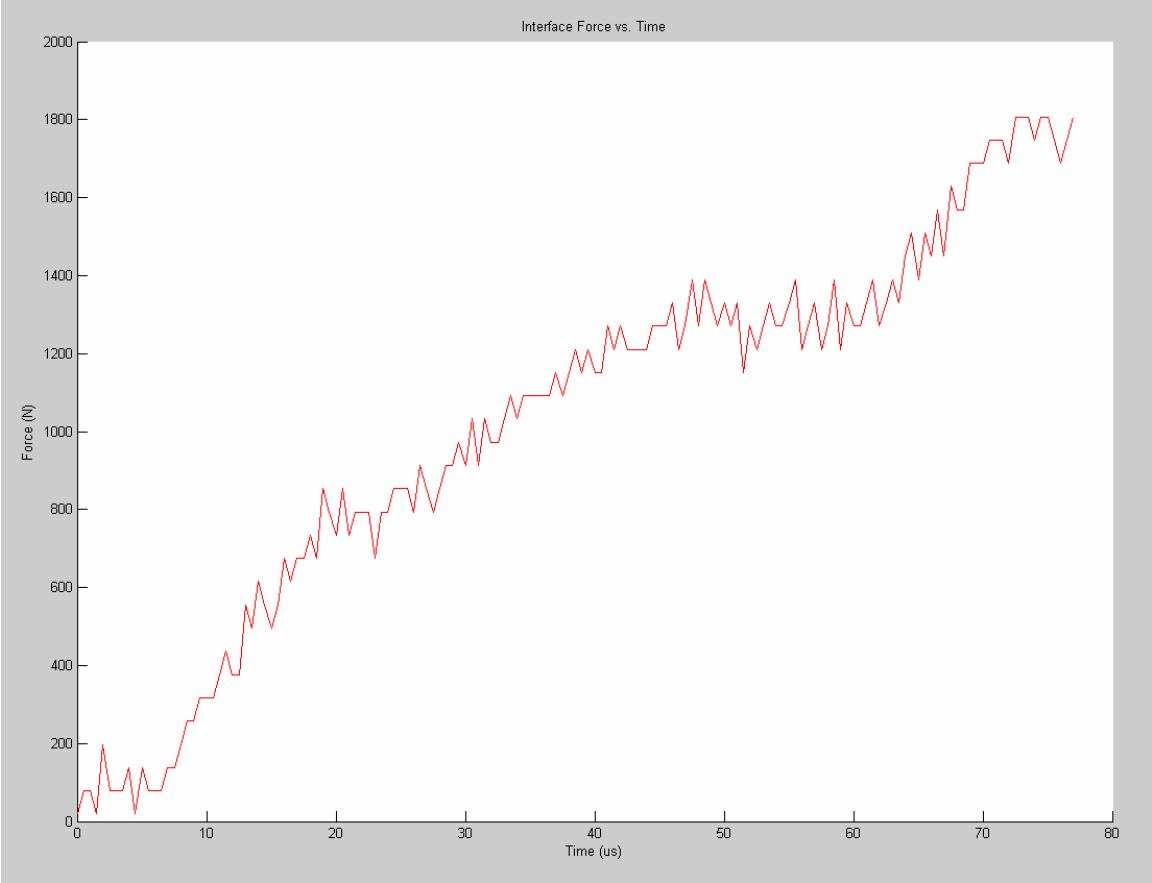

Figure 61: Output figure dh.m Matlab program

APPENDIX F
MATLAB: HASAN-BOYCE MODEL

This program fits the experimental data collected in this study to the Hasan-Boyce model (1995). The input for this program is the dynamic stress-strain curve for the specimens tested. The parameters for the model are changed within the program under the Constants and Initial Conditions sections of the code. Figure 62 is an output of variables that are used in the model; Figure 63 is an output of the fit of the model prediction and the experimental data. The "Data2" variable contains the history of the variables within the calculations.

```
format long g
orient landscape
clear

DataFile = load('C:\Documents and Settings\nitinp\My Documents\Research\Hasan-
Boyce Model\Input Data\100%.dat');
q = length(DataFile);

%Extract Stress and Strain columns from input file
sigma = DataFile(:,3);          %Uniaxial Stress in MPa
sigma_Pa = sigma*10^6;          %Convert from MPa to Pa
epsilon = DataFile(:,2);        %Uniaxial Strain
time = DataFile(:,1);           %Time (us)

E = 5536.3e6;                   %Young's Modulus in Pa
epsilon_plastic = epsilon - sigma/E;

%Convert Uniaxial Stress and Strain to Shear Stress and Strain
tau_Pa = sigma_Pa/sqrt(3);
gamma = epsilon*sqrt(3);
```

```
gamma_plastic = epsilon_plastic*sqrt(3);
for i = 1:length(gamma_plastic)
   if gamma_plastic(i)<0
      gamma_plastic(i)=0;
   end
end
for i = 2:length(gamma_plastic)
   if gamma_plastic(i-1)==0
      if gamma_plastic(i+1)==0
         gamma_plastic(i)=0;
      end
   end
end

energyconv = 1.602176462e-19;
stressconv = 160217646200;
E = E/stressconv;                %Elastic Modulus in eV/Angstroms^3
tau_i = tau_Pa'/stressconv;      %Shear Stress in eV/Angstroms^3

%----------------------------
%  Constants
%----------------------------
k = 8.617385e-5;               %Boltzmann's Constant  (J/K)
rho = 1.164e3;                 %Density in kg/m^3
c = 2.0e3;                     %Specific Heat in J/kg/K
mu = (E/(2*(1+.379)));         %Shear Modulus in eV/Angstroms^3
T_0 = 297;                     %(K)
delta_t = 0.5e-6;              %(s)
omega_0 = 7e15;                %(Hz)
gamma_dot_0 = 4.55e16;         %(s^-1)
xi = 5;
lamda = 2.4;                   %Angstroms^3/K
alpha_inv_eq = 1.87;           %eV^-1
a_eq = 0.800;                  %eV
beta1 = 50;
beta2 = 600;
beta3 = 1000;

%----------------------------
%  Initial Conditions
%----------------------------
delta_v(1) = 19.5;             %Angstroms^3
alpha_inv(1) = 1;              %eV^-1
a(1) = 0.531;                  %eV
S(1) = -0.001;                 %eV
gamma_dot_p(1) = 0;
```

```
omega(1) = 0;
tau(1) = 0;
tau_dot(1) = 0;
gamma_total(1)=0;
gamma_p(1)=0;
f(1) = 0;
gamma_dot_plastic(1) = 0;
T(1) = T_0;
eta(1) = 1/(k*T_0);
gamma_dot_p_1(1) = 0;
a_prime(1) = a(1)+(pi*alpha_inv(1))/2;
gamma_dot_p_2(1) = 0;
beta(1) = 0;
T_dot(1) = 0;
integral(1) = 0;

for i = 2:q
        gamma_dot_plastic(i) = (gamma_plastic(i)-gamma_plastic(i-1))/delta_t;
        eta(i) = 1/(k*T(i-1));
        T_dot(i) = (1/(2*rho*c))*stressconv*(tau_i(i-1)*gamma_dot_p(i-1)+tau_dot(i-
1)*gamma_p(i-1));
        T(i) = T(i-1)+delta_t*T_dot(i-1);
        f(i) = exp(-xi*exp(-xi*gamma_p(i-1)));
        beta(i) = beta1*(1+beta2*exp(-beta3*gamma_p(i-1)));
        omega(i) = (omega_0/gamma_dot_0)*gamma_dot_p(i-1);
        a_dot(i) = (a(i-1)-a_eq)*f(i-1)*omega(i-1);
        a(i) = a_dot(i)*delta_t+a(i-1);
        alpha_inv_dot(i) = -(alpha_inv(i-1)-alpha_inv_eq)*omega(i-1);
        alpha_inv(i) = alpha_inv_dot(i)*delta_t+alpha_inv(i-1);
        S_dot(i) = beta(i-1)*(tau_i(i-1)*gamma_dot_p(i-1))-S(i-1)*omega(i-1);
        S(i) = S_dot(i)*delta_t+S(i-1);
        delta_v(i) = delta_v(1)+lamda*(T(i-1)-T_0);
        h1(i) = (sqrt(2)+(2-eta(i-1))*exp(3*pi*(1-eta(i-1))/4))/((1+(1-eta(i-1))^2)*
(sqrt(2)+2*exp(3*pi/4)));
            h2(i) = (sqrt(2)*exp(pi*(1/4-eta(i-1)))+(2+eta(i-1))*exp(pi*(1-eta(i-1)/4)))/
((1+(1+eta(i-1))^2)*(sqrt(2)*exp(pi/4)+2*exp(pi)));
        a_prime(i) = a(i-1)+(pi*alpha_inv(i-1))/2;
        gamma_dot_p_2(i) = gamma_dot_0*exp(-a_prime(i-1)*eta(i-1))*h2(i);
        r1(i) = eta(i-1)*tau_i(i-1)*delta_v(i-1);
        r2(i) = (-tau_i(i-1)*delta_v(i-1)+S(i-1))*eta(i-1);
        x1(i) = exp(r1(i));
        x2(i) = exp(r2(i));
        y(i) = gamma_dot_p_1(i)+gamma_dot_p_2(i);
        gamma_dot_p(i) = y(i)*(x1(i)-x2(i));
        gamma_p(i) = gamma_dot_p(i)*delta_t+gamma_p(i-1);
        gamma_dot_total(i) = tau_dot(i-1)/mu+gamma_dot_p(i-1);
```

```
        gamma_total(i) = gamma_dot_total(i)*delta_t+gamma_total(i-1);
        tau_dot(i) = (tau_i(i)-tau_i(i-1))/delta_t;
end

epsilon_total = gamma_total/sqrt(3);

Data(1,:) = gamma_dot_plastic;
Data(2,:) = gamma_plastic';
Data(3,:) = tau_i;
Data(4,:) = T;
Data(5,:) = eta;
Data(6,:) = f;
Data(7,:) = beta;
Data(8,:) = omega;
Data(9,:) = a_dot;
Data(10,:) = a;
Data(11,:) = alpha_inv_dot;
Data(12,:) = alpha_inv;
Data(13,:) = a_prime;
Data(14,:) = S_dot;
Data(15,:) = S;
Data(16,:) = delta_v;
Data(17,:) = gamma_dot_p_1;
Data(18,:) = gamma_dot_p_2;
Data(19,:) = x1;
Data(20,:) = x2;
Data(21,:) = y;
Data(22,:) = gamma_dot_p;
Data(23,:) = gamma_p;
Data(24,:) = T_dot;
Data(25,:) = gamma_dot_total;
Data(26,:) = gamma_total;
Data(27,:) = epsilon_total;

Data2 = Data';

figure(1), clf
subplot(4,4,1), hold on, plot(gamma_plastic, 'r'), plot(gamma_p), hold off,
title('\gamma^p & \gamma^p^l^a^s^t^i^c')
subplot(4,4,2), hold on, plot(gamma_dot_plastic,'r'), plot(gamma_dot_p), title('\gamma
dot^p & \gamma dot^p^l^a^s^t^i^c')
subplot(4,4,3), plot(T), title('Temperature'), title('Temperature'),
subplot(4,4,4), plot(tau_dot,'r'), title('\tau dot')
subplot(4,4,5), plot(f), title('f')
subplot(4,4,6), plot(beta), title('\beta')
subplot(4,4,7), plot(a_prime), title('a prime')
```

```
subplot(4,4,8), plot(a), title('a')
subplot(4,4,9), plot(S), title('S')
subplot(4,4,10), plot(x1), title('x1')
subplot(4,4,11), plot(delta_v), title('\Delta v')
subplot(4,4,13), plot(omega), title('\omega')
subplot(4,4,14), hold on, plot(gamma_total), plot(gamma, 'r'), hold off,
title('\gamma^t^o^t^a^l & \gamma')
subplot(4,4,15), hold on, plot(gamma_total, tau_i), plot(gamma, tau_i, 'r'), title('\tau vs.
\gamma'), hold off

%Display boxes on figure with information
uicontrol('string', 'omega_0', 'position',[775 325 75 20]);
uicontrol('string', omega_0, 'position',[850 325 75 20]);
uicontrol('string', 'gamma dot_0', 'position',[775 305 75 20]);
uicontrol('string', gamma_dot_0, 'position',[850 305 75 20]);
uicontrol('string', 'xi', 'position',[775 285 75 20]);
uicontrol('string', xi, 'position',[850 285 75 20]);
uicontrol('string', 'lamda', 'position',[775 265 75 20]);
uicontrol('string', lamda, 'position',[850 265 75 20]);
uicontrol('string', 'alpha_inv_eq', 'position',[775 245 75 20]);
uicontrol('string', alpha_inv_eq, 'position',[850 245 75 20]);
uicontrol('string', 'a_eq', 'position',[775 225 75 20]);
uicontrol('string', a_eq, 'position',[850 225 75 20]);
uicontrol('string', 'beta1', 'position',[775 205 75 20]);
uicontrol('string', beta1, 'position',[850 205 75 20]);
uicontrol('string', 'beta2', 'position',[775 185 75 20]);
uicontrol('string', beta2, 'position',[850 185 75 20]);
uicontrol('string', 'beta3', 'position',[775 165 75 20]);
uicontrol('string', beta3, 'position',[850 165 75 20]);
uicontrol('string', 'delta_v', 'position',[775 145 75 20]);
uicontrol('string', delta_v, 'position',[850 145 75 20]);
uicontrol('string', 'alpha_inv_0', 'position',[775 125 75 20]);
uicontrol('string', alpha_inv(1), 'position',[850 125 75 20]);
uicontrol('string', 'a_0', 'position',[775 105 75 20]);
uicontrol('string', a(1), 'position',[850 105 75 20]);
uicontrol('string', 'S_0', 'position',[775 85 75 20]);
uicontrol('string', S(1), 'position',[850 85 75 20]);

figure(2), clf, hold on, plot(gamma_total, tau_i), plot(gamma, tau_i, 'r'), title('\tau vs.
\gamma'), xlabel('Shear Strain'), ylabel('Shear Stress (eV/Angstroms^3'),
legend('Hasan-Boyce Model', 'Experimental Data', 2), hold off

%Write output file 'tecplot_data.dat' with columns of Time, Stress, and Strain into same
directory as waveform file
data(:,1) = epsilon;              %Experimental Strain
data(:,2) = epsilon_total';       %Calculated Strain (using Hasan-Boyce Model)
```

```
data(:,3) = sigma;                  %Experimental Stress
data(:,4) = time;                   %Time
output_filename = 'C:\Documents and Settings\nitinp\My Documents\Research\Hasan-
Boyce Model\Results\100%_output.dat';
dlmwrite(output_filename,data,'\t');
```

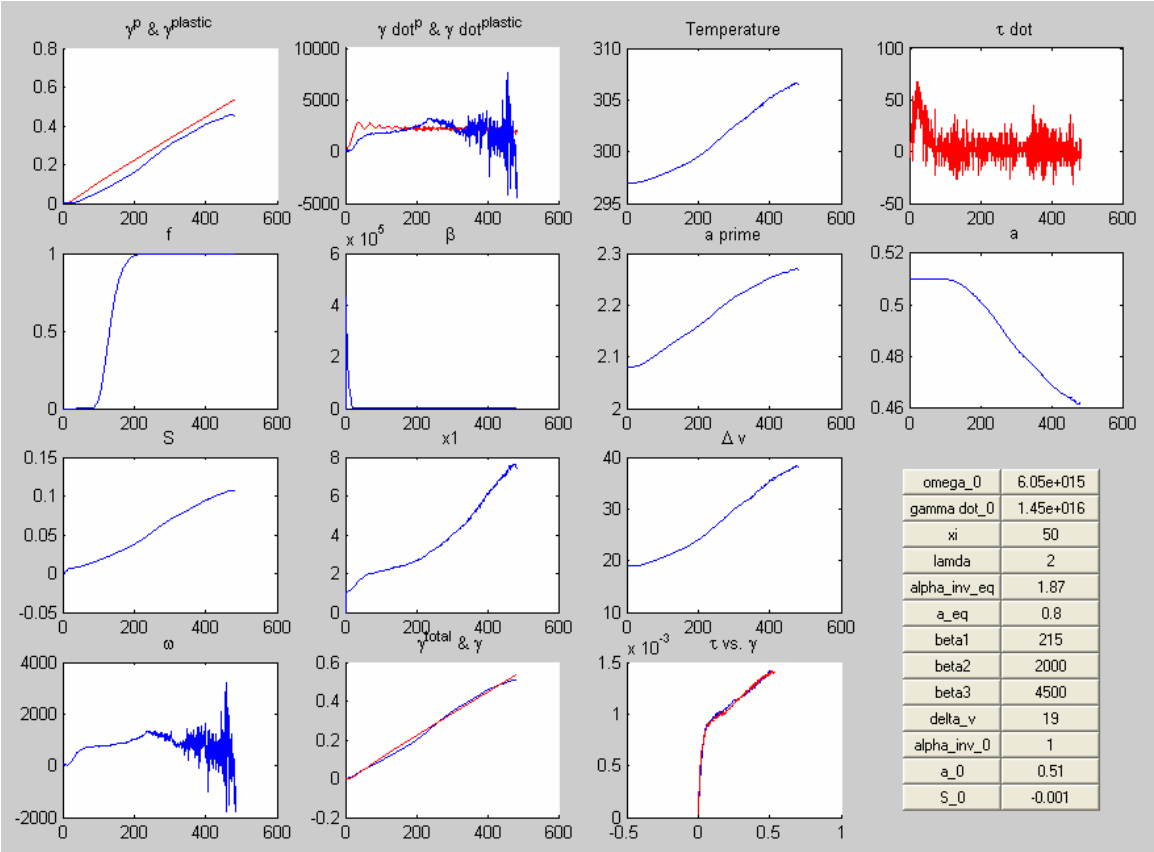

Figure 62: Output of parameters in Hasan-Boyce Model

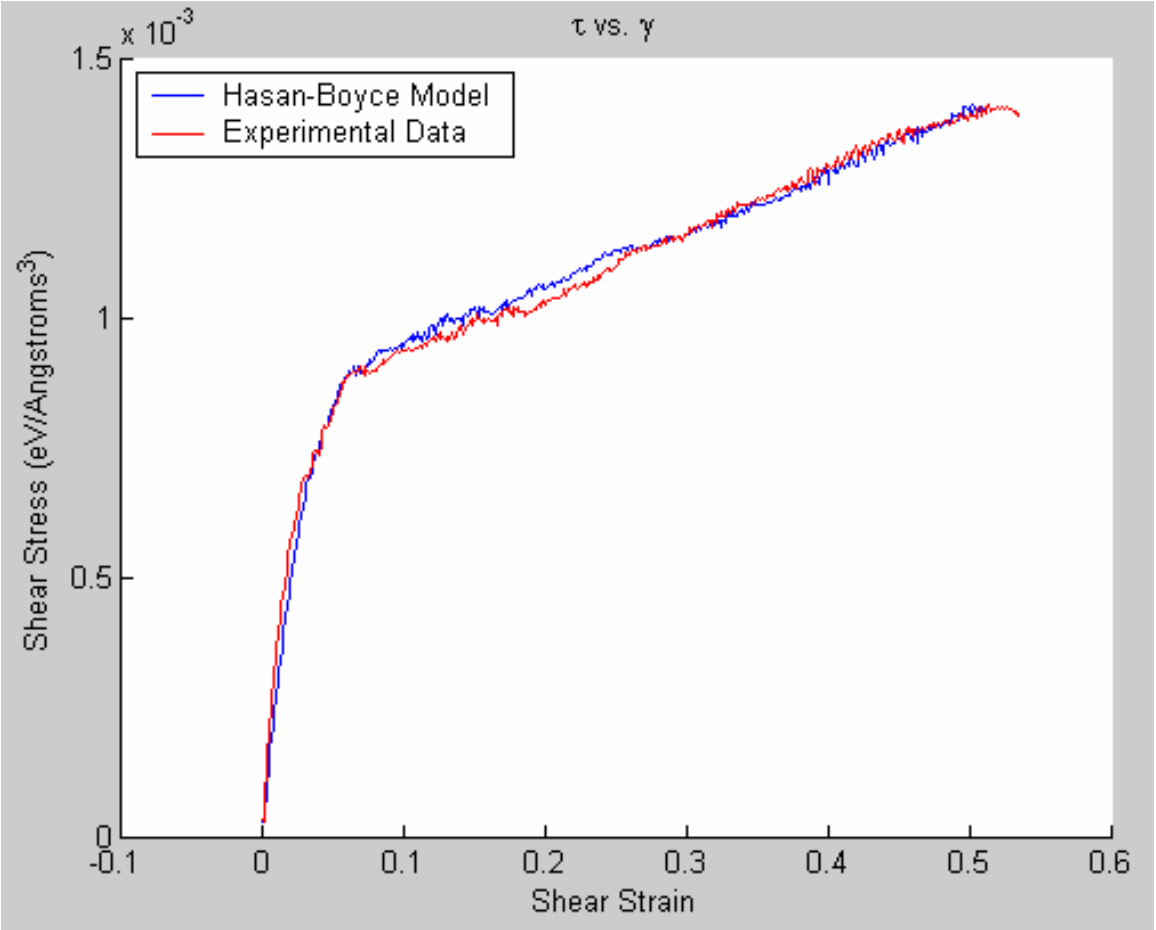

Figure 63: Fit of Hasan-Boyce Model to experimental data

REFERENCES

Al-Haik, M. S., Garmestani, H., Li, D. S., Hussaini, M. Y., Sablin, S. S., Tannenbaum, R. and Dahmen, K. (2004). "Mechanical properties of magnetically oriented epoxy." Journal of Polymer Science, Part B: Polymer Physics **42**(9): 1586-1600.

ASTM E-10 (2001). Standard Test Method for Brinell Hardness of Metallic Materials. ASTM International.

ASTM E-384 (2002). Standard Test Method for Microindentation Hardness of Materials. ASTM International.

Chen, W., Lu, F. and Cheng, M. (2002). "Tension and compression tests of two polymers under quasi-static and dynamic loading." Polymer Testing **21**(2): 113-121.

Chen, W. and Zhou, B. (1998). "Constitutive Behavior of Epon 828/T-403 at Various Strain Rates." Mechanics of Time-Dependent Materials **2**: 103-111.

Curran, M. D., Gedris, Thomas E., and Stiegman, A.E. (1999). "Synthetic Control over the Production of Multicomponent Sol-Gel Materials: Fabrication of Homogenous Vanadia-Silica Xerogels with High Vanadium Content." Chem. Mater. **11**: 1120-1127.

Davies, R. M. (1948). "A Critical Study of the Hopkinson Pressure Bar." Philosophical Transactions of the Royal Society of London. Series A. Mathematical and Physical Sciences **240**(821): 375-457.

Follansbee, P. S. (1985). "The Hopkinson Bar." Mechanical Testing, Metals Handbook **8**(9th Edition): 198-217.

Garmestani, H., Al-Haik, M. S., Dahmen, K., Tannenbaum, R., Li, D., Sablin, S. S. and Yousuff Hussaini, M. (2003). "Polymer-Mediated Alignment of Carbon Nanotubes under High Magnetic Fields." Advanced Materials **15**(22): 1918-1921.

Hasan, O. A. and Boyce, M. C. (1995). "Constitutive model for the nonlinear viscoelastic viscoplastic behavior of glassy polymers." Polymer Engineering and Science **35**(4): 331-344.

Hopkinson, B. (1914). "A Method of Measuring the Pressure Produced in the Detonation of High Explosives or by the Impact of Bullets." Philosophical Transactions of the Royal Society of London. Series A, Containing Papers of a Mathematical or Physical Character **213**: 437-456.

Kolsky, H. (1949). "An Investigation of the Mechanical Properties of Materials at very High Rates of Loading." Proc. Phys. Soc. **B62**: 676-700.

Lee, J.-H. and Thadhani, N. N. (1998). "Enhanced solid-state reaction kinetics of shock-compressed titanium and carbon powder mixtures." Journal of Materials Research **13**(11): 3160-3173.

Li, Z. and Lambros, J. (2001). "Strain rate effects on the thermomechanical behavior of polymers." International Journal of Solids and Structures **38**(20): 3549-3562.

Lindholm, U. S. (1964). "Some experiments with the split Hopkinson pressure bar." Journal of the Mechanics and Physics of Solids **12**: 317-335.

Lu, H., Tan, G. and Chen, W. (2001). "Modeling of constitutive behavior for epon 828/T-403 at high strain rates." Mechanics Time-Dependent Materials **5**(2): 119-130.

Lundberg, B. and Henchoz, A. (1977). "Analysis of elastic waves from two-point strain measurement." Experimental Mechanics **17**(6): 213-218.

Nemat-Nasser, S., Isaacs, J. B. and Starrett, J. E. (1991). "Hopkinson Techniques for Dynamic Recovery Experiments." Proceedings: Mathematical and Physical Sciences **435**: 371-391.

Owens, F. J. (1996). "Calculation of energy barriers for bond rupture in some energetic molecules." Journal of Molecular Structure (Theochem) **370**: 11-16.

Park, S. W. and Zhou, M. (1999). "Separation of elastic waves in split Hopkinson bars using one-point strain measurements." Experimental Mechanics **39**(4): 287-294.

Subhash, G., Koeppel, B. J. and Chandra, A. (1999). "Dynamic Indentation Hardness and Rate Sensitivity in Metals." Journal of Engineering Materials and Technology **121**: 257-263.

Tabor, D. (1948). "A Simple Theory of Static and Dynamic Hardness." Proceedings of the Royal Society of London. Series A. Mathematical and Physical Sciences **192**(1029): 247-274.

Tillotson, T. M., Hrubesh, L. W., Simpson, R. L., Lee, R. S., Swansiger, R. W. and Simpson, L. R. (1998). "Sol-gel processing of energetic materials." Journal of Non-Crystalline Solids **225**: 358-363.